ACTA UNIVERSITATIS SZEGEDIENSIS

ACTA MINERALOGICA-PETROGRAPHICA

Tomus XLIV

SZEGED, 2003

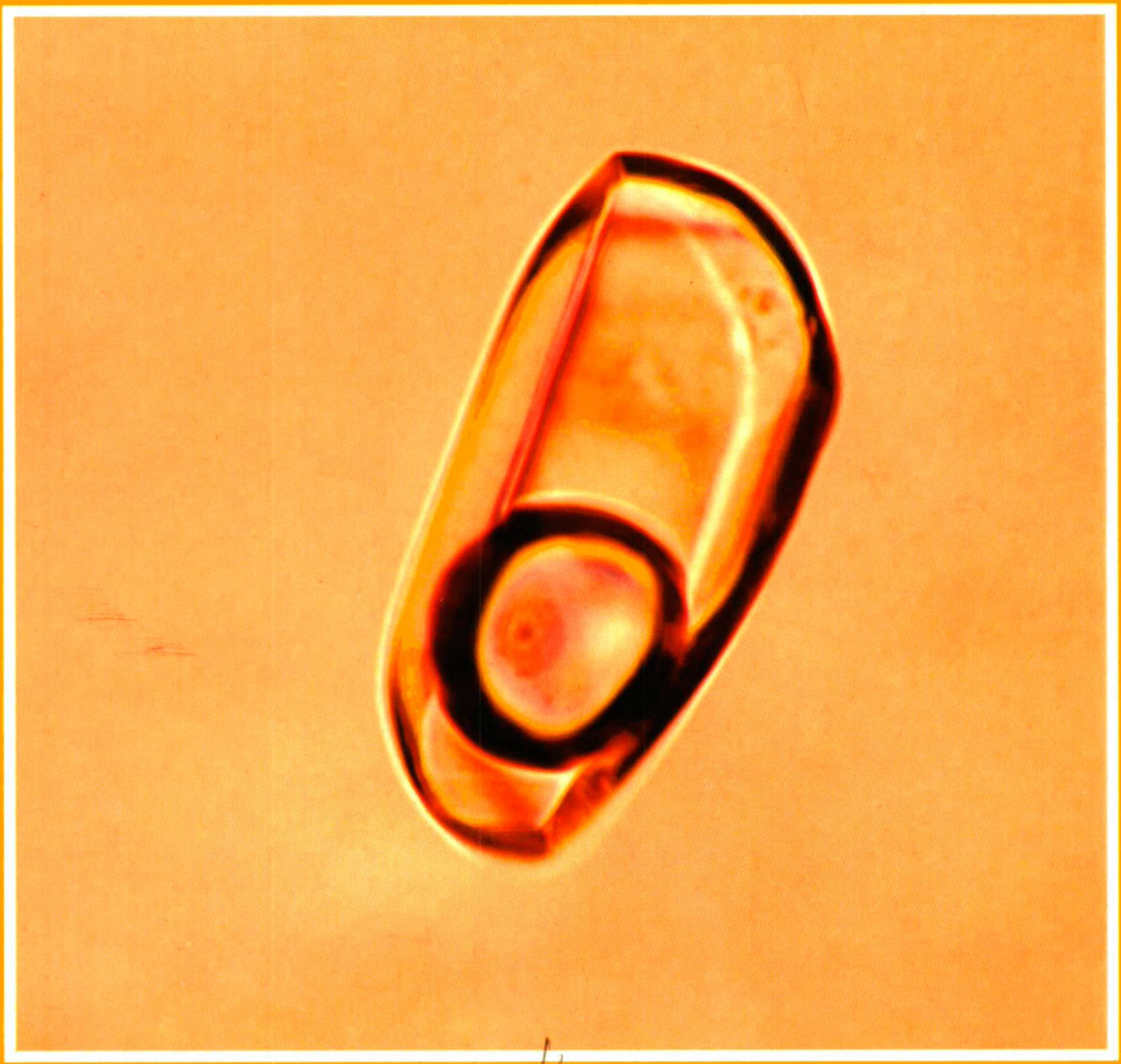

Published by the Department of Mineralogy, Geochemistry and Petrology, University of Szeged

ACTA MINERALOGICA-PETROGRAPHICA
established in 1922
HU ISSN 0365-8066

Abbreviated title:

Acta Mineral. Petrogr., Szeged

The Acta Mineralogica-Petrographica is published by the Department of Mineralogy, Geochemistry and Petrology, University of Szeged

---

On the cover: Primary petroleum inclusion from the fracture-filling quartz phase of the Szeghalom-167 well. The negative crystal shape refers to the recrystallization of the inclusion cavity. The diameter of the gas bubble is 15 mm. (see Schubert and M. Tóth, pp. 9-17)

Designed by: Elemér Pál-Molnár & György Sipos ©

Acta Mineralogica-Petrographica, Szeged 2003, Vol. 44, pp. 1-8

ACTA
Mineralogica
Petrographica

CORRENSITE IN METABASALTS AND METAGABBROS FROM MT. MEDVEDNICA, CROATIA

KATALIN JUDIK[1], TIBOR NÉMETH[1], DARKO TIBLJAŠ[2], PÉTER HORVÁTH[1], PÉTER ÁRKAI[1]

[1] Laboratory for Geochemical Research, Hungarian Academy of Sciences
Budaörsi út 45, H-1112, Budapest, Hungary
[2] University of Zagreb, Faculty of Science
Horvatovac bb, HR-10000 Zagreb, Croatia
e-mail: judik@geochem.hu

ABSTRACT

Complex mineral paragenetic and mineral structural and -chemical studies were carried out on metabasite samples from the ophiolitic mélange unit of Mt. Medvednica, Croatia using petrographic microscopic, XRPD and EMP techniques. According to XRPD studies of the <2 μm and < 0.6 μm grain-size fractions, chlorite and corrensite (regularly interstratified chlorite/smectite) are the predominant phyllosilicate components. Randomly interstratified chlorite/smectite and discrete smectite are also found in minor amounts. On the basis of the EMP analyses chemical composition of "chloritic materials" from different textural positions reveals that they contain not only chlorite layers but certain amount of trioctahedral smectite (saponite) interlayers also occur being responsible for their relatively high Ca and/or Na contents, large excess of Al(VI) relative to Al(IV) and high octahedral vacancy. The formation temperature of the "chloritic materials" is suggested to be in the range of ca. 160-200 °C using the geothermometer of Cathelineau (1988). Metabasalt samples from the ophiolitic mélange could be affected by minimum alteration, and the appearance of corrensite, together with mixed-layered chlorite/smectite and discrete smectite suggest "intermediate" temperature conditions (Shau and Peacor, 1992). According to Proust (1982) and Proust et al. (1986) corrensite as chlorite/vermiculite forms as an intermediate product of the weathering but the occurrence of chlorite/smectite in the studied samples may indicate that rather the diagenetic-incipient metamorphic alteration is the process that may be the main mechanism responsible for its formation.

Key words: corrensite, smectite-to-chlorite transition, hydrothermal metamorphism, weathering.

INTRODUCTION

Corrensite is an R1 50/50 regularly interstratified chlorite/smectite or chlorite/vermiculite named after C. W. Correns whose former student, F. Lippmannn identified it first in 1954 (Lippman, 1954). The presence of corrensite in different rock types has recently been receiving much attention. Corrensite occurs in variable geological settings, e.g. in contact metamorphic zones of shales, carbonate sequences, Lake Superior iron ores, in metabasalts and metagabbros affected by hydrothermal metamorphic alteration or weathering. Corrensite forms during burial diagenesis or weathering of sedimentary rocks containing sufficient amount of Mg (Reynolds and Moore, 1997).

The conversion of trioctahedral smectite into chlorite is a well-known process during diagenesis and under very low-grade metamorphic conditions. It is a very common feature of phyllosilicate reaction progress (in the sense of Merriman and Peacor, 1999) during hydrothermal metamorphism of the ocean crust. A common path of the smectite to chlorite transition process starts with smectite and involves a continuous sequence of interstratified chlorite/smectite phases with increasing proportion of chloritic layers as the alteration proceeds, and reaches chlorite as a stable phase (Liou et al., 1985; Bettison-Varga et al., 1991; Schiffman and Fridleifsson, 1991; Robinson et al., 1993). The second way is considered to be discontinuous with steps from smectite to corrensite and from corrensite to chlorite without any continuous sequence of mixed-layering (Tribble, 1991; Shau and Peacor, 1992; Schmidt and Robinson, 1997). In this model corrensite is considered to be a discrete phase and only smectite/corrensite and chlorite/corrensite interstratifications are suggested (Reynolds, 1988; Shau et al., 1990; Shau and Peacor, 1992). Recently, a third pathway has also been recognized, namely a direct transformation from smectite to chlorite (Robinson et al., 2002). Another debated consideration in connection to the smectite to chlorite transformation is whether this change represents equilibrium or disequilibrium processes. According to Robinson et al. (2002) the smectite to chlorite transition involving the above mentioned three pathways proves disequilibrium progression in which these pathways are interpreted as irreversible, episodic reactions that proceed in one or more steps with a minimization of free energy (Peacor, 1992; Essene and Peacor, 1995). Robinson et al. (2002) claim that there are several kinetic factors that control the smectite to chlorite transition besides the temperature, pressure and the whole rock composition. The fluid/rock ratio, the porosity and the permeability of the rock are proved to be the most important kinetic controls clearly affecting fluid transport and nutrient supply for recrystallization (Schiffman and Staudigel, 1995; Schmidt and Robinson, 1997).

Weathering is another important corrensite-forming process in basic rocks of the ocean crust, as first described by Johnson (1964). According to Proust (1982) and Proust et al. (1986) corrensite as an intermediate product of the

weathering is characterized as chlorite/vermiculite. This process involves loss of Fe and Mg to such an extent that the chlorite gradually loses its trioctahedral character transforming into the end-member vermiculite being strictly dioctaherdal, which may evolve into smectite.

The aim of the present paper is to provide a characterization of phyllosilicates of metabasite samples from the ophiolitic mélange unit of Mt. Medvednica, using petrographic microscopic, X-ray powder diffractometric and electron-microprobe techniques in order to give additional data on its metamorphic and/or post-metamorphic evolution.

GEOLOGICAL SETTING AND PREVIOUS DATA ON METAMORPHISM

The Zagorje–Mid-Transdanubian Zone (ZMTZ) is located in the triple junction of the Dinaridic, Alpine and Pannonian units (Fig. 1). In the north and northwest it is bordered by the Periadriatic-Balaton Lineament. The Zagreb-Zemplén Lineament is considered to be its southeastern boundary, while in the south it is bordered by the north-northeastern margin of Adriatic-Dinaridic carbonate platform, i.e. by the External Dinarides (Pamić and Tomljenović, 1998).

Mt. Medvednica is one of the few outcrops within ZMTZ composed of four pre-Neogene tectono-stratigraphic units. These are (1) the Middle Jurassic–Early Cretaceous ophiolitic mélange; (2) the Paleo–Mesozoic complex affected by Eoalpine (122-110 Ma) very low- to low-grade regional metamorphism; (3) the Late Cretaceous–Paleocene overlying sequence and (4) the dominantly Triassic Medvednica-Žumberak nappe.

Field work coupled with collection of representative samples was carried out on the Middle Jurassic–Early Cretaceous ophiolitic mélange characterized mainly by sheared pelitic-silty matrix, containing fragments of ophiolites (predominantly metabasalt and metagabbro), graywackes, radiolarites, shales and limestones. On the basis of the radiolarite biostratigraphy the ages of the radiolarite fragments are considered to be Late Ladinian – Late Carnian (Halamić and Goričan, 1995) and Jurassic (Halamić et al., 2000). Diabase and gabbro samples gave Early to Middle Jurassic (189-185 Ma) and Early to Late Cretaceous (110-66 Ma) K/Ar whole rock apparent ages (Pamić, 1997a, b).

METHODS

X-ray powder diffraction patterns were obtained using a Philips PW-1730 diffractometer (with computerized APD system) with the following instrumental and measuring conditions: Cu K_α radiation, 45 kV/35 mA, proportional counter, graphite monochromator, divergence and detector slit of 1°, and collection of data with 0.02° 2Θ steps, using time intervals of 5 s.

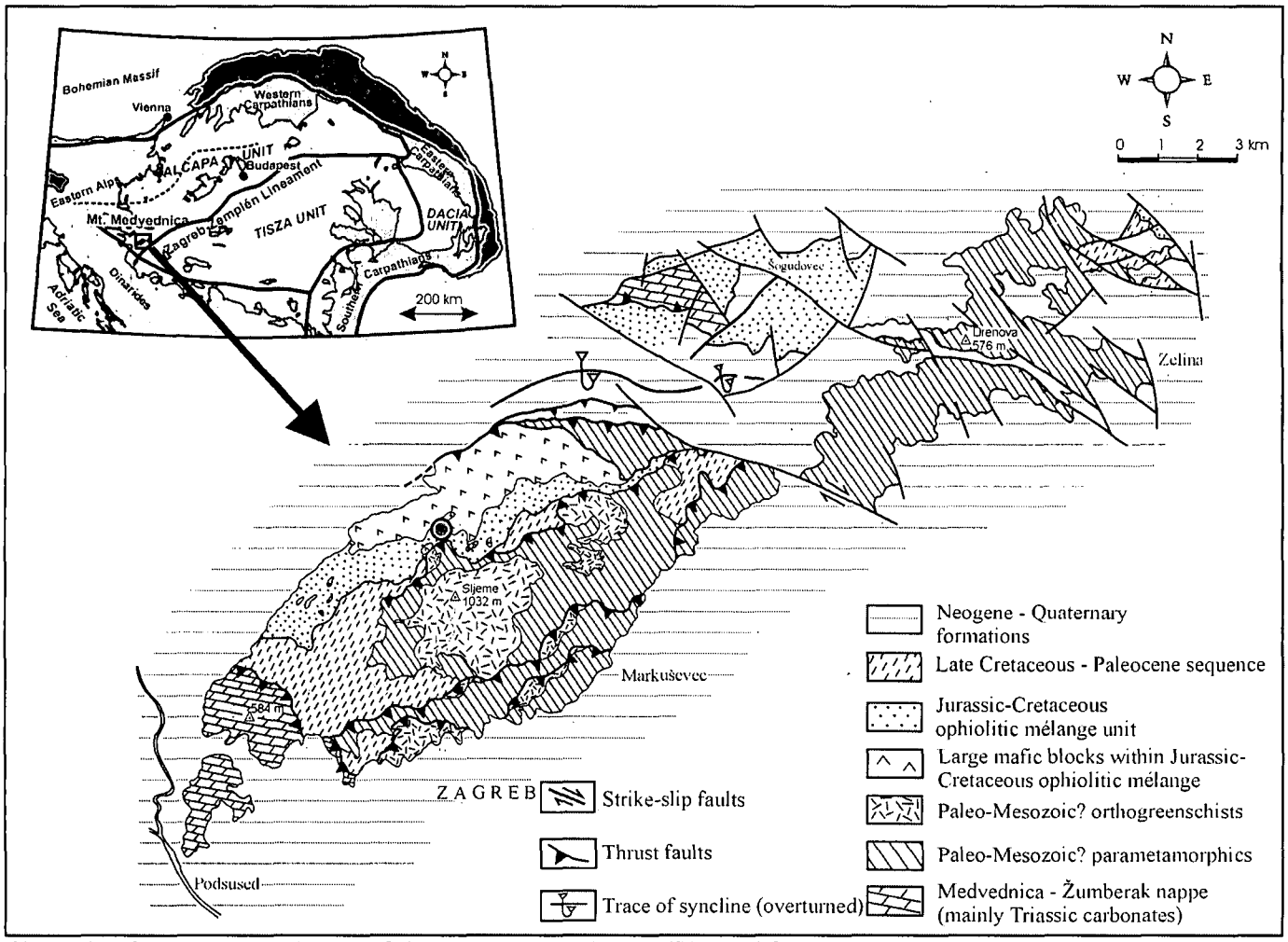

Fig. 1. (A) Geological sketch map of the Pannonian Basin and *(B)* simplified geological map of Mt. Medvednica modified after Šikić (1978), grey circle shows the sample locality.

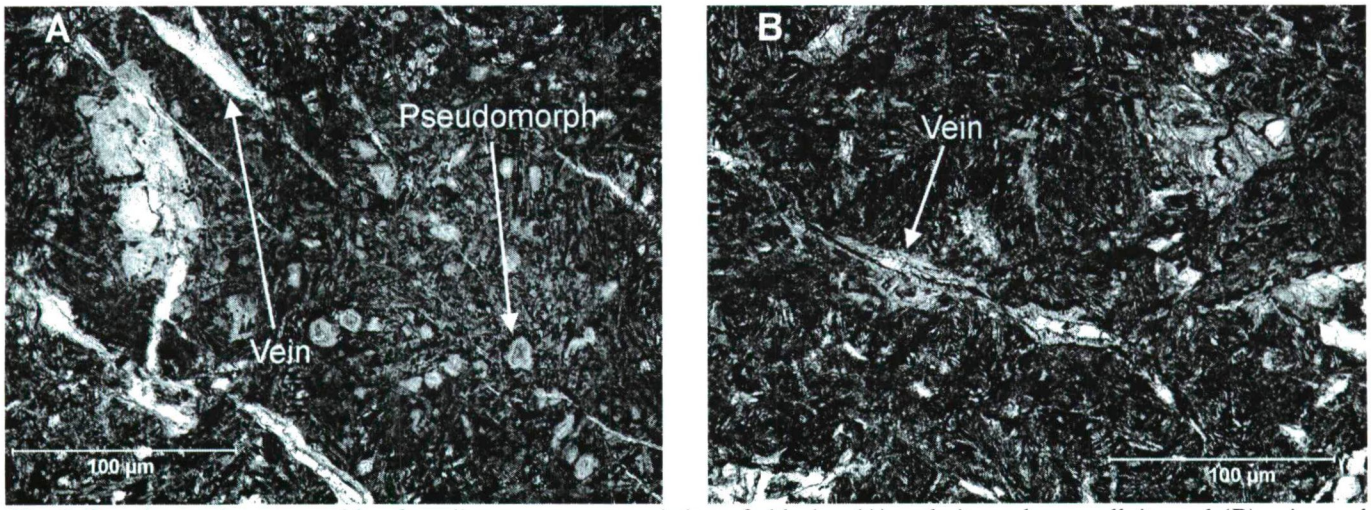

Fig. 2. Pseudomorphs presumably after clinopyroxenes consisting of chlorite, ***(A)*** prehnite and pumpellyite and ***(B)*** veins and aggregates containing dominantly chlorite and calcite in metabasalt sample PA 2/C.

Diffraction patterns were performed from non-oriented and highly oriented powder mounts of whole rock, <2 and <0.6 µm spherical equivalent diameter (SED) size fractions. The <2 and <0.6 µm grain-size fraction samples were obtained using the following procedure. Rock samples were disaggregated under standard conditions using a jaw crusher followed by crushing in a mortar mill (type Pulverisette 2, Fritsch) for 3 min. Final disaggregation was achieved by repeated shaking in deionized water. The <2 and <0.6 µm grain-size fractions were separated from aqueous suspension based on the differential settling of grains of different diameters. Following the technique of Kübler (1975), aqueous suspensions of the given fraction were pipetted onto glass slides and dried at room temperature to produce thin-layer, highly orientated preparates with a density of 3 mg/cm^2. Portions of air-dried <2 and <0.6 µm grain-size fraction were saturated with 1 mol/l $MgCl_2$, 1 mol/l KCl and LiCl solutions. Air-dried (AD), Mg-saturated and air-dried (Mg+AD), K-saturated and air-dried (K+AD) and Li-saturated and air-dried (Li+AD) mounts were obtained. Ethylene glycol (EG) and glycerol solvation (60 °C and 95 °C/ overnight) of AD mounts, as well as glycerol solvation of the Mg+AD samples, and heating of the Li+AD mounts at 250°C/16 h followed by glycerol solvation (Green-Kelly test) were carried out. AD samples were heat treated at 350 and 550 °C in order to complete the sample preparation procedure.

Electron microprobe analyses were carried out with a JEOL JXCA-733 instrument equipped with Oxford INCA 200 energy dispersive spectrometer (EDS) using periclase (Mg), corundum (Al), orthoclase (K), quartz (Si), albite (Na), hematite (Fe) and wollastonite (Ca) (C. M. Taylor Corporation) standards and PAP correction procedure (Pouchou and Pichoir, 1984). The measuring conditions were the followings: 15 keV acceleration voltage, 4 nA sample current 100 s measuring time and electron beam with a diameter of ca. 5-10 µm.

RESULTS

Petrographic microscopic features

Metagabbro fragments contain strongly chloritized clinopyroxene relics rimmed by actinolite needles, plagioclase grains completely altered into K-white mica, albite and quartz, as well as 3-4 mm thick veins containing prehnite and calcite. In the metabasalt samples chloritic pseudomorphs, presumably after clinopyroxene are the most abundant mafic constituents (Fig. 2A). Veins built up by chlorite, calcite, quartz and subordinate albite are recognized in these samples (Fig. 2B). Fibrous or rosette-like arrays of "chloritic materials" occur in veins and amygdules. In some metabasalts two separate domains can be distinguished; one is composed of mainly calcite, albite and "chloritic materials", whereas the other domain contains predominantly pseudomorphs presumably after clinopyroxenes, as well as albite and "chloritic materials".

XRPD characterizations

On the basis of the XRPD studies carried out on the <2 µm and < 0.6 µm grain-size fractions of metabasalt and metagabbro samples, chlorite and corrensite (regularly interstratified chlorite/smectite) are the predominant phyllosilicate phases. Additionally, randomly interstratified chlorite/smectite and discrete smectite can also be found. Corrensite was first identified by its 29 Å peak which shifted to 31 Å after ethylene glycol solvation. Mg-saturation and glycerol solvation confirm rather the smectitic nature of its swelling component than vermiculitic on the basis of the expansion of the 29 Å peak to 31-32 Å (Fig. 3). The appearance of the reflection at 18 Å after the same treatment proves the presence of a small amount of discrete smectite phase. Ethylene glycol solvation and Mg-saturation coupled with glycerol solvation suggest that irregularly interstratified chlorite/smectite is also present in the samples because of the slight broadening of the 14 Å peak and its shift towards the low angle values. After Li-saturation and heat treatment at 250 °C for 16 h (Green-Kelly test) of the <0.6 µm grain-size fractions, corrensite, irregularly interstratified chlorite/smectite and the minor smectite all keep their expansion capacity suggesting tetrahedral origin of the layer charge of their smectitic component (Fig. 4). Slight collapse of the 29 Å peak to 26 Å after K-saturation probably indicate the low layer charge of the expanding component(s). The 060 reflection at about 1.545 Å reveals the trioctahedral type of both the chlorite and smectite components.

EMP data

EMP analyses were carried out on "chloritic materials" situated in different textural positions and mineral parageneses in metabasalt sample PA 2/C. It was selected because of the highest amount of corrensite suggested by the XRPD measurements. On the basis of petrographic results "chloritic materials" from both the calcite-rich and the pseudomorph-rich domains were analyzed (Table 1).

Figure 5A shows that all the analyzed "chloritic materials" are classed as diabantite. All these "chloritic materials" contain Ca and/or Na, show large excess of Al(VI) relative to Al(IV) and have significant apparent octahedral vacancy (Figs. 5B, C and 6). These facts prove that analyses were in part contaminated by "inclusions" of materials other than ideal chlorite layers within the volume of interaction of the electron beam and sample (Árkai et al., 2000). Considering the electron beam diameter (5-10 μm) and the energy of the electron bombardment, the volume of the analyzed material may be ca. 100-800 μm^3.

As it is shown in Figures 5B and 6 the composition of the "chloritic mineral" suggests trioctahedral smectitic (saponitic) "contamination". Comparing to data obtained on "chloritic materials" from the matrix of the calcite-rich part (Fig. 7A) to data from the matrix of the pseudomorph-rich part (Fig. 7B) it is clear that "chloritic materials" from the carbonate enriched part contain more Si and Fe, and less Al(IV) and Mg, whereas they have the highest interlayer cation content. "Chloritic materials" from veins (Fig. 7C) have

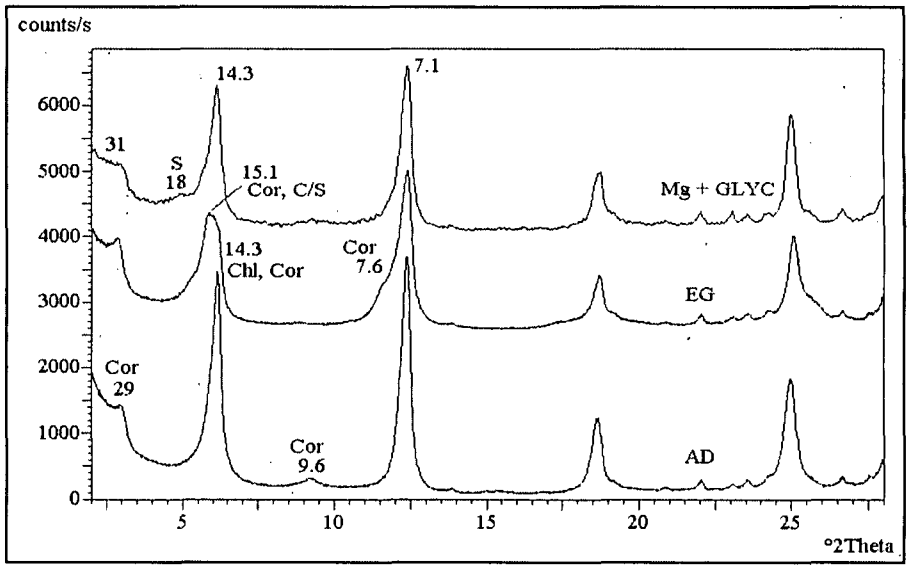

Fig. 3. X-ray powder diffraction patterns obtained on <2 μm grain size fraction of metabasalt sample PA 2/C. Air-dried (AD), ethylene glycol solvated (EG), Mg-saturated and glycerol solvated (Mg+GLYC) mounts. Abbreviation of mineral names are: Chl: chlorite, Cor: corrensite, C/S: irregularly interstratified chlorite/smectite, S: smectite. d values are in Ångstroms.

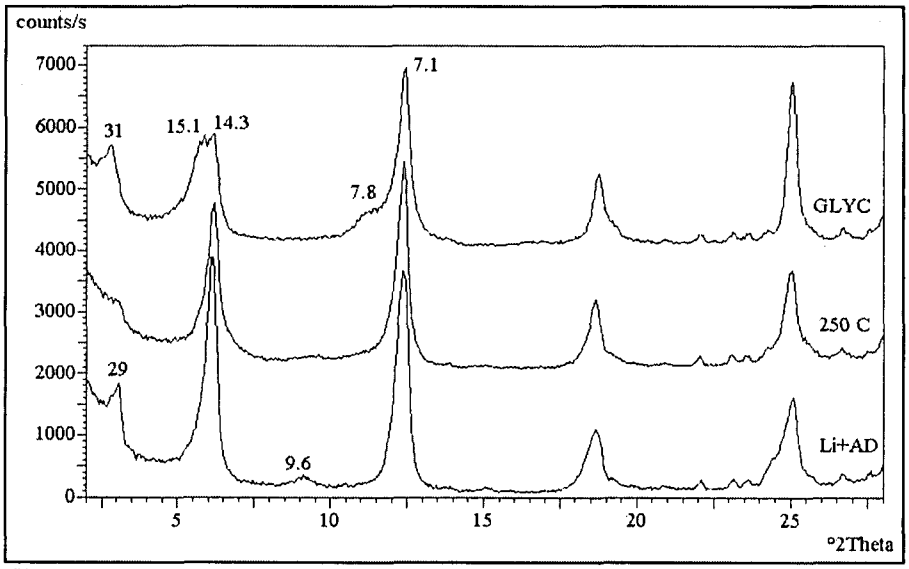

Fig. 4. X-ray powder diffraction patterns obtained on <0.6 μm size fraction of metabasalt sample PA 2/C. Li-saturated (Li+AD), Li-saturated and heated at 250 C (250 °C), and Li-saturated, heated and glycerol solvated (GLYC) sample mounts.

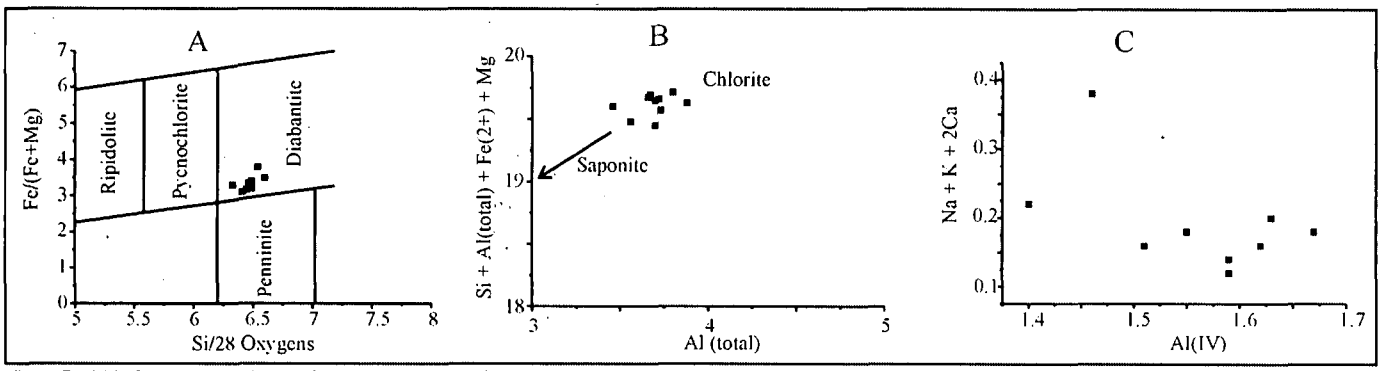

Fig. 5. (A) Fe/(Fe+Mg) vs. Si compositional variations of chlorites from metabasites modified after Hey (1954), *(B)* chlorites in metabasites as plotted after Schiffman and Fridleifsson (1991) and *(C)* relations between the Al(IV) content and the total interlayer charge expressed by Na+K+2Ca values (c). Cation numbers on the basis of 28 oxygens.

homogenous chemical composition, they contain more Al but their Fe content is lower than the matrix "chloritic materials" from the carbonate-rich part.

Discussion

According to XRPD studies of the <2 μm and < 0.6 μm grain-size fractions of the metabasalt and metagabbro samples the predominant phyllosilicate components are chlorite and corrensite (regularly interstratified chlorite/smectite) with minor amounts of irregulary interstratified chlorite/smectite and discrete smectite. On the basis of the EMP analyses chemical composition of all "chloritic materials" ("chlorites" in Table 1) from different textural positions reveals that they contain not only chlorite layers, but certain amounts of trioctahedral smectite (saponite) layers also occur causing relatively high Ca and/or Na contents, large excess of Al(VI) relative to Al(IV) and high octahedral vacancy.

Using the chlorite-Al(IV) geothermometer of Cathelineau (1988) the temperature of the formation of the "chloritic materials" analyzed by EMP ranges between ca. 160-200 °C. This range is in agreement with the data obtained by Kristmanndóttir (1975, 1979) and Evarts and Schiffman (1983) who claimed that the temperature of the disappearance of corrensite is ca. 230-250 °C in the Islandic geothermal fields and 225 °C in the Del Puerto Ophiolite, respectively. Cathelineau and Nieva (1985) and Cathelineau and Izquierdo (1988) suggest 220-260 °C for the disappearance of corrensite in the Los Azufres geothermal system.

Shau and Peacor (1992) give additional information to the formation conditions of corrensite. They claim that intense alteration of basalts with high fluid/rock ratio and high permeability is characterized by pervasive albitization and zeolitization. By contrast, minimal alteration in basalts with low permeability and low fluid/rock ratio results in sporadic albitization and zeolitization accompanied by the occurrence of saponite±mixed-layered chlorite/smectite in low-temperature alteration zone and mixed-layered chlorite/corrensite or mixed-layered talc/chlorite in the high-temperature alteration zone. According to the above mentioned observations metabasalt samples from the ophiolitic mélange could be affected by minimum alteration and the appearance of corrensite, together with irregulary interstratified chlorite/smectite and discrete smectite suggest "intermediate" temperature conditions.

Certainly, the weathering as a possible mechanism being responsible for the formation of corrensite cannot be

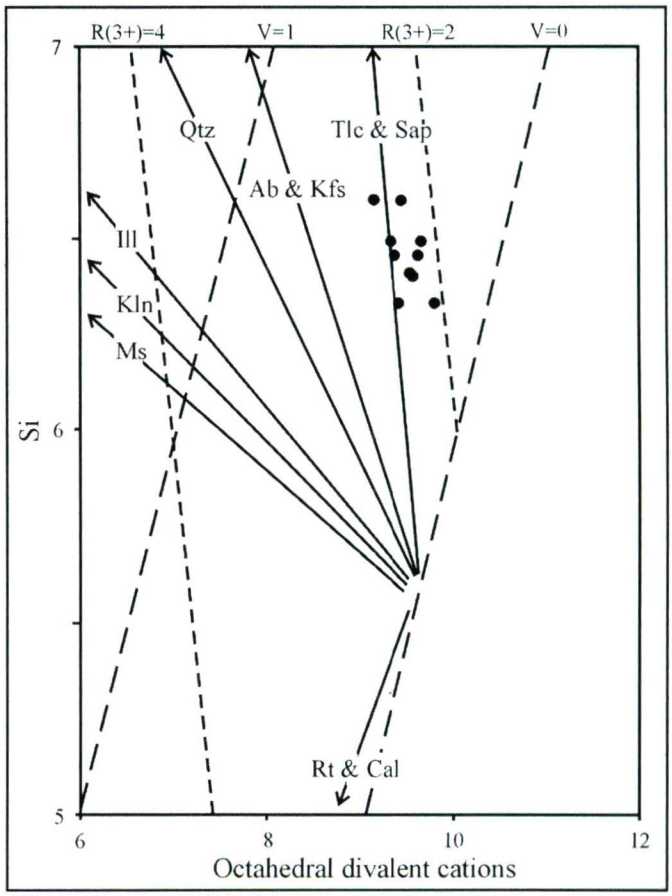

Fig. 6. Si *vs.* octahedral divalent cations plotted after Jiang et al. (1994). Arrows indicate schematic trends of compositional deviations generated from mixtures of an assumed composition of chlorite and other minerals. V: apparent octahedral divalent cations. Cation numbers on the basis of 28 oxygens.

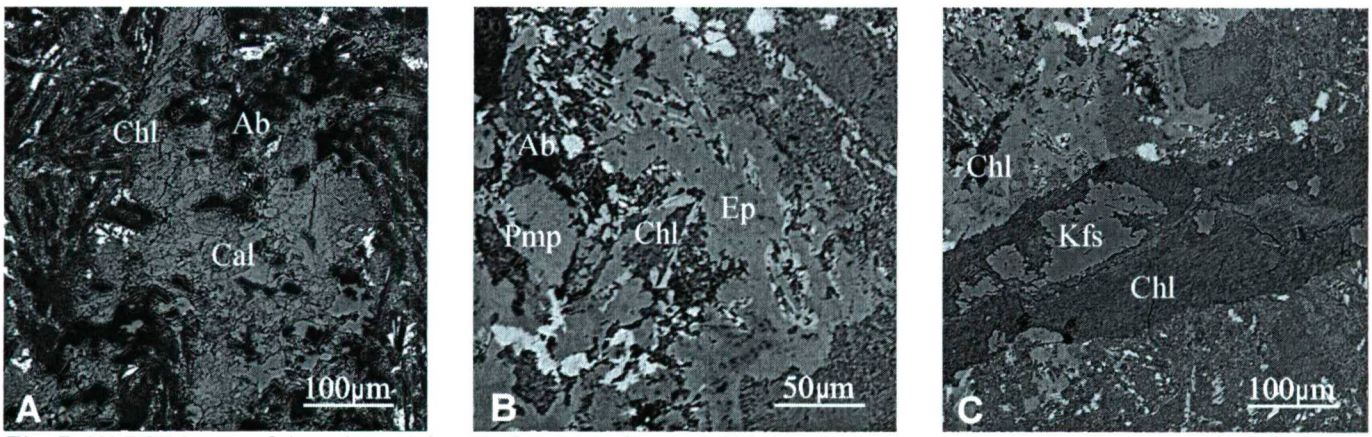

Fig. 7. (A) BSE image of the calcite-rich part of metabasalt sample PA 2/C containing mainly "chloritic materials" and albite, ***(B)*** pseudomorphs presumably after clinopyroxene and plagioclase containing "chloritic materials", pumpellyite, epidote and albite in the pseudomorph-rich part and ***(C)*** vein containing dominantly "chloritic materials" and K-feldspar, "chloritic materials", albite and prehnite in the matrix of the metabasalt.

Table 1. Chemical composition of "chloritic materials" ("chlorites") in metabasalt sample PA 2/C from the ophiolitic mélange of Mt. Medvednica (* all Fe is calculated as Fe^{2+}, T: total, Oct.: octahedral cations, Int.: interlayer cations, K_2O and MnO are below detection limit). All formulae are normalized to 28 oxygens.

	"chlorites" from the pseudomorphs-rich part								chlorites from matrix of the carbonate rich	
	chlorites from veins		"chlorites from the		"chlorites" from veins		"chlorites" fom the			
SiO_2	31,38	31,11	32,10	31,05	31,56	31,64	30,30	31,18	31,13	32,18
Al_2O_3	15,37	15,30	14,59	15,13	15,33	16,01	16,03	15,19	14,38	15,30
FeO	17,45	17,13	19,05	18,29	17,76	17,38	17,87	18,01	20,39	18,75
MgO	21,53	21,36	22,08	21,36	21,83	21,72	20,72	20,03	18,52	19,41
Na_2O	0,00	0,00	0,00	0,00	0,00	0,00	0,00	0,00	0,20	0,00
CaO	0,28	0,32	0,45	0,48	0,29	0,39	0,40	0,36	0,65	0,49
Total	86,01	85,22	88,27	86,31	86,77	87,14	85,82	84,78	85,27	86,13
Si	6,41	6,41	6,45	6,37	6,41	6,38	6,33	6,49	6,54	6,60
Al(IV)	1,59	1,59	1,55	1,63	1,59	1,62	1,67	1,51	1,46	1,40
Al(VI)	2,11	2,13	1,91	2,03	2,08	2,18	2,21	2,22	2,10	2,30
Al (T)	3,70	3,72	3,46	3,66	3,67	3,80	3,88	3,73	3,56	3,70
Fe^{2+}*	2,98	2,96	3,20	3,14	3,02	2,93	3,07	3,14	3,58	3,22
Mg	6,56	6,57	6,61	6,53	6,61	6,53	6,35	6,21	5,80	5,93
Oct.	11,65	11,66	11,72	11,70	11,71	11,64	11,63	11,57	11,48	11,45
Na	0,00	0,00	0,00	0,00	0,00	0,00	0,00	0,00	0,08	0,00
CA	0,06	0,07	0,09	0,10	0,06	0,08	0,09	0,08	0,15	0,11
Int.	0,06	0,07	0,09	0,10	0,06	0,08	0,09	0,08	0,23	0,11
Total	19,71	19,73	19,81	19,80	19,77	19,72	19,72	19,65	19,71	19,56

disregarded, but according to Proust (1982) and Proust et al. (1986) corrensite as an intermediate product of the weathering is characterized as chlorite/vermiculite thus the occurrence of chlorite/smectite in the studied samples may indicate that it is probably not the weathering that may be the main mechanism responsible for its formation. To assure the previous explanation further transmission electron microscopical studies are needed on the "chloritic materials".

Summarizing the above mentioned observations, the formation of the "chloritic materials" in metabasites of the ophiolitic mélange of Mt. Medvednica may be related to one or any combinations of the following mechanisms. One is considered to be the smectite to chlorite transition during diagenetic-incipient metamorphic conditions (a prograde process). Superficial weathering of the metabasites regarding their recent geological position can not be precluded. Progressive burial diagenesis and/or low-grade metamorphism followed by exhumation and superficial weathering being responsible for the formation of irregularly interstratified chlorite/smectite and discrete smectite seem to be an other plausible, although rather complicated alternative.

Conclusions

"Chloritic materials" in metabasalt and metagabbro samples from the ophiolitic mélange unit of Mt. Medvednica were studied by petrographic microscopy, XRPD and electron microprobe techniques. "Chloritic materials" are composed of chlorite, corrensite, first described in this paper from the site, irregularly interstratified chlorite/smectite and discrete smectite (saponite).

Using the empirical chlorite-Al(IV) geothermometer of Cathelineau (1988) the formation temperature of the "chloritic materials" is suggested to be in the range of ca. 160-200 °C.

According to Shau and Peacor (1992) metabasalts from the ophiolitic mélange could be affected by minimum alteration, and the appearance of corrensite, together with irregulary interstratified chlorite/smectite and discrete smectite suggest "intermediate" temperature conditions.

According to Proust (1982) and Proust et al. (1986) corrensite as chlorite/vermiculite can form as an intermediate product of the weathering but the occurrence of chlorite/smectite in the studied samples may indicate that it is not the weathering that may be the main mechanism responsible for its formation.

Acknowledgements

This paper presents preliminary results of the scientific co-operation project titled "Comparative metamorphic petrogenetic study of the complexes in the southern part of the Tisia Unit, as well as the Internal Dinarides and the Bükk Unit and their relative position during metamorphism" leaded by Acad. Prof. Jakob Pamić (Zagreb) and Péter Árkai within the frame of bilateral agreement held between the Croatian Academy of Sciences and Arts and Hungarian Academy of Sciences. The authors are grateful to Mr. P. Sipos (Laboratory for Geochemical Research, Hungarian Academy of Sciences) for providing bulk chemical data. Thanks are due to Mrs. M. Tóth, M. Sándor, O. Komoróczy, P., Ms. K. Temesvári, N. Szász, R. Winkler and N. Keresztes (Laboratory for Geochemical Research, Hungarian Academy of Sciences) for their technical assistance. Thorough reviews of K. Török and anonymous referee are gratefully acknowledged. The authors are indebted to the Hungarian National Research Fund (OTKA, Budapest), project No. T-050350/2001-2004 to P. Á. and to the Croatian Ministry of Science and Technology, project No. 0119412 for financial support.

REFERENCES

ÁRKAI, P., MATA, M. P., GIORGETTI, G., PEACOR, D. R., TÓTH, M. (2000): Comparison of diagenetic and low-grade metamorphic evolution of chlorite in associated metapelites and metabasites: an integrated TEM and XRD study. Journal of Metamorphic Geology, **18**, 531-550.

BETTISON-VARGA, L. A., MACKINNON, D. R., SCHIFFMAN, P. (1991): Integrated TEM, XRD and electron microprobe investigations of mixed-layered chlorite/smectite from the Point Sal ophiolite, California. Journal of Metamorphic Geology, **9**, 697-710.

CATHELINEAU, M. (1988): Cation site occupancy in chlorites and illites as a function of temperature. Clay Minerals, **23**, 471-485.

CATHELINEAU, M., IZQUIERDO, G. (1988): Temperature-composition relationships of authigenic micaceous minerals in the Los Azufres geothermal system. Contributions to Mineralogy and Petrology, **100**, 418-428.

CATHELINEAU, M., NIEVA, D. (1985): A chlorite solid solution geothermometer. The Los Azufres (Mexico) geothermal system. Contributions to Mineralogy and Petrology, **91**, 235-244.

ESSENE, E. J., PEACOR, D. R. (1995): Clay mineral thermometry – a critical perspective. Clays and Clay Minerals, **43**, 540-553.

EVARTS, R. C., SCHIFFMAN, P. (1983): Submarine hydrothermal metamorphism of the Del Puerto ophiolite, California. American Journal of Science, **283**, 289-340.

HALAMIĆ, J., GORIČAN, Š. (1995): Triassic Radiolarites from Mts. Kalnik and Medvednica (NW Croatia). Geologica Croatica, **48/2**, 129-146.

HALAMIĆ, J., GORIČAN, Š., SLOVENEC, D., KOLAR-JURKOVŠEK, T. (2000): A Middle Jurassic Radiolarite-Clastic Succession from the Medvednica Mt. (NW Croatia). Geologica Croatica, **52/1**, 29-57.

HEY, M. H. (1954): A new review of the chlorites. Mineralogical Magazine, **30**, 272-292.

JIANG, W. T., PEACOR, D. R., BUSECK, P. R. (1994): Chlorite geothermometry? – contamination and apparent octahedral vacancies. Clays and Clay Minerals, **42**, 593-605.

JOHNSON L. J. (1964): Occurrence of regularly interstratified chlorite-vermiculite as a weathering product of chlorite in a soil. American Mineralogist, **49**, 556-572.

KRISTMANNSDÓTTIR, H. (1975): Clay minerals formed by hydrothermal alteration of basaltic rocks in Icelandic geothermal fields. Journal of Metamorphic Geology, Geol. Foren Stockholm Forhand **97**, 289-292.

KRISTMANNSDÓTTIR, H. (1979): Alteration of basaltic rocks by hydrothermal activities at 100-130 °C. In Mortland, M. M., Farmer, V. C. (eds): International Clay Conference 1978, 359-367. Elsevier, Amsterdam.

KÜBLER, B. (1975): Diagenese-anchimétamorphisme et métamorphisme. Institut national de la recherche scientifique-Pétrole, Quebec.

LIOU, J. G., SEKI, Y., GUILEMETTE, R. N., SAKAI, H. (1985): Composition and parageneses of secondary minerals in the Onikobe geothermal system, Japan. Chemical Geology, **49**, 1-20.

LIPPMAN, F. (1954): Über einen Keuperton von Keiserweiher bei Maulbron. Heidelberg Beitr. Mineral. Petrol. **4**. 30-144.

MERRIMAN, R. J., PEACOR, D. R. (1999): Very low-grade metapelites: mineralogy, microfabrics and measuring reaction progress. In Frey, M., Robinson, D. (eds): Low-Grade Metamorphism, 10-60. Blackwell Science, Oxford.

PAMIĆ, J., (1997a): The development of the Croatian geoscience as reflected by the study of Dinaric Ophiolites. Geologica Croatica, **50/2**, 173-180.

PAMIĆ, J., (1997b): Volcanic rocks from the Sava-Drava interfluve and Baranja in the south Pannonian Basin (Croatia). Nafta, Zagreb.

PAMIĆ, J., TOMLJENOVIĆ, B. (1998): Basic geologic data from the Croatian part of the Zagorje-Mid-Transdanubian Zone. Acta Geologica Hungarica, **41/4**, 389-400.

PEACOR, D. R. (1992): Diagenesis and low grade metamorphism of shales and slates. In Buseck, P. R. (ed): Minerals and Reactions at the atomic scale: Transmission Electron Microscopy Reviews in Mineralogy 27, 335-380. Mineralogical Society of America, Washington D C.

POUCHOU, J. L., PICHOIR, F. (1984): A new model for quantitative X-ray microanalyses, Part I. Application to to the analyses of homogenuous samples. La Recherche Aérospatiale, **3**, 13-38.

PROUST, D. (1982): Supergene alteration of metamorphic chlorite in an amphibolite from Massif Central, France. Clay Minerals, **17**, 159-173.

PROUST, D., EYMERY, J. P., BEAUFORT, D. (1986): Supergene vermiculitization of a magnesian chlorite: iron and magnesium removal process. Clays and Clay Minerals, **34**, 572-580.

REYNOLDS, R. C. (1988): Mixed-layer chlorite minerals. Mineralogical Society of America. In Bailey, S. W. (ed): Hydrous phyllosilicates (Exclusive of Micas) Reviews in Mineralogy 19, 601-629. Mineralogical Society of America, Washington DC.

REYNOLDS, R. C., MOORE D. M. (1997): X-ray Diffraction and the Identification and Analysis of Clay Minerals, Oxford University Press, 378 pp.

ROBINSON, D., BEVIS, R. E., ROWBOTHAM, G. (1993): The characterization of mafic phyllosilicates in low grade metabasalts from eastern North Greenland. American Mineralogist, **78**, 377-390.

ROBINSON, D., SCHMIDT, S. TH, SANTANA DE ZAMBORA, A. (2002): Reaction pathways and reaction progress for the smectite-to-chlorite transformation: evidence from hyrothermally altered metabasites, Journal of Metamorphic Geology, **20**, 167-174.

SCHIFFMAN, P., FRIEDLEIFSSON, G. O. (1991): The smectite to chlorite transition in drillhole NJ-15, Nesjavellir Geothermal Field, Iceland: XRD, BSE and electron microprobe investigations, Journal of Metamorphic Geology, **9**, 679-696.

SCHIFFMAN, P., STAUDIGEL, H. (1995): The smectite to chlorite transition in a fossil seamount hydrothermal system: the basement complex of La Palma, Canary Islands. Journal of Metamorphic Geology, **13**, 487-498.

SCHMIDT, S., ROBINSON, D. (1997): Metamorphic grade and porosity/permeability controls on mafic phyllosilicate distributions in a regional zeolite to greenschist facies transition of the North shore Volcanic Group, Minnesota. Geological Society of America Bulletin, **109**, 638-397.

SHAU, Y. H., PEACOR, D. R. (1992): Phyllosilicates in hydrothermally altered basalts from DSDP Hole 4504 B, Leg 83 – a TEM and AEM study. Contributions to Mineralogy and Petrology, **112/1**, 119-133.

SHAU, Y. H., PEACOR, D. R., ESSENE, E. J. (1990): Corrensite and mixed-layer chlorite/corrensite in metabasalt from northern Taiwan: TEM/AEM, EMPA, XRD and optical studies. Contributions to Mineralogy and Petrology, **105/2**, 123-142.

ŠIKIĆ, K., BASCH, O., ŠIMUNIĆ, A. (1978): Basic geological map 1:100.000, sheet Zagreb. Fed. Geological Institution, Belgrad.

TRIBBLE, J. S. (1991): Clay mineral and zeolite diagenesis in the Toa-Baja well, Puerto Rico. Geophysical Research Letters, **18**, 529-532.

Received: February 9, 2003; accepted: June 16, 2003

Acta Mineralogica-Petrographica, Szeged 2003, Vol. 44, pp. 9-17

ACTA Mineralogica Petrographica

SUCCESSIVE, ISOTHERMAL HYDROCARBON MIGRATION EVENTS RECORDED BY FLUID INCLUSIONS IN FRACTURE-FILLING QUARTZ OF THE SZEGHALOM DOME (SE HUNGARY)

FÉLIX SCHUBERT, TIVADAR M. TÓTH

Department of Mineralogy, Geochemistry and Petrology, University of Szeged
H-6701 Szeged, P. O. Box 651, Hungary
e-mail: schubert@geo.u-szeged.hu

ABSTRACT

The largest sub-basin in the south-eastern part of the Pannonian Basin is the Békés Basin (BB). The BB is surrounded by metamorphic and magmatic basement highs, which produce considerable amount of petroleum due to their high fracture porosity. One of the most intensively explored basement highs is located on the northern margin of the BB, called Szeghalom Dome (SzD). Former studies revealed remnants of an ancient hydrocarbon migration event preserved as fluid inclusions in the fracture-filling, idiomorphic quartz crystals of the SzD. This quartz phase occurs in 6 wells in the central part of the dome.

The several growth zones suggest that the quartz phase is the product of a successive cementation process. Two markedly different petroleum inclusion types could be distinguished along the growth zones characterised by different colours, vol. % of the gas phase and fluorescence emission. Simultaneously with the HC inclusions also aqueous inclusions occur in lower quantity and rather unequal spatial distribution.

The appearance of the different petroleum inclusions shows a well-defined temporal and spatial distribution during the HC-bearing fluid migration in the SzD. Based on co-genetic aqueous inclusions the quartz cementation preceded at isothermal conditions and decreasing salinity, while the HC-bearing fluid turned into a lower density (higher maturity?) type.

Key words: Pannonian Basin, metamorphic basement, fracture-filling minerals, fluid inclusion, microthermometry, petroleum migration.

INTRODUCTION

In the Pannonian Basin system (PB) hydrocarbon reservoirs exist not only in the basin-filling Neogene sediments, but also in its fractured metamorphic basement. The high fracture porosity of these rocks is the result of a multistage tectonic (in several parts brittle) evolution from the Pre-Variscan events up to present, which movements also produced a basement surface of remarkable orography. At present, the deepest sub-basins are as deep as 8000 metres below the present surface, while the mostly elevated highs are covered only with around 2000 metres of young (essentially Mio-Pliocene) clastic sediments. Thanks to all these structural and topographical reasons, a significant part of the crystalline mass can play an active role in the current hydrological system of the PB (Teleki et al., 1994). Incompatible chemical compositions of the oils (and water) produced form neighbouring wells, on the other hand suggest, that there also co-exist independent fluid regimes in the basement, which are not in hydrological contact (Pap et al., 1992).

There are several basement reservoirs throughout the PB, which even at present supply a significant amount of oil and gas. The largest one among them is called Szeghalom Dome (SzD), which is situated on the northern rim of the deepest sub-basin (Békés Basin).

Based on a detailed evaluation of organic geochemical data, the age of the currently explored hydrocarbons is thought to be of Middle-Upper Miocene age (Teleki et al., 1994) suggesting percolation into the basement coeval to the main subsidence phase of the basin. Juhász et al. (2002) report HC-bearing fluid inclusions in fracture-filling quartz crystals from several basement cores. Including chemical and fluid inclusion data of the other vein forming minerals as well, they link this quartz phase to the exhumation stage of the basement high. Such a model suggests that the enclosed hydrocarbon migrated to the basement fractures prior to the sedimentation of the source rocks of the present-day oils, consequently it should be older and different from those produced currently.

The aim of this study is to determine the distribution of the fracture-filling, HC-bearing quartz phase in the SzD, to classify the temporal and spatial differences of the HC-bearing parent fluid, as well as to characterize the relationship between the petroleum migration and the quartz cementation. By means of the co-genetic aqueous inclusions we also aim to determine the variation of composition and the temperature of the brines co-genetic with the successive quartz precipitation events.

GEOLOGICAL SETTING

The Pannonian Basin (PB) system is a result of a rather complex, structural evolution from the Pre-Variscan events up to present. Currently, its Paleozoic-Mesozoic basement can be considered as an amalgamated mosaic of incompatible crystalline blocks, sedimentary nappes and sliders. Morphologically, PB consists of deep (down to -7000 m below surface) sub-basins and relatively uplifted basement highs (ca. -2000 m) among them. The deepest and largest sub-basin in the PB is the Békés Basin (BB), which is surrounded by basement highs from all directions.

During the Neogene, the BB developed due to a multistage subsidence history. According to current models (Teleki et al., 1994), the basin evolution of the BB can be divided into three main steps; the pre-rift, syn-rift and the post-rift episodes. Paleozoic and Mezozoic sediments represent the pre-rift formations, which are covered by Middle Miocene to Holocene sediments above a sharp erosional discordance surface. The syn-rift phase of the basin evolution started during the early Miocene and can be characterised by the uplift and exhumation of the basement highs as well as the subsidence of the sub-basins. The post-rift episode started with the coeval subsidence of both the basins and the previously elevated high regions. As a result, at present, pre-Neogene formations can exclusively be followed below the flat surface (2-7 kms) throughout the basin.

The subject of the present study is the Szeghalom Dome (SzD), which forms the boundary of BB in the north representing one of the most intensively explored basement highs all over the PB (Fig. 1A-C). The pre-Neogene basement of the SzD is composed mainly of medium and high-grade polymetamorphic rocks essentially representing the Variscan orogeny (M. Tóth et al., 2000). The most elevated central part of the high is covered by 1800 m thick Miocene-Holocene sediments at present.

Due to the Neogene movements, crystalline basement formed a horst/graben structure (Royden and Horváth, 1988; Tari et al., 1999), the basement rocks deformed ruptually developing a dense fracture system. A detailed investigation of the microtectonic features on borecores of the SzD revealed a steeply-dipping (70-80°), conjugate system of normal faults and a set of sub-horizontal fractures (Szűcs, 2001). In some cases the members of the conjugate system are crosscut by the sub-horizontal fractures and are dragged away along them. The frequency and the aperture of the steeply dipping set are much higher than those of the low-angle one.

According to mineral chemical and fluid inclusion data (Juhász et al., 2002), exhumation is characterised by a general pyrite - illite - calcite1 - quartz - calcite2 - laumontite fracture-filling sequence in the steeply-dipping fractures. The sub-horizontal fractures are filled by laumontite, only (Szűcs, 2001). The early phases up to calcite1 form a very thin (< 1 mm) coating on the fracture walls. From the subsequent, free- standing quartz crystals Juhász et al. (2002) report presence of the hydrocarbon inclusions, which are focused in the present study.

During the exhumation, at the highest structural position of the SzD a pervasive calcite phase (calcite2) precipitated in the fractures. This phase contains pure liquid primary brine inclusions with Thom values as low as 50 °C. Its light $\delta^{13}C$ and $\delta^{18}O$ stable isotopic compositions suggest that the calcite precipitated from meteoric water typical of the Lower Pannonian time and not from former sea-water (Juhász et al., 2002). Calcite crystals also enclose terrestrial pollens not

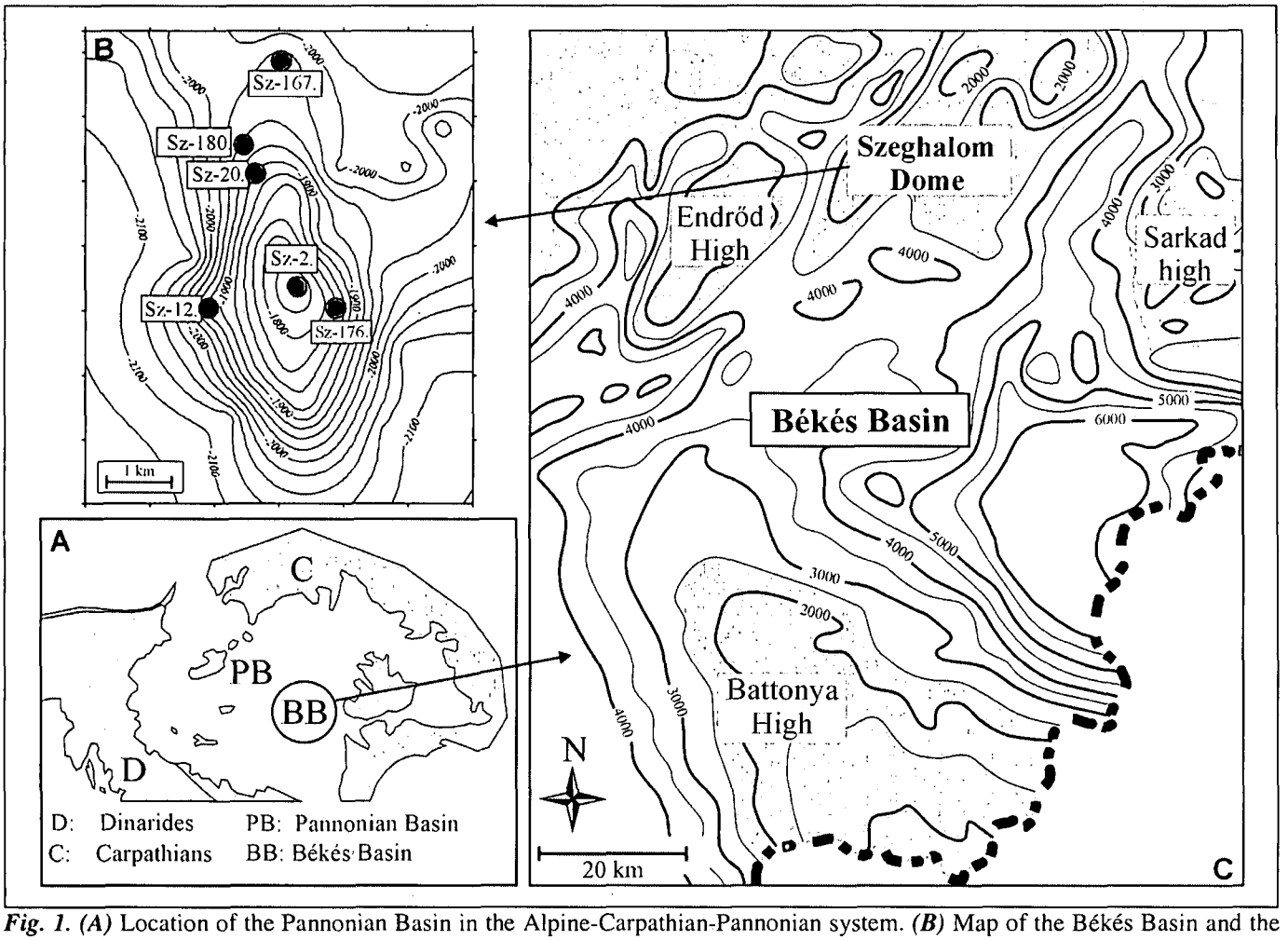

Fig. 1. (A) Location of the Pannonian Basin in the Alpine-Carpathian-Pannonian system. *(B)* Map of the Békés Basin and the surrounding basement highs. *(C)* The location of the wells on the Szeghalom Dome, which contain HC-bearing quartz crystals.

older than the Oligocene *(Chanepodiaceae, Ericaceae)* as well as other terrestrial plant fragments (M. Tóth et al., 2003) fixing the age of the fracture-filling mineralization to the Neogene.

The steep fractures stayed usually open even after the quartz precipitation but they were partially filled in due to the calcite2 phase.

ANALYTICAL METHODS

The walls of the fractures were investigated by hand-lens and by binocular microscope. A number of over 500 specimens were checked for open and filled fractures; grown-up quartz crystals were, however, found only in 6 wells. Fluid inclusions were observed on double polished single quartz crystals, using a modified spindle stage (Anderson and Bodnar, 1993) with immersion oil (n=4.17). During the use of UV-light, the immersion oil was omitted to avoid a disturbing emission.

Fluid inclusion measurements were carried out using a Linkam MDS-600 and a THMS-600 heating-freezing stage connected to an Olympus BX-60 microscope using objectives with a 40x and 100x magnification at the Montanuniversität in Leoben (Austria) and at the University of Szeged (Hungary). The instruments were calibrated using synthetic fluid inclusions of the *FLUID Inc.* at –56.6 (TmCO2), 0.0 (TmH2O) and 374 °C (ThH2O). Prior to microthermometry, fluid inclusions were checked for any presence of petroleum, under UV-light. The petroleum-bearing aqueous inclusions were ruled out of this measurement. The salinity calculations were performed by the computer software Aqso2e developed by Bakker (2003) using the equation of Naden (1996).

The Raman spectra of the inclusions were detected by a LABRAM HR-800 microprobe at the Montanuniversität in Leoben (Austria) using 532.2 and 632.8 nm incident radiations. The spectral resolution of the vibration is 4 cm^{-1}; the maximal size of the analysed circular area is about 3 μm. The recording time generally was 150 s, the reference spectra were recorded on artificial silicon. The Raman spectra were evaluated using different literature data (Pironon et al., 1995; Orange et al., 1996)

SAMPLES

Open and healed fractures that contain fracture-filling quartz crystals were looked for in the cores of all 87 wells of the SzD. In agreement with the previous results (Szűcs, 2001), a mutual vertical/sub-vertical fracture network characterizes the cores. The shape and the dip of the fractures are highly variable depending on the host rock fabric, in which they formed. The average aperture of the steep fractures varies around 0.5-1 cm, but they locally form 3-5 cm deep vugs, as well. The wall of the fractures, especially, in the vugs is rough and is covered by different mineral phases.

Up-grown quartz crystals were found in six wells in the SzD (Sz-2, 12, 20, 167, 176, 180) (Fig. 1B). The crystals are faceted (prism: 10-10, trapezoid: 10-11) with a size of up to 10 millimetres; they are free from apparent imperfections. At some places the crystals show a well-developed bipyramidal habit. The crystals are colourless and translucent; except the samples of the Sz-167 wells, where the inner parts of the crystals have a light brown colour. The extinction of the quartz crystals is homogenous, there could not be any subgrains or other microstructural features observed. The quartz phase of each of the six wells contains significant amount of petroleum inclusions, while HC-free quartz phase has not been found so far. Quartz crystals do not come out along the subsequent, sub-horizontal fractures.

FLUID INCLUSION PETROGRAPHY

The quantity and the distribution of the fluid inclusions (FIs) in the fracture-filling quartz phase are rather different from one crystal to another. The FIs contain either a brine- or a hydrocarbon-dominated fluid fill. Because the colour of the HC liquid phase in the FIs varies from dark brown to a completely colourless type, UV excitation was applied to distinguish them from the brine, and also to classify the single HC fluid inclusion assemblages (FIAs).

Size distribution and the amount of the FIs representing the two main fluid types (i.e. the brine- and hydrocarbon-dominated, respectively) show similar characteristic features in all of the six wells. Namely, the brine inclusions are several orders of magnitude smaller and less frequent than the other ones.

Based on the petrographic properties (colour, vol. % of the gas phase, fluorescence colour, etc.) three main FI types (and additional subtypes) can be distinguished in the quartz crystals:

Type IA: Two-phase inclusions showing a V+L→ V type homogenisation. The vol. % of the gas phase is 0.8-0.9 (all vol. % values were measured on microphotographs). Both phases are colourless, during the UV excitation a weak, bluish fluorescent colour of the liquid phase can be observed. The inclusions might be as large as 1 mm in size. The shape of the inclusions is usually tabular, hand-like or rounded; they often form a tooth rack-like habit.

Type IB: The trapped fluid of this subtype is similar to that of Type IA but the homogenisation occurs as a L+V → L transition. The size of these inclusions never exceeds the size of Type IA inclusions; they usually are several orders of magnitude smaller.

The above subtypes sometimes occur within small, isolated inclusion clusters, whose members show highly variable liquid-vapour ratios.

When cooling, in some cases, a solid phase as black-coloured spots appears on the surface of the bubbles of the Type IA inclusions. During subsequent heating, this solid phase disappears between 20 and 22 °C. The occurrence adjacent to the (methane) bubble and the homogenisation temperature above 0 °C suggest that this solid phase is probably a gas-clathrate.

Type II: Type II inclusions can be characterised by a dark or pale brown liquid, a colourless vapour phase and solid phases of highly variable quantity (L+V±S). The liquid phase fluoresces very intensively with greenish blue colour under UV light. The vol. % of the gas phase varies between 0.2 and 0.3. These inclusions often show negative crystal shape. The size of Type II petroleum inclusions (PIs) does not exceed 80 μm.

In Type II PIs two solid phases (Sp and Sb) could be distinguished at room temperature, or during the cooling process (Fig. 2). At room temperature the Sp phase forms groups in the liquid phase, the particles show a dendrite-, needle-like or amorphous, translucent habit. The crystals show birefrigent behaviour under crossed polarizers. During the cooling process the quantity of the solid phase increases, while below 0 °C it fills up the inclusions cavity, completely. The colourless, dendritic habit of the Sp phase prevents the estimation of its exact volumetric proportion.. Within the same FIA in some cases a yellowish brown, amorphous mass (Sb) occupies almost the whole inclusion cavity, while in other PIs it forms small (3-6 μm) particles, only. The extremely different quantity of the Sb phase relative to the liquid or vapour phases suggests an accidental origin.

Type III: The liquid phase of these FIs consists of brine, while the composition of the vapour phase is in most cases unknown. The inclusions of Type III usually form isolated clusters with a maximal inclusion size of 15 μm. These aqueous inclusions are rather rare and they are distributed unevenly among and inside the growth zones. Type III inclusions occur together with Type I-II PIs in several growth zones.

Type I-II PIs occur either separated or in small groups. These groups define weakly developed planes, which usually terminate within the crystals. The small (< 10 μm) FIs often form curved planes, which at places seemingly crosscut each other. Varying the position of the focal plane of the microscope, these FIs-defined planes show a chaotic, often crosscutting texture. The clusters of Type III FIs always occur within or along planes defined by the PIs.

In crystals, which contain only a few inclusions, the planar arrangement of the FIs can be noticed by changing the point of view, only. Detailed petrographic observations using a modified spindle-stage (Anderson and Bodnar, 1993) show evidence for multistage quartz precipitation in each studied wells. The crystals can be characterised by several parallel growth zones with primary FIs trapped along them. The angles between the planes defined by the FIs give about 60°, the value corresponds to the angle between the faces of a hexagonal prism. The FIs are often flat, parallel to each other and to certain faces of the enclosing crystal (Fig. 3).

The frequent occurrence of the sceptre-shaped quartz crystals is a macroscopic evidence of this multistage precipitation.

RAMAN MICROSPECTROSCOPY

Although the spectra of Type IB inclusions were often masked by the (weak) fluorescence of the liquid phase as well, the composition of the IA subtype could be determined by this method, qualitatively. The major part of the vapour phase consists of methane with a subordinate quantity of ethane (Fig. 4). The characteristic peaks of the liquid phase are located on a hump between 2800 and 2950 cm^{-1}. The most intensive peak can be found at 2909 cm^{-1} referring to the presence of the methane dissolved in the liquid phase (Orange et al., 1996). Although they all occur systematically, the positions of the peaks at 2875, 2942 and 2963 cm^{-1} vary slightly in the different samples suggesting the contribution of diverse alkanes and/or cyloalkanes to the liquid phase. The

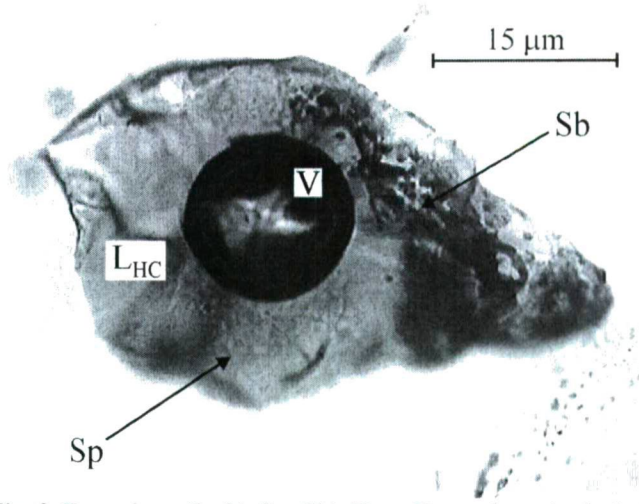

Fig. 2. Four phase (L+V+Sp+Sb), Type II petroleum inclusion from the Sz-167 well.

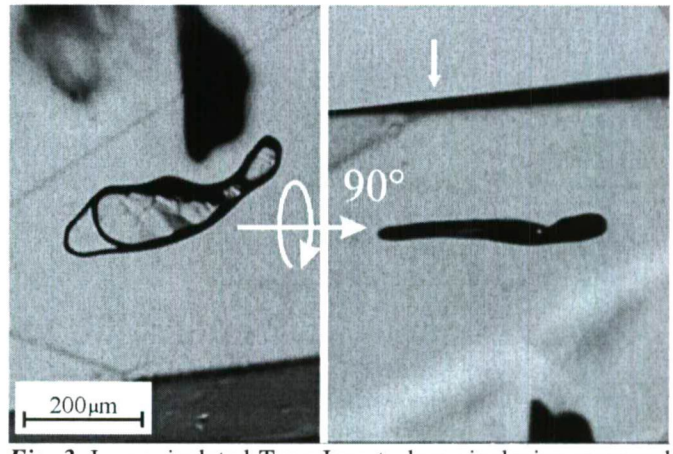

Fig. 3. Large, isolated Type Ia petroleum inclusion arranged parallel to the certain faces of the enclosing crystal (Sz-180 well).

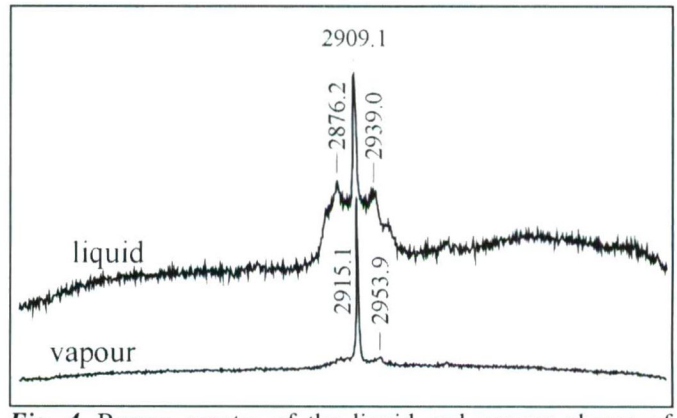

Fig. 4. Raman spectra of the liquid and vapour phases of Type Ia fluid inclusion.

weak fluorescence and the colourless habit of the Type I fluid inhibit the optical observation of the co-existing water phase probably present in the hydrocarbon inclusions.

The strong fluorescence inhibited the investigation of Type II inclusions by Raman spectroscopy.

Because of the small size and the arrangement of the aqueous inclusions (Type III), its semi-quantitative composition was specified only in two cases. In these cases

on the spectrum of the aqueous L phase the peak at 2909 cm^{-1} suggests the symmetric stretching band of dissolved methane (Dubessy et al., 2001). The determination of the composition of the vapour phase has been failed.

The distribution of Type I and II hydrocarbon inclusions shows a well-defined sequence in the studied wells and in the successive growth zones. Based on the results of petrography (performed under normal and UV light) and the micro-Raman spectroscopy, all of the petroleum inclusions occurring in quartz crystals of the Sz-20 and 180 wells belong to the Type I group, while the samples from the Sz167 well contain Type II PIs, exclusively. The precipitation of the quartz phase in the Sz-2, 12 and 176 wells took place in the presence of a more complex, changing fluid regime. The inner zones of the quartz crystals represent the above three wells contain Type II FIs, exclusively, while following a "sudden" change, in the outer (younger) growth zones Type I inclusions became dominant (Fig. 5). Both Type I and Type II FIs occur simultaneously within the same growth zone in one case, in the Sz-2 well.

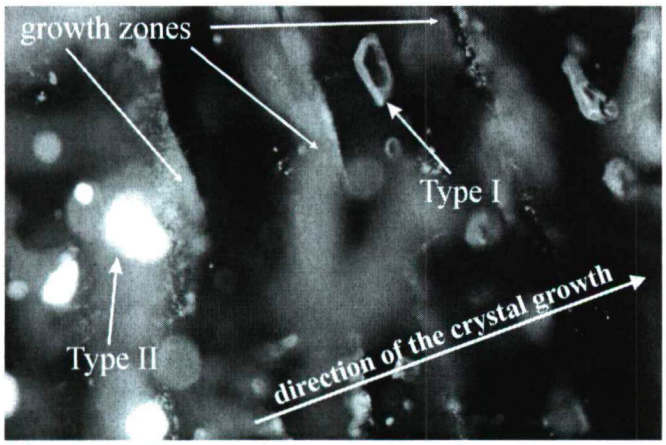

Fig. 5. Parallel growth zones with Type II petroleum inclusions occurring in the inner, and Type I PIs in the outer zones (Sz-173 well). The width of the picture is 1 mm.

MICROTHERMOMETRY

Aqueous FIAs suitable for microthermometry were found in three wells; Sz-2 (in two well sections: ÁGK-1131 (1900-1902.5 m) and 1134 (1990-1990.2 m), respectively), Sz-167 (2074 m) and Sz-180 (in well section: ÁGK-4644 (2011 m)). Because of the small size and the poor optical resolution, the homogenisation temperature in most cases was measured using the cycling method described by Goldstein and Reynolds (1994). We attempted to determine the final ice melting temperature in the presence of the vapour phase; in cases it was impossible, the temperature data are marked on the histograms.

Two aqueous FIAs of the Sz-2 well may be distinguished: in the well section AGK-1131 it is co-genetic with Type II PIs, while in the well section ÁGK-1134 it is co-genetic with Type I PIs. The measured Thom and TmICE values are shown in Fig. 6.

We were able to determine the homogenisation temperatures of Type IA and IB petroleum inclusions, which occur side by side in the same growth zone of the Sz-20 well (in well section ÁGK-4921 (2069 m)) Fig. 7. shows the distribution of the measured data. The flat morphology of the

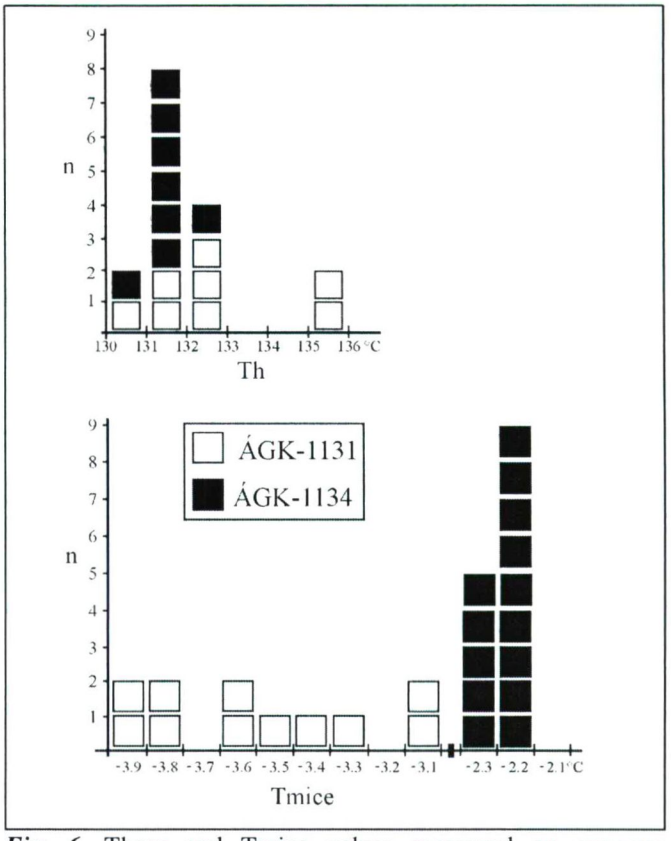

Fig. 6. Thom and Tmice values measured on aqueous incluison of the ÁGK-1131 and -1134 well sections of the Sz-2 well.

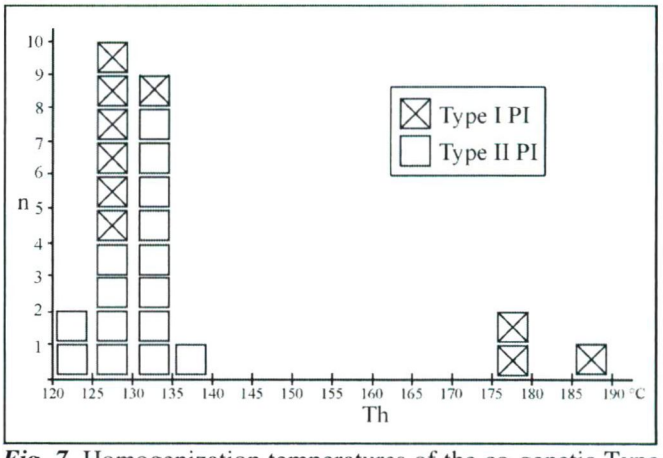

Fig. 7. Homogenization temperatures of the co-genetic Type Ia and Ib petroleum inclusions of the Sz-20 well (well section ÁGK-4921)

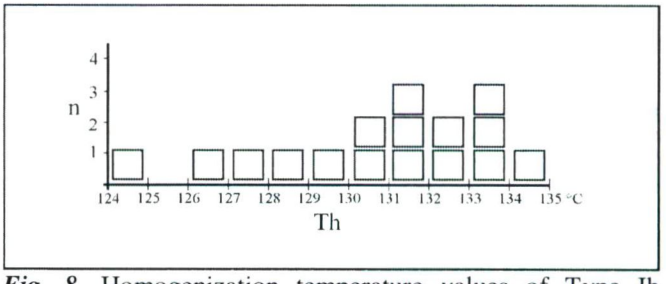

Fig. 8. Homogenization temperature values of Type Ib petroleum incluisons of the Sz-180 well (well section ÁGK-4648).

Type IA inclusions make the observation of the temperature of the L→V mode homogenisation easier, however, these values must be regarded as minimal temperatures.

Measurable quantity of HC inclusions of the Sz-180 well was found in the 4848 well section (2020 m). The primary FIA exclusively contains Type IB fluid inclusions, which homogenized between 124 and 135 °C, by V→L transition (Fig. 8). In the 4644 well section (2011 m) of the same well aqueous FIA co-genetic with the Type I inclusions was observed. Thom values show a quite uniform distribution varying between 131 and 133 °C (Fig. 9).

Microthermometry was performed on both aqueous and petroleum inclusions (trapped along the same growth zone) of the Sz-167 well. The Thom and Tmice values are shown on Fig. 10.

At low temperatures, Type I FIs show a characteristic phase transition of L+L+V→L+V type. During the cooling run, after the initial shrinkage of the vapour phase at about -77 °C a new liquid phase appears, which homogenises at about -63 °C during subsequent heating (Fig. 11). This transition can be observed on both Type IA and IB inclusions.

The S→L type homogenisation of the Sp phase occurs at slightly different temperatures in different wells containing Type II PIs. In Type II inclusions of the Sz-2, 12 and 176 wells the S→L homogenisation proceeds at 18 ± 5 °C, while in case of the Sz-167 well it occurs at 21 ± 8 °C. The S→L type homogenisation of the Sb solid phase proceeds above the V→L homogenisation temperature (it was not exactly determined).

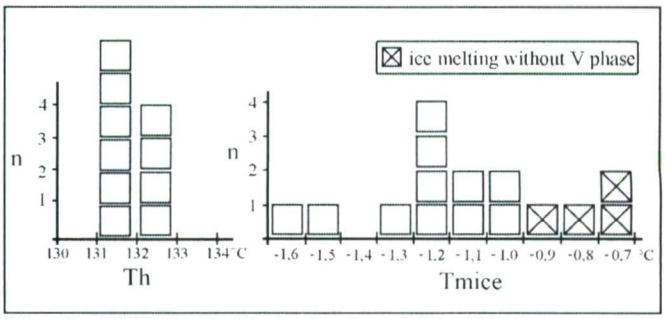

Fig. 9. Thom and Tmice values measured on aqueous incluison from the Sz-180 well (well section ÁGK-4644).

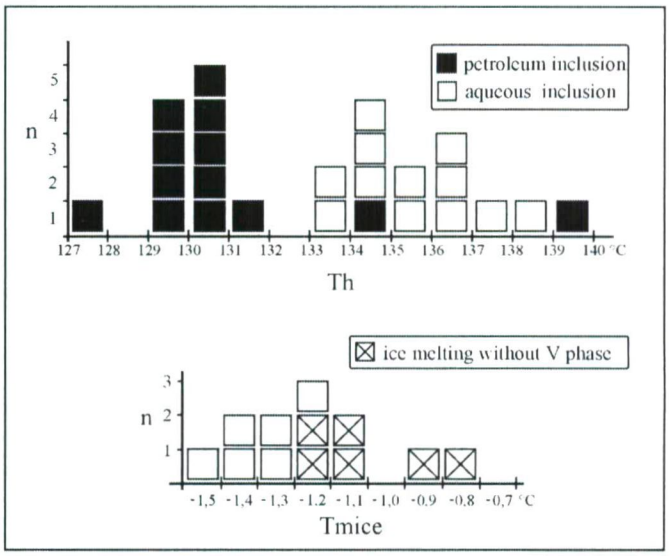

Fig. 10. Thom and Tmice values of the co-genetic aqueous and petroleum inclusions from the Sz-167 well.

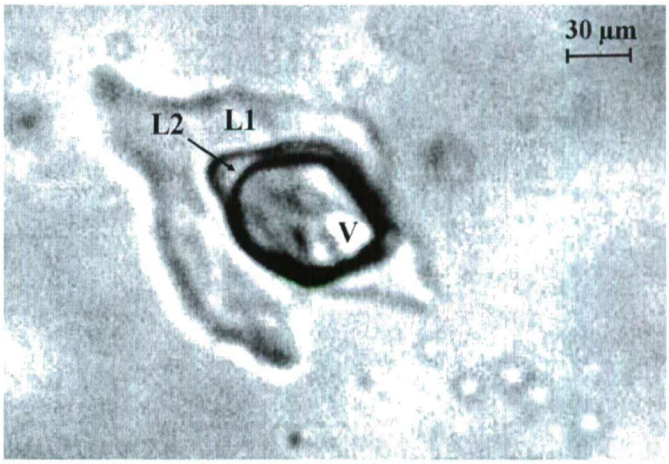

Fig. 11. Type Ib fluid inclusion from the Sz-180 well (well section ÁGK-4648) showing L + L + V equilibrium at – 89 °C.

Discussion

In the central part of the SzD HC-bearing quartz were found in 6 wells, while quartz crystals free from organic fluid remnants were not observed (see Schubert and M. Tóth, 2001). The relative position of this quartz phase in the fracture-filling mineral sequence is of overriding importance in studied reservoir. Although fluid inclusion and stable isotope measurements of the subsequent calcite2 phase are available only from a few wells analysed by Juhász et al. (2002), our observations in all studied wells support their fracture-filling model. Namely, the precipitation of the quartz phase in the whole SzD precedes the formation of the calcite2 phase. Based on the newest palynological data of M. Tóth et al. (2003), the calcite2 phase precipitated at the most exhumed vertical position of the SzD during the Badenian. As a consequence, the HC fluid entrapped in the quartz crystals cannot be identical to the nowadays produced oil and gas, which have a source rock of Badenian, Sarmatian and lower Pannonian age (Teleki et al., 1994). So the known composition of the produced HC fluid could not be used even as a starting-point for investigation of the trapped fluid. Although there are some Mesozoic formations near the study area that contain members of high organic matter content (e.g. Szolnok Flysch Formation, Juhász et al., 2002), the source rock of the enclosed petroleum is still unidentified.

The studied fluid inclusions form planar arrangement supposing a secondary (or pseudosecondary) origin for the FIAs in question. The petrographical observations performed by the modified spindle stage (Anderson and Bodnar, 1993), however, suggest that the planar arrangement coincides well with an early-late primary origin of these inclusions (Roedder, 1979), which were probably trapped along the faces of the earlier quartz crystals. Thus the petroleum (and aqueous) inclusions trapped along parallel growth zones were formed simultaneously with the precipitation of the host quartz (primary inclusions; Goldstein and Reynolds, 1994).

HC-bearing idiomorphic quartz crystals were reported from several localities in the world, e.g. the so-called "Marmarosh diamonds" (Dudok et al., 2000), "Quebéc diamonds" (Levine

et al., 1991), etc. Several works studied the obvious relationship between the precipitation of quartz and the host rock rich in organic matter, as well (e.g. Levine et al., 1991; Bennett, 1991; Wilkinson et al., 1998). Wilkinson et al. (1998) suppose that the organic acids, which liberate during the thermal maturation of the organic matter, could be of primary importance in the local silica transport.

Based on the negligible solubility of silica in petroleum, in spite of the extremely low amount of aqueous inclusions relative to the HC-bearing ones, it can be supposed that even those quartz crystals, which exclusively enclose petroleum inclusions, were precipitated from an aqueous solution. Nedkvitne et al. (1993) studied the temporal relationship between diagenesis and oil emplacement in sandstone reservoirs of the North Sea. They could demonstrate that in contrast to the former conception, cementation does not terminate after oil emplacement in all geological situations.

The fracture-filling quartz phase of the SzD contains two markedly different HC fluids. They differ in colour, density, presence of solid phases, intensity and colour of fluorescence, (relative) time of trapping, as well as spatial occurrence in the SzD. The PIs of Type I and II occur either separated or together in the studied wells, but the temporal sequence of these fluid types is identical everywhere.

The colourless liquid phase, the different vol. % of the gas phase and the lack of the solid phases unambiguously distinguish Type I fluid from Type II, although, these deviations may account for completely different reasons. The above-mentioned features of Type I fluid suggest a low density; possibly mature HC fluid (light oil/condensate). Similar HC-bearing FIs were introduced by Munz et al. (1999) from the Brent Group Reservoirs among many others. Based on the observed bluish fluorescent colour, they considered the trapped fluid as a condensate. Referring to the results of Luks et al (1983), Teinturier et al (2002) classified PIs from the Haltenbanken Area as condensate based on appearance of a new liquid phase during cooling. The new liquid phase homogenised below 0°C by L+L+V→L+V transition.

The usually typical low amount of the aromatic components of the gas condensates (e.g. Goldstein and Reynolds, 1994) is proved indirectly by the applicability of the visible Raman spectroscopy in case of Type I fluid inclusions. The contribution of methane and ethane to the vapour and alkanes/cycloalkanes to the liquid phase is revealed by the Raman microspectroscopy. Even if their compositions agree, there is not unquestionable evidence that the Type I fluid must be a condensate, because the measured components are most common in crude oils, too (Tissot and Welte, 1978). The termogenic formation of condensate is typical of the higher part of the oil window (Tissot and Welte, 1978). Nevertheless, there also are other mechanisms (e.g. evaporative fractination, Thompson, 1987), which may produce condensates that are seemingly similar to those produced by thermal maturation.

By reason of the coloured liquid phase, the lower API gravity (presence of different solid phases) and the bluish green fluorescence colour (red shift relative to the emission of the Type I fluid), Type II HC fluid can unambiguously be distinguished from the Type I fluid. To form subcategories within the Type II fluid using the above-mentioned indirect methods is not possible. Therefore, the Type II fluid found in the Sz-167 well cannot undoubtedly be correlated with those of Sz-2, 12, 176 wells, whose outer growth zones contain even the Type I fluid. The similar homogenisation temperature data (about 130 °C) of the co-genetic aqueous inclusions and occurrence of the solid phases stand for the relationship to the other three wells, while the significantly lower salinity (2.07-2.57 wt% NaCleq) and the uniquely coloured host quartz tell against.

We have constructed a relative sequence for the different HC fluid types using the occurrence of the different HC-bearing FIAs in the subsequent growth zones of the six wells. Then the studied wells of the SzD were classified based on similar PIs or PI sequences.

The most common HC FIs in the SzD belong to Type IA and IB. In the Sz-20 and 180 wells these two HC types occur exclusively. The FIs arise along several parallel growth zones but there is no systematic difference in the appearance (vol. % of the gas phase, colour, fluorescence properties) of the HC-bearing FI assemblages of the adjacent zones. The succeeding growth zones of the Sz-167 well contain Type II PIs, without any difference between the FIAs. A well-defined temporal difference can be observed in the appearance of Type I and Type II fluids in the centre and the southern flank of the SzD; in case of the Sz-2, 12, 176 wells. While the inner growth zones are defined, exclusively, by Type II PIs, following a sudden appearance of Type I inclusions (Fig. 5), this type becomes dominant in the outer zones. In these wells Type I fluid appears only in the outer (younger) growth zones.

There is not any significant change in any measured properties of the FIs/PIs with depth.

If the aqueous inclusions at the time of entrapment were saturated respecting methane, then the homogenisation temperature coincidences with the trapping temperature (Hanor, 1980; Pironon et al., 2001). Because of the minute size, rarity and position of the aqueous inclusions, we were able to prove the presence of methane by Raman microprobe in the vapour (and the liquid) phase in two cases only. As the common occurrence of petroleum and aqueous fluids within the same inclusion unambiguously prove the co-genetic trapping of the two fluids (Fig. 12), we consider that the aqueous phase was methane-saturated at the time of trapping (Munz, 2001).

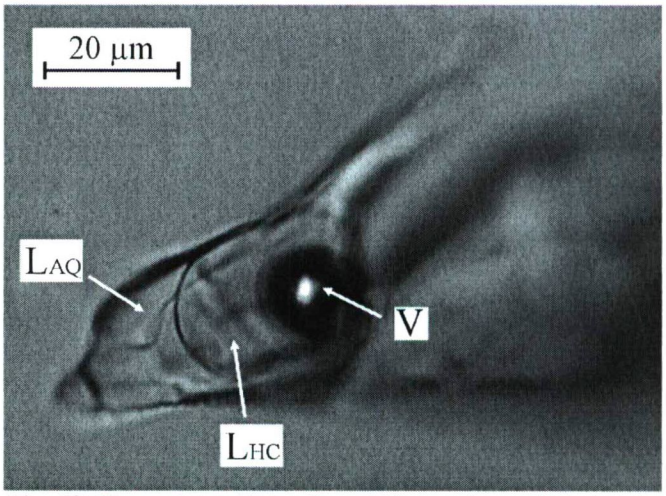

Fig. 12. Three phase (L_{AQ} + L_{HC} + V) petroleum inclusion from the Sz-167 well.

The generally observable small size and unequal distribution of the aqueous inclusions makes comparison of the studied wells concerning the trapping temperature problematic. Nevertheless, we suppose that the measured aqueous FIAs do not represent contemporaneous growth zones of the different wells, on the contrary they record different moments of the quartz precipitation. Accepting the above assumption, the precipitation of the fracture-filling quartz phase of the SzD took place during static temperature regime but intensively changing fluid composition.

The common recrystallisation phenomenon (e.g. by necks connected inclusions) and the overall observable size difference between Type IA and IB inclusions may suggest that the liquid-rich (Type IB) inclusions were possibly formed by post-entrapment modification of the originally Type IA PIs. In this case Type IB inclusions should give a rather scattering Thom pattern caused by the accidental change in the volume of the inclusion cavity yielded by recrystallisation (Shepperd et al., 1985). In the present case, however the Thom values of Type IB inclusions are quite similar (Fig. 7), and the typical range falls near that of Type IA. Although the fact that the size of Type IA inclusions always exceeds the dimension of Type IB would support the above assumption, the size difference may be explained by the different wetting properties of the co-existing vapour and liquid phases, as well (Diamond personal communication, 2003).

Considering a multi-component hydrocarbon fluid, there are mechanisms that may result in formation of heterogeneous FIAs, i.e. simultaneous trapping of liquid- and vapour-rich petroleum inclusions introduced by Teinturier et al. (2002). They described condensate-type fluid showing analogous behaviour to ours from the Haltenbanken area (North Sea). Based on the similar Thom values of the L→V and V→L type fluid inclusions they supposed a near critical trapping. However, they have found several inclusions with critical homogenisation behaviour as well, which was not observable in the studied SzD samples. Here, the frequent occurrence of the partially necking-downed FIs, the negative crystal shape, the pointed inclusion shape as well as some Thom values differing from the average suggest that the effect of recrystallisation could not be ignored either.

Since the measurable aqueous FIAs of the Sz-2 well were found in different samples (crystals), the temporal relationship between the two growth zones (FIAs) were identified based on the co-genetic petroleum inclusions. Systematic sequence of Type I and II HC inclusions is well-defined in the studied wells, i.e. the growth zones containing Type I fluid inclusions always post-date the Type II-bearing zones. Therefore we consider the aqueous FIA in the sample 1131 co-genetic with Type II petroleum inclusions as a marker of the former stage of quartz precipitation in the SzD. Since the aqueous inclusions of the sample 1134 co-exist exclusively with Type I HC fluid, it must represent the parent fluid composition of the later (younger) stage. A similar change in the composition of the HC fluid during the charging of a hydrocarbon reservoir is a common phenomenon (e.g. Munz et al., 2002). The types and distribution of the petroleum inclusions in the Sz-12 and 176 wells are identical to those observed in the Sz-2 well, in these cases, however, aqueous inclusions occur sporadically.

Although, formation temperatures of the quartz phase in the early and late growth zones (Sz-2) are similar, a significant change in the salinity can be observed. While the aqueous inclusions of the well section 1131 show a salinity of 5.1-6.3 wt% NaCleq, those values of the well section 1134 vary between 3.7-3.8 wt% NaCleq. The salintiy measured on the aqueous inclusions of the Sz-180 well changes between 1.2-2.7 wt% NaCleq, while the trapping temperature is identical to those measured in the Sz-2.

Although, the relative time of precipitation of the quartz phase between the Sz-180 and the outer growth zones of the Sz-2 wells is unclear, we suppose a trend of decreasing salinity from the time of migration of Type II petroleum towards the appearance of Type I fluid. So, the intermediate salinity received from the outer growth zones of the Sz-2 well may probably represent the mixing "event" of Type I and Type II fluids. There is no reason for changing salinity if we assume that the Type I fluid formed by phase separation from the "original" Type II fluid, to further discuss this dilemma quantitative information of the petroleum inclusions of the three growth zones is needed.

Conclusions

- Six wells of the central part of the SzD contain HC-bearing, euhedral quartz crystals, which was formed unambiguously prior to the calcite2 phase, which represents the most exhumed state of the SzD.
- The several growth zones and the flat PIs arranging parallel to certain crystallographic directions of the host quartz suggest a primary origin of the HC-bearing FIs and the co-genetic brine inclusions.
- Based on colour, fluorescent properties and low temperature phase transition, the HC fluid of the Sz-20 and 180 wells probably represent a condensate-like fluid (Type 1).
- In the Sz-2, 12 and 176 wells the precipitation of the quartz phase took place in a changing HC fluid regime. The early liquid-rich PIs (Type II) are followed by the condensate-like, translucent HC fluid in the outer (younger) growth zones of the quartz crystals. Based on the introduced data it is impossible to decide whether this condensate is the product of advanced thermal maturation or was formed by phase separation from a former petroleum fluid (e.g. by evaporation fractionation).
- Based on the aqueous inclusions co-genetic with the PIs, the trapping of the primary FIAs and the precipitation of the different quartz phases happened at isothermal conditions (at about 130 °C) but in the presence of different HC fluids. The quartz cementation in Sz-167 well took place at a temperature identical to those observed in the other five wells.
- During the fluid evolution devised using the subsequent PIs, a decreasing salinity (5.1-6.3 → 3.7-3.8 → 1.2-2.7 wt% NaCleq) of the aqueous inclusions can be revealed. The significant salinity change relates to the abrupt appearance of the condensate-like fluid suggesting a phase separation rather than the increasing thermal maturation of the same organic matter.
- Based on colour, fluorescence properties, trapping temperature, vol. % of the gas phase and the presence of higher molecular weight components (solid phases), the Type II PIs of the Sz-167 well seem to be related to those found in the Sz-2, 12 and 176 wells. Because Sz-167 well

can be found rather far from the three wells mentioned, and Type II fluid is completely missing from the two wells (Sz-20 and 180, respectively), which are situated among them (c.f. Fig. 1C), we suppose that the Type II fluid of the Sz-167 well is probably different from that found in the Sz-2, 12 and 176 wells. The lower salinity of the aqueous inclusions measured in the Sz-167 well support this assumption, however, to decide this question compositional data of the different HC types are needed.

- Although, the different liquid-vapour ratios of Type I PIs were presumably resulted from heterogeneous trapping, the morphology of the inclusions suggest a possible effect of the recrystallization, as well.

ACKNOWLEDGEMENTS

The financial background of this work was ensured by the OMAA (grant no. 45öu1 and 53öu4), the Hungarian Ministry of Culture (grant no. FKFP 0139/2001) and Hungarian Research Found (grant no. OTKA F32792 and D45921).

REFERENCES

ANDERSON, A. J., BODNAR, R. J. (1993): An adaption of the spindle stage for geometric analysis of fluid inclusion. American Mineralogist, **78**, 657-664.

BAKKER, R. J. (2002): http://www.unileoben.ac.at/~buero62/minpet/Ronald/Programs/Computer.html. accessed: November 15, 2003.

BENNETT, P., SIEGEL, D. I. (1987): Increased solubility of quartz in water due to complexation by dissolved organic compounds. Nature, **326**, 684-687.

BENNETT, P. (1991): Quartz dissolution in organic-rich aqueous systems. Geochimica et Cosmochimica Acta, **55**, 1781-1797.

CSONTOS, L., NAGYMAROSI, A. (1999): Late Miocene inversion versus extension in the Pannonian Basin. Tübinger Geowissenschaftliche Arbeiten, Series A, **52**, 132.

DUBESSY, J., BUSCHAERT S., LAMB, W., PIRONON, J., THIÉRY, R. (2001): Methane-bearing aqueous fluid inclusions: Raman analysis, thermodynamic modelling and application to petroleum basins. Chemical Geology, **173**, 193-205.

DUDOK, I., JARMOLOWICZ-SZULC, K. (2000): Hydrocarbon inclusions in vein quartz (the „Marmarosh diamonds") from the Krosno and Dukla zones of the Ukrainian Carpathians. Geological Quarterly, **44**, 415-425.

GOLDSTEIN, R. H., REYNOLDS, T. J. (1994): Systematics of fluid inclusions in diagenetic minerals. SEPM Short Course 31.

HANOR, J. S. (1980): Dissolved methane in sedimentary brines: potential effect on the PVT properties of fluid inclusions. Economic Geology, **75**, 603-617.

JUHÁSZ, A., M. TÓTH, T., RAMSEYER, K., MATTER, A. (2002): Connected fluid evolution in fractured crystalline basement and overlying sediments, Pannonian Basin, SE Hungary. Chemical Geology, **182**, 91-120.

KARLSEN, D. A., NEDKVITNE, T., LARTER, S. R., BJORLYKKE, K. (1993): Hydrocarbon composition of authigenic inclusions: Application to elucidation of petroleum reservoir filling history. Geochemica and Cosmochemica Acta, **57**, 3641-3659.

LEVINE, J. R., SAMSON, I. M., HESSE, R. (1991): Occurence of fracture-hosted impsonite and petroleum fluid inclusions, Quebec City Region, Canada. AAPG Bulletin, **75**(1), 139-155.

LUKS, K. D., MERRILL, R. C., KOHN, J. P. (1983): Partial miscibility behavior in cyrogenicnatural gas systems. Fluid Phase Equilibria, **14**, 193-201.

M. TÓTH, T., SCHUBERT, F., ZACHAR, J. (2000): Neogene exhumation of the Variscan Szeghalom Dome, Pannonian Basin, E. Hungary. Geological Journal, **35**, 265-284.

M. TÓTH, T., KEDVES, M., SCHUBERT, F. (2003): Az Alföld metamorf aljzatának exhumációja a Szeghalom-dóm területén: palinológiai bizonyítékok. Földtani Közlöny, **133/4**, 547-562.

MUNZ, I. A., JOHANSEN, H., HOLM, K., LACHARPAGNE, J.-C. (1999): The petroleum characteristics and filling history of the Froy field and the Rind discovery, Norwegian North Sea. Marine and Petroleum Geology, **16**, 633-651.

MUNZ, I. A. (2001): Petroleum inclusions in sedimentary basins: systematics, analytical methods and applications. Lithos, **55**, 195-212.

MUNZ, I. A., YARDLEY, B. W. D., GLEESON, S. A. (2002): Petroleum infiltration of high-grade basement, South Norway: Pressure-Temperature-time-composition (P-T-t-X) constraints. Geofluids, **2**, 41-53.

NEDKVITNE, T., KARLSEN, D. A., BJORLYKKE, K., LARTER, S. R. (1993): Relationship between reservoir diagenetic evolution and and petroleum emplacement in the Ula Field, North Sea. Marine and Petroleum Geology, **10**, 255-270.

ORANGE, D., KNITTLE, E., FARBER D., WILLIAMS, Q. (1996): Raman spectroscopy of crude oils and hydrocarbon fluid inclusions: A feasibility study. In Dyar, M. D., McCammon, C., Schaefer, M. W. (eds): The Geochemical Society, Special Publication No. 5.

PAP, S., SŐREG, V., PAPNÉ HASZNOS, I, (1992): A Dévaványa-déli metamorf medencealjzati szerkezet szénhidrogénkutatási problémái - esettanulmány. Geophysical Transactions, **37**(2-3), 211-228. (in Hungarian)

ROEDDER, E. (1979): Fluid inclusion: Mineralogical Society of America, Reviews in Mineralogy, v. 12.

ROYDEN, L. H., HORVÁTH, F. (eds.) (1988): The Pannonian Basin: A Study in Basin Evolution. AAPG, Tulsa, Oklahoma. Memoir **45**, 27-48.

SCHUBERT, F., M. TÓTH, T. (2001): Structural evolution of mylonitized gneiss zone from the northern flank of the Szeghalom dome (Pannonian Basin, SE Hungary). Acta Mineralogica et Petrographica Szeged, **42**, 59-64.

SHEPHERD, T. J., RANKIN, A. H., ALDERTON, D. H. M. (1985): A Practical Guide to Fluid Inclusion Studies. Blackie.

SZŰCS, É. (2001): Polimetamorfitok mikrotektonikai vizsgálata a Békési-medence északi részén. Kézirat, SZTE, Ásványtani, Geokémiai és Kőzettani Tanszék. (in Hungarian)

TARI, G., DÖVÉNYI, P., DUNKL, I., HORVÁTH, F., LENKEY, L., STEFANESCU, M., SZAFIÁN, P., TÓTH, T. (1999): Lithospheric structure of the Pannonian Basin derived from seismic, gravity and geothermal data. In Durand, B., Jolivet, L., Horváth, F., Séranne, M. (eds): The Mediterranean Basins: Tertiary Extension within the Alpine Orogen. Geological Society: London. Special Publications **156**, 215-250.

TEINTURIER, S., PIRONON, J., WALGENWITZ, F. (2002): Fluid inclusion and PVTX modelling: examples from the Garn Formation in well 6507/2-2, Haltenbanken, Mid-Norway. Marine and Petroleum Geology, **19**, 755-765.

TISSOT, B. P., WELTE, D. H. (1978): Petroleum Formation and Ocurence. Springer-Verlag.

WILKINSON, J. J., LONERGAN, L., FAIRS, T., HERRINGTON, R. J. (1998): Fluid inclusion constraints on conditions and timing of hydrocarbon migration and quartz cementation in Brent Group reservoir sandstones, Columba Terrace, northern North Sea. In Parnell, J. (ed): Dating and Duration of Fluid Flow and Fluid-Rock Interaction. Geological Society Special Publications **144**, 69-89.

Received: March 12, 2003; accepted: September 25, 2003

Acta Mineralogica-Petrographica, Szeged 2003, Vol. 44, pp. 19-22

ACTA
Mineralogica
Petrographica

EXPERIMENTAL INSTRUMENT ON HUNVEYOR FOR COLLECTING BACTERIA BY THEIR ELECTROSTATIC COAGULATION WITH DUST GRAINS (FOELDIX): OBSERVATION OF ELECTROSTATICAL PRECIPITATED COAGULATED UNITS IN A NUTRIENT DETECTOR PATTERN

TIVADAR FÖLDI[1], SZANISZLÓ BÉRCZI[2], ERZSÉBET PALÁSTI[1]

[1] FOELDIX, H-1117 Budapest, Irinyi József u. 36/b. Hungary

[2] Department of General Physics, Cosmic Materials Space Research Group, Eötvös Loránd University
H-1117 Budapest, Pázmány Péter sétány 1/C, Hungary
e-mail: bercziszani@ludens.elte.hu

ABSTRACT

Electrostatic coagulation properties of dust above planetary surfaces (CRISWELL, 1972, RHEE ET AL., 1977, REID, 1997, HORÁNYI ET AL., 1998, SICKAFOOSE ET AL., 2001) were studied by FOELDIX instrument of Hunveyor. We developed FOELDIX by a detector unit in order to observe biomarkers on Mars by collecting dust thrown out from dusty regions. The dust collector experiment (FÖLDI ET AL., 1999), with the observation capability of the size dependent dust particles (FÖLDI ET AL., 2002), was developed by fitting a nutrient container detector pattern which can show various types of bacteria in the inner detector-wall of the modified FOELDIX instrument (FÖLDI ET AL., 2001). Coagulation of electrostatically charged dust particles, rare H_2O molecules and suggested extremophile bacteria from the dusty Martian surface is carried out by our experimental assemblage through the space with electrodes. Coagulated grains are allowed to precipitate in the vicinity of some specially charged electrodes (FÖLDI, BÉRCZI, 2001a). If living units form a community, a consortia of bacteria and fungal spores with the attached soil then the cryptobiotic crust (PÓCS, 2002) components of Mars may also be found and distinguished by this measuring technology.

INTRODUCTION

Levitating charged dust particles were measured on Surveyors (Criswell, 1972), Apollo's LEAM experiments (Rhee et al., 1977) and their models were shown (Reid, 1997; Horányi et al., 1998; Sickafoose et al., 2001). Windstorms on Mars are known since old times and were photographed. We also studied levitating dust particle phenomenon in the experiment of FOELDIX where coagulation of lunar quasiatmospheric dust were modelled (Földi et al., 1999, 2001). We placed the FOELDIX instrument among the Hunveyor (Bérczi et al., 1998, 1999) electrostatic assemblage. To search the possibility of life on Mars we developed our instrument with bacteria and spora detector unit.

The FOELDIX detector unit consists of stripes with nutrient containers. They are placed on the inner wall of the dust collector. They form a coordinate system. (In terrestrial conditions the containers can be replaced with other ones.) In principle the detector unit is similar to the Magnetic Properties Experiment of the Mars Pathfinder, where magnetic materials were fixed on a curtain on the surface of the lander. Magnetic materials were arranged in a characteristic pattern of spots. Magnetic forces glued the magnetized particles on the spots. The repeated dust interaction with this curtain amplified the pattern of the colored dust particles attracted on the spots till the visibility of the pattern. Even by camera observation of the curtain the magnetic spot pattern - with various megnetisation strength of the spots in the curtain magnets - allowed estimation of the magnetisation of the dust particles flown by winds (Hviid et al., 2000).

THE SOIL AND BACTERIA TOGETHER

Extremophile bacteria are among the main constituents of the cryptobiotic crust on the Earth. The FOELDIX instrument has a benefit to colllect the fragments of such living consortia in glued and coagulated units. This way not only dust but the glued bacteria or other living units (i.e. fungal spores) can be collected into the instrument's container detector. Selected detecting mechanism is necessary to distinguish the various components of the cryptobiotic type living unit fragments of the windblown dry powder material. Therefore a detecting surface with a selective nutrient stripe arrangement was constructed for the FEOLDIX. On the Hunveyor we measure the CBC collecting capacity of the instrument in the Great Hungarian Plain where dry alkaline grounds can be found, especially in the Hortobágy.

THE MEASURING DETECTOR ARRANGEMENT

In our measuring detector an inner wall-curtain with various nutrients are fixed in the vicinity of special electrodes. These electrodes allow the coagulated dust and bacteria grains (and other complex particles) to precipitate and sediment from the streaming particles in the instrument. The coagulated materials with various bacterial components can grow on the nutrient stripes with different effectivity. Repeated interaction of the precipitated dust-and-bacteria coagulates will change the color and extent of the nutrient stripe regions and amplifies the pattern of the nutrients till the visibility of the arrangement of stripes. Microcamera observation of the detector's stripe pattern will show the types of bacteria (or fungal spores) existing inside the coagulated dust particles.

COAGULATION OF PARTICLES CONTAINING DUST + BACTERIA + WATER MOLECULES

On the inner surface of the electron tube, even in the case of hypervacuum, a monomolecular water molecule layer can be found (Tungsram Factory, Bródy and Palócz, 1953). These water molecules are small negative ions and have far longer lifetime then that of the small positive ions (Israel, 1957).

In the vicinity of a dusty planetary surface there exist a space charge of electron cloud. The rare water molecules will act as if they were negatively charged and they preserve their charge. The negatively charged water molecules frequently collide with particles of a positively charged dust cloud producing a complex coagulated particle. This particle is a loose aggregate of ions, has great mass and has lower velocity compared to the small mass particles. While colliding with a negatively charged water molecule the water molecule will attach to the larger one. This process enlarges the complex aggregate larger and larger (we measured coagulation up to 450.000 times mass in the FOELDIX instrument). The living units are embraced and included into this coagulated large particles. Living units are shielded by the dust components from UV and other radiations, and the presence of water allows to continue their life activity, too.

LOCATION OF PROMISFUL OBSERVATION CHANCES FOR MARTIAN LIVING ORGANISMS: SOUTH POLE

On the MOC MGS images there are promisful regions where to land in order to observe Martian life components of bacteria or fungal spores with dust. In winter these dark dunes are covered with frost. Dark dune spots are formed in late winter and early spring. They show a characteristic defrosting pattern on the frost covered surface where the soil material is partially exposed on the surface activity (Horváth et al., 2002a). The frost-free uncovered region is the dark spot itself. In these periods wind blows out the dark dune material from the spots and the ejected dark dust forms a thin layer on the surface of the frost cover.

On the basis of the analyses of the dark dune spots (DDSs) morphogenetics DDSs were estimated as probable sites for biogenic activity (Horváth et al., 2001, 2002a, 2002b). The Hungarian group suggested that Martian surface organisms (MSOs) are the main agents of the DDS phenomenon, and they were considered as promisful candidates of the recent life on Mars. If the MSOs exist, then they must be flown out from the dark dune spots by the strong winds during the late winter and early spring period of the DDS activity. Dark wind-streaks emanating from DDSs can be observed in these seasons.

PRESENCE OF WATER ON DDS SITES

As we referred earlier the water molecule content of the atmosphere helps the electrostatic coagulation of the dust particles (Földi and Bérczi, 2001b). The Southern Polar region of Mars where the DDS sites were found and studied is therefore promisful source for the FOELDIX experiment because Mars Odyssey also found higher concentration of

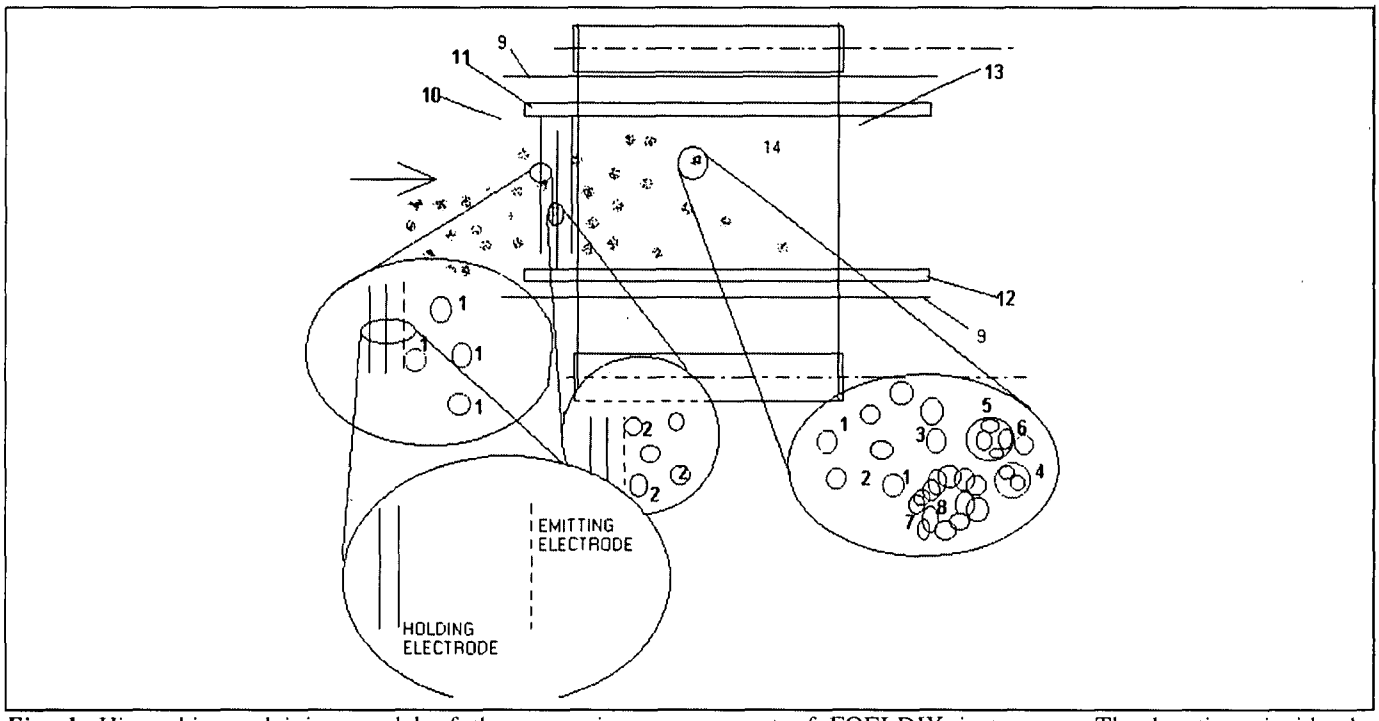

Fig. 1. Hierarchic explaining model of the measuring arrangement of FOELDIX instrument. The locations inside the instrument are the followings: 1. Dust (or aerosol) particles with positive charge; 2. Dust (or aerosol) particles with negative charge; 3. Coagulated dust (or aerosol) particles; 4. Coagulated dust (or aerosol) particles with positive charge, 5. Recharged coagulated dust (or aerosol) particles with negative charge; 6. Recharged coagulated dust (or aerosol) particles with positive charge; 7. Multiple coagulated, cluster-like dust (or aerosol) particles, (max. 540.000 times mass); 8. Bacteria or virus (or other particles with biologic information) inside the multiple coagulated, cluster-like dust (or aerosol) particles; [in this location these bacteria, etc. are shielded for UV radiation]; 9. The wall of the box of the instrument; 10. The entrance gate for the dust (or aerosol) particles; 11. Electrode with positive potential; 12. Electrode with negative potential; 13. Discharging and sedimenting electrode; 14. Nutrient containing zero potential electrode surface.

water in this region (Mitrofanov, et al., 2003; Kuzmin, et al., 2003; Horváth et al., 2003a). Although the 2003/2004 Mars missions will not go to the polar regions, a more detailed imaging may reveal special sites with extensive wind activity in the given late winter early spring period (Córdoba-Jabonero et al., 2003; Horváth et al., 2003b).

THE HUNVEYOR EXPERIMENTAL SPACE PROBE MODEL

Hunveyor experimental university space probe model - a Surveyor-like lander - has been first constructed on the Eötvös University, Budapest, (Department of General Technology) in 1997 (Bérczi et al., 1998). Next year we made planetary geology park around Hunveyor-1 1997 (Bérczi et al., 1999), and the Pécs University group also began to build his Hunveyor-2 (Hegyi et al., 2001). The minimal space probe was built with camera and robotic arm. Since that first instrumentation various new experiments were improved like soil analyzer and measuring unit, spectrometer, opto-chemical sensor unit, electrostatic unit. A Martian desert landscape study was also carried out. The Hunveyor-3 (Kovács et al., 2001) and Hunveyor-4 (Hudoba et al., 2003) are also built in the Berzsenyi College, Szombathely and the Kandó College, Székesfehérvár, respectively. The recent development of FOELDIX instrument is a great step forward a real space instrument constrution on Hunveyors.

CONCLUSIONS

The new FOELDIX instrument with the bacteria and spore detector unit is capable to observe various Martian living units coagulated by the instrument and deposited by special electrodes on nutrient containing stripes of the detector. The growing spots can be observed by microcamera units built into the FOELDIX instrument. Such detector can measure not only bacteria but the soil type which is glued with the bacteria. Therefore it is probable that components of the cryptobiotical crust (Pócs, 2002) units may be discovered by this measuring technology.

ACKNOWLEDGEMENTS

This work has been supported by the fund of the Hungarian Space Office No. MÜI-TP-190/2002-2003.

REFERENCES:

BÉRCZI, SZ., CECH, V., HEGYI, S., BORBOLA, T., DIÓSY, T., KÖLLŐ, Z., TÓTH, SZ. (1998): Planetary geology education via construction of a planetary lander probe. In Lunar and Planetary Science XXIX, Abstract #1267, Lunar and Planetary Institute, Houston (CD-ROM).

BÉRCZI, SZ., DROMMER, B., CECH, V., HEGYI, S., HERBERT, J., TÓTH, SZ., DIÓSY, T., ROSKÓ, F., BORBOLA, T. (1999): New Programs with the Hunveyor Experimental Lander in the Universities and High Schools in Hungary. In Lunar and Planetary Science XXX, Abstract #1332, Lunar and Planetary Institute, Houston (CD-ROM).

BRÓDY I., PALÓCZ K. (1953): Lecture on Techn. Univ. Budapest (personal communication).

CÓRDOBA-JABONERO, C.; FERNÁNDEZ-REMOLAR, D.; GONZÁLEZ-KESSLER, C.; LESMES, F.; C. MANRUBIA, S.; PRIETO BALLESTEROS, O.; SELSIS, F.; BÉRCZI, S.; GESZTESI, A.; HORVÁTH, A. (2003): Analysis of geological features and seasonal processes in the Cavi Novi region of Mars. EGS Conference, Nizza, EAE03-A-13011.

CRISWELL, D. R. (1972): Horizon glow and motion of Lunar dust. Lunar Science III. p. 163. LPI, Houston.

DIÓSY, T., ROSKÓ, F., GRÁNICZ, K., DROMMER, B., HEGYI, S., HERBERT, J., KERESZTESI, M., KOVÁCS, B., FABRICZY, A., BÉRCZI, SZ. (2000): New instrument assemblages on the Hunveyor-1 and -2 experimental university lander of Budapest and Pécs. In Lunar and Planetary Science XXXI, Abstract #1153, Lunar and Planetary Institute

FÖLDI, T., EZER, R., BÉRCZI, SZ., TÓTH, SZ. (1999): Creating Quasi-Spherules from Molecular Material Using Electric Fields (Inverse EGD Effect). LPSC XXX. #1266, LPI, Houston.

FÖLDI, T., BÉRCZI, SZ., PALÁSTI, E. (2001): Water and bacteria transport via electrostatic coagulation and their accumulation at the poles on the dusty planet. LPSC XXXII, #1059, LPI, Houston.

FÖLDI, T., BÉRCZI, SZ. (2001a): The source of water molecules in the vicinity of the Moon. LPSC XXXII, #1148, LPI, Houston.

FÖLDI, T., BÉRCZI, SZ. (2001b): Quasiatmospheric Electrostatic Processes on Dusty Planetary Surfaces: Electrostatic Dust and Water molecule Coagulation and Transport to the Poles. 26th NIPR Symposium Antarctic Meteorites, Tokyo, p. 21.

FÖLDI, T., BÉRCZI, SZ., PALÁSTI, E. (2002): Time Dependent Dust Size Spectrometry (DUSIS) Experiment: Applications in Interplanetary Space and in Planetary Atmospheres/Surfaces on Hunveyor. Meteoritics & Planetary Science, **37**, No. 7. Suppl., p. A49.

HEGYI, S., BÉRCZI, SZ., KOVÁCS, ZS., FÖLDI, T., KABAI, S., SÁNDOR, V., CECH, V., ROSKÓ, F. (2001): Antarctica, Mars, Moon: Comparative planetary surface geology and on site experiments and modelling via robotics by Hunveyor experimental lander. 64. Met. Soc. Ann. Meeting, #5402, (Rome, Vatican City, Sept, 2001) Meteoritics & Planetary Science, **36**, Supplement, p.A77.

HORÁNYI, M., WALCH, B., ROBERTSON, S. (1998): Electrostatic charging of lunar dust. LPSC XXIX. #1527, LPI, Houston

HORVÁTH, A., GÁNTI, T., GESZTESI, A., BÉRCZI, SZ., SZATHMÁRY, E. (2001): Probable evidences of recent biological activity on Mars: Appearance and growing of Dark Dune Spots in the South Polar Region. LPSC XXXII, #1543, LPI, Houston.

HORVÁTH, A., GÁNTI, T., BÉRCZI, SZ., GESZTESI, A., SZATHMÁRY, E. (2002a): Morphological Analysis of the Dark Dune Spots on Mars: New Aspects in Biological Interpretation. LPSC XXXIII, #1108, LPI, Houston. (CD-ROM)

HORVÁTH, A., BÉRCZI, SZ., GÁNTI, T., GESZTESI, A., SZATHMÁRY, E. (2002b): The "Inca City" Region of Mars: Testfield for Dark Dune Spots Origin. LPSC XXXIII, #1109, LPI, Houston.

HORVÁTH, A., GÁNTI, T., BÉRCZI, SZ., GESZTESI, A., SZATHMÁRY, E. (2003a): Evidence for Water by Mars Odyssey is Compatible with a Biogenic DDS-Formation Process. LPSC XXXIV, #1134, LPI, Houston.

HORVÁTH, A.; MANRUBIA, S. C., GÁNTI, T., BÉRCZI, S., GESZTESI, A., FERNANDEZ-REMOLAR, D., PRIETO BALLESTEROS, O., SZATHMÁRY, E. (2003b): Proposal for Mars Express: detailed DDS-test in the "Inca City" and "Csontváry" areas. EGS Conference, Nizza, EAE03-A-14142.

HUDOBA, GY., SASVÁRI, G., KERESE, P., KISS, SZ., BÉRCZI, SZ. (2003): Hunveyor-4 Construction at Kandó Kálmán Engineering Faculty of Budapest Polytechnik, Székesfehérvár, Hungary. In Lunar and Planetary Science XXXIV, #1543, LPI, Houston.

HVIID, S. F.; KNUDSEN, J. M.; MADSEN, M. B.; HARGRAVES, R. B. (2000): Spectroscopic Investigation of the Dust Attracted to the Magnetic Properties Experiment on the Mars Pathfinder Lander. LPSC XXXI, #1641, LPI, Houston.

ISRAEL, H. (1957): Atmospherische Elektricitet. Leipzig.

KOVÁCS, ZS. I., KŐVÁRI, I. E., BALOGH, R., VARGA, V., KOVÁCS, T., HEGYI, S., BÉRCZI, SZ. (2001): Planetary science education via construction of the Hunveyor-3 experimental planetary lander on Berzsenyi College, Szombathely, Hungary: Rock radioactivity measurements. In Lunar and Planetary Science XXXII, Abstract #1130, LPI, Houston.

KUZMIN, R. O., MITROFANOV, I. G., LITVAK, M. L., BOYNTON, W. V., SAUNDERS, R. S. (2003): Mars: Detaching of the Free Water Signature (FWS) Presence Regions on the Base of HEND/ODYSSEY Data and Their Correlation with Some Permafrost Features from MOC Data. LPSC XXXIV, #1369, LPI, Houston.

MITROFANOV, I. G. (2003): Global Distribution of Shallow Water on Mars: Neutron Mapping of Summer-Time Surface by HEND/Odyssey. LPSC XXXIV, #1104, LPI, Houston.

PÓCS, T. (2002): A kriptobiotikus kéreg és szerepe a szárazföldi ökoszisztémákban. (The Cryptobiotic Crust and its Role in the Continental Ecosystems) Akadémai székfoglaló előadás. (Presentation at the Hungarian Academy of Science) MTA, Budapest. (in Hungarian)

REID, G. C. (1997): On the influence of electrostatic charging on coagulation of dust and ice particles in the upper mesosphere. Geophysical Res. Letters, **24**, No. 9., p. 1095.

RHEE, J. W., BERG, O. E., WOLF, H. (1977): Electrostatic dust transport and Apollo 17 LEAM experiment. Space Research XVII, p. 627.

SICKAFOOSE, A. A., COLWELL, J. E., HORÁNYI, M., ROBERTSON, S. (2001): Dust particle charging near surfaces in space. LPSC XXXII, #1320, LPI, Houston.

Received: September 2, 2003; accepted: October29, 2003

*Acta Mineralogica-Petrographica, Szeged 2003, Vol. **44**, pp. 23-29*

ACTA
Mineralogica
Petrographica

HEAVY METAL LOAD OF SOILS AROUND A WASTE ROCK DUMP IN THE MÁTRA MTS., HUNGARY

TIVADAR M. TÓTH[1], ANDREA FARSANG[2]

[1] Department of Mineralogy, Geochemistry and Petrology, University of Szeged, H-6701 Szeged, Hungary
e-mail: mtoth@geo.u-szeged.hu

[2] Department of Physical Geography and Geoinformatics, University of Szeged, H-6701 Szeged, Hungary
e-mail: andi@earth.geo.u-szeged.hu

ABSTRACT

Soils around a waste rock dump were studied in the Recsk-Lahóca sulphide ore mining area (NE Mátra Mts., N Hungary). Three soil profiles were examined with a 50 m lag along a slope of the dump. Heavy metals (Cu, Co, Fe, Mn, Ni, Zn, Pb) were measured as well as Al, pH(H_2O) and C_{org}. Soil chemical and statistical analyses show that Zn and Cu accumulate in the topsoil due to resedimentation from the dump material. Fe, Mn, Ni and Co are of lithogene origin in each profile. In sections close to the dump a significant increase of pH can be observed in the topsoil (up to 7.5) due probably to calcite dissolution. Calcite, as a rock forming constituent of the ore-bearing limestone, is present only in the dump material, because the study area consists mainly of volcanic rocks. Although pH is regionally low (around 5.5) in the study area, and the common clay mineral in the soils is kaolinite, the local control of pH is responsible for hindering mobility of the possibly pollutant metals both vertically and horizontally. Due to this effect the dump studied is no risk to its environment.

Key words: waste rock dump, soil pollution, heavy metal mobility, carbonate buffer.

INTRODUCTION

In the Mátra Mts. in Northern Hungary several inactive dumps of the earlier mining activity can be found. Until the last decade sulphide ore minerals, chalcopyrite, enargite, sphalerite, galena as well as precious metals were extracted from underground mines. The dump material still contains a significant amount of heavy metals and may have an important role in heavy metal pollution of the soils nearby (e.g. Korte et al., 1976; Merrington and Alloway, 1994). At the NE foot of the mountains a 20 km^2 large drainage basin was examined (Fig. 1). In the framework of a complex geoecological evaluation (Mezősi and Rakonczai, 1997) among several problems (natural vegetation, drainage system, soil erosion, etc.) also chemical and physical features of the soil was investigated and mapped. Using data of 150 soil profiles, these studies (Farsang, 1996a) showed that the major element as well as the heavy element distribution of the soils over the study area exhibit a natural signal and essentially is free from significant external pollution. No small-scale examination has, however, been carried out yet, there is no information about soil chemistry around the heavy element accumulating dumps. The aim of the present study is to examine the change of the heavy metal concentration in soil profiles moving away from one dump, as well as to test how well soil could buffer occasional pollution.

GEOGRAPHY, GEOLOGY, PEDOLOGY

The study area lies at the NE foot of the Mátra Mts. at 200-800 m above see level (Fig. 1) with increasing average elevation to the west. The 20 km^2 small catchment area is surrounded by peaks in all directions defining the drainage divide, its main stream flows out the area on the eastern end. The average relief is in the range of 95-150 m/km^2. The area is characterized by a temperate climate with 650-750 mm/year rainfalls and 8.3-8.5 °C annual average temperature (Somogyi, 1990). There is only one small village in the basin, Bodony.

Geologically, Paleogene volcanic and sedimentary rocks dominate on the surface. The most common rock types over the whole study area are Eocene andesite, dacite, rhyolite as well as their tuffaceous equivalents with a small amount of

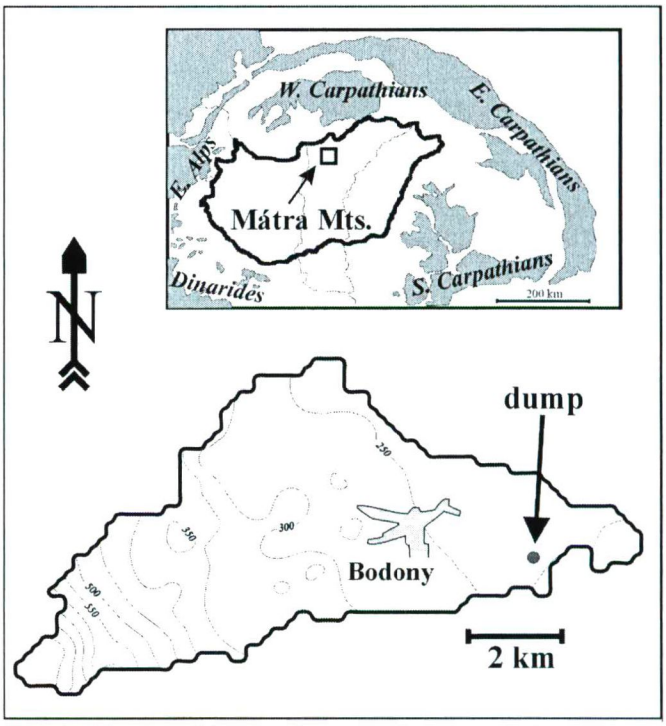

Fig. 1. Topographic sketch map of the studied catchment area. Inset: position of the Mátra Mts. within the framework of the Alp-Carpathian system.

Oligocene clayey sediments in the deeper sub-basins (Báldi, 1983). At places Miocene pyroxene andesite lava flows cover the underlying strato-volcanic complex. Ore minerals of epithermal, porphyry, vein and skarn types are associated with the Eocene andesite. Also Triassic limestone, below the Paleogene formations contains sulphide ore bodies of Cu, Zn, (Cd) and Pb skarn and vein types. Carbonate rocks do not crop out in the area; along the small streams and creeks Pleistocene and Holocene fluvial sediments cover the older formations.

The characteristic soils of the whole catchment area are different subtypes of brown earth (Cambisols and Luvisols). In small patches also Fluvisols, Leptosols (according to the FAO classification; FAO, 1974) occur, following the lithological and/or topographical diversity. Texturally the soils are clayey with only a little regional variation. Physical as well as chemical characters of the soils were mapped based on 150 sampling points with random spatial distribution (Farsang, 1996a, b). Organic material content defines a background of around 2% with a sharp contrast in the forest areas (5%). pH follows the lithological conditions being close to neutral above the loamy sediments and varying around 5 in the parts covered by the volcanic rocks (Fig. 2). The geological background essentially determines large-scale variation of heavy metal content of the soils as well. All studied elements show maximum values at the most elevated areas, where the large relief energy results in thin, lithomorphic soil profiles. Here the volcanic rocks at the surface act as the most important source causing high concentration values. In this paper we recall topsoil (0-20 cm depth) concentration maps of Co and Pb as examples (Fig. 3A, B). On these maps one can follow the co-variation tendency of heavy metal contents with pH and topography. The highest regions consist of volcanic rocks and consequently serve low pH and large heavy element concentration values.

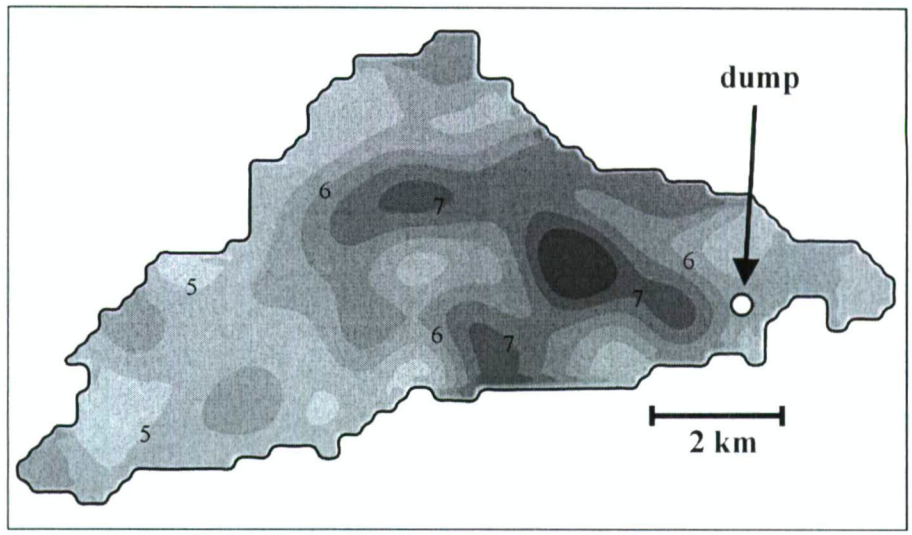

Fig. 2. Spatial pH distribution of the studied catchment area follows lithological variation being around neutral above the loamy sediments and 5-6 on volcanic bedrocks.

The waste rock dump studied can be found at the SE part of the catchment area (Fig. 1). It is a 15 m high hill with a diameter of ~60-70 m at the base (Fig. 4A). The bedrock is andesite, the typical brown earth soil profiles around it are 70-80 cm thick and are covered by a thin layer (up to 3 cm) of the resedimented dump material (Fig. 4B).

Methods

During the geoecological examination of the area, soil samples were collected from 150 points, which represent the topsoil (0-20 cm) and 40 cm depths, respectively. Additional soil profiles represent the surroundings of the potential sources of pollution, including the dump in question. One profile was made at the foot of the dump (P1), and two others away from with a 50 m lag downstream along the northern slope (P2, P3). Each profile was sampled down to the bedrock at every 5 cm.

Following extraction in aqua regia (in a Gerhardt-Kjeldaltherm block), concentrations of Cu, Co, Fe, Mn, Ni, Zn, Cd, Pb and Al were measured using a Perkin Elmer 3010 AAS machine at the University of Tübingen (Germany), following the instructions of Beck et al. (1995). Analytical errors are as listed: Cu: 4%, Co: 3%, Fe: 4%, Mn: 2%, Ni: 5%, Zn: 7%, Cd: 4%, Pb: 8%, Al: 8%. Also pH(H_2O) was measured being a key variable governing heavy metal mobility (Maskall et al., 1995; Gäbler and Schneider, 2000).

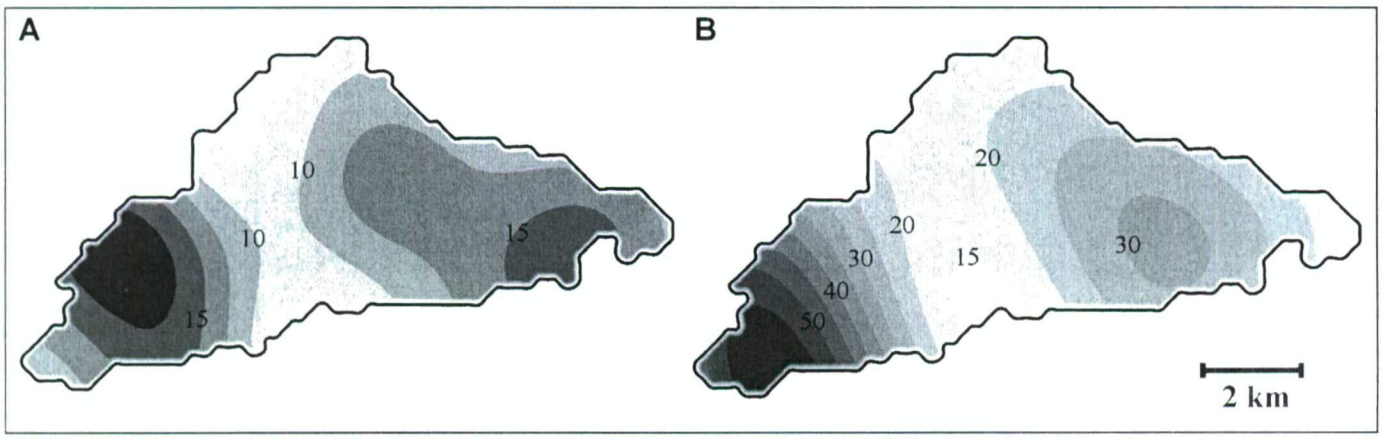

Fig. 3. Regional distribution of selected elements in the whole catchment area. ***(A)*** Co, ***(B)*** Pb. (Isolines in ppm).

The main mineral components of the soil samples were determined by standard XRD methods for different size fractions (0-2 μm, 2-5 μm, 5-10 μm, 10-20 μm, >20 μm) along all profiles. Clay minerals were determined by swelling with glycole in settled preparates. Organic matter (C_{org}) was determined in a Philips PU8675 VISible spectrophotometer following oxidation with $K_2Cr_2O_7$.

In order to specify how different heavy elements do accumulate, XRF measurement on different size fractions (0-2 μm, 2-5 μm, 5-10 μm, 10-20 μm, >20 μm) of the soil profiles P1 and P3 were carried out. Because the amount of the material was insufficient for a standard XRF measurement, we used the energy dispersive spectra. These were compared with standard 10, 50 and 100 ppm spectra for estimating concentrations.

RESULTS

Heavy metal content of the soil profiles

Heavy metal concentration as well as Al, pH(H_2O) and C_{org} data from the 3 soil profiles are given in Table 1. Typical concentrations for each element are in the range common for brown earths (Kloke, 1980), they do not exceed the health limit according to the current Hungarian directives. Only Cu in the topsoil (0-2 cm) of P1 is rather close to it (93 ppm). Vertical distributions of the studied elements exhibit characteristic trends following their common geochemical features. Siderophile elements (Fe, Mn, Co, Ni), which accumulate in the silicate phases of the bedrock reach their maxima in the B horizon at around 40 cm depth. Chalcophile elements (Zn, Cu, Pb) show different kinds of trends (Fig. 5); Zn is decreasing downwards in all cases similarly to Cu in the cases of P1 and P2. Cu is equally low along the whole P3 profile. Pb has a random distribution along the profiles and shows no significant tendency to accumulate.

In the case of the P3 profile, pH does not alter along the section (5.2-5.5) and has similar characteristics to common brown earth soils in the study area. In the two other cases, however, pH exhibits a disturbed trend with a significant increase towards the surface (5.5 → 7.5, Fig. 5).

Qualitative XRD measurements suggest that above 2 μm quartz and K-

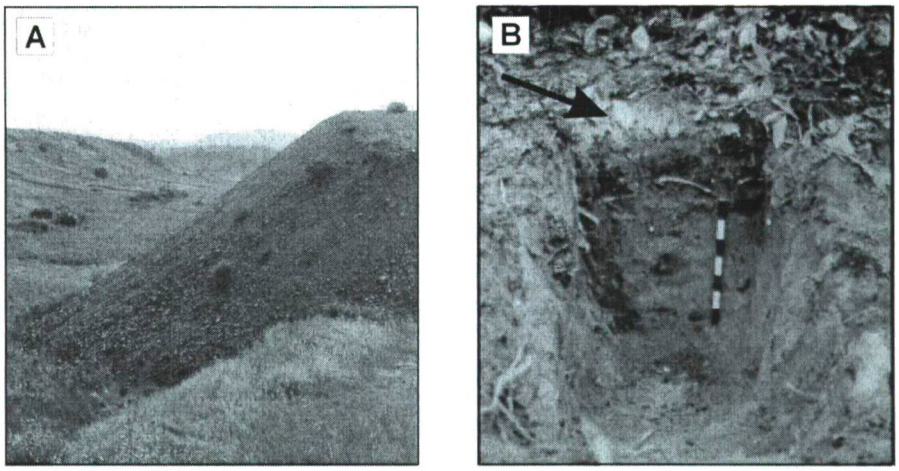

Fig. 4. ***(A)*** Photograph of the studied ore dump looking to the East. Northern slope of the dump was sampled. ***(B)*** The P1 soil profile. Arrow points to the resedimented dump material at the top of the section.

Table 1. Heavy metal and pH data in the soil profiles studied (depth in cm, concentrations in ppm)

	Depth	pH	C_{org}	Zn	Cu	Pb	Co	Ni	Fe	Mn
	2	7.6		80.0	43.0	32.1	15.8	13.0	21350	1063
	5	7.6		80.0	45.0	25.0	15.9	14.8	22310	875
	10	7.6		67.5	37.5	37.5	15.5	14.4	22537	975
	15	7.4		62.5	29.5	36.2	13.7	15.3	21612	1200
	20	7.3		63.8	25.7	19.7	17.4	16.0	22932	1375
	25	7.2		60.0	18.8	25.0	18.2	14.7	20475	1275
	30	6.8		50.0	22.5	35.3	23.3	11.9	22168	1650
P1	35	6.0		53.8	24.0	26.6	22.1	10.3	20783	1400
	40	6.2		52.5	22.2	29.5	15.2	10.1	21400	1062
	45	5.9		48.8	17.5	21.6	16.9	11.4	19806	1012
	50	6.1		52.5	24.7	33.7	13.4	11.6	20993	900
	55	6.3		47.5	27.3	25.3	18.4	13.1	21985	1037
	60	6.3		55.0	28.0	20.0	17.9	16.0	23867	887
	65	6.6		52.5	28.0	14.4	18.4	10.8	23798	825
	70	6.7		55.0	35.7	20.2	17.4	17.6	25595	812
	75	6.7		55.0	32.2	18.7	14.6	12.0	24797	675
	2	7.6		141.3	93.3	33.7	4.7	10.5	12706	112
	5	7.8		58.8	44.0	17.5	12.6	8.3	18987	662
	10	7.7		65.0	36.5	41.3	13.9	11.8	22740	812
	15	7.4		62.5	22.0	38.0	13.5	13.5	22150	1037
	20	7.2		55.0	18.5	23.7	14.9	12.4	20337	1000
	25	7.0		61.3	20.6	32.7	19.4	14.0	23533	1250
	30	6.2		58.8	22.0	39.0	14.9	13.5	23837	1062
P2	35	5.7		55.0	23.7	29.5	16.9	12.1	23450	1187
	40	5.5		52.5	24.3	9.5	18.5	12.2	22672	1275
	45	5.6		50.0	25.1	30.0	23.1	16.8	23626	1275
	50	5.7		80.0	40.8	37.5	24.2	17.7	39125	1437
	55	5.7		52.5	23.8	15.0	14.3	12.1	21568	762
	60	6.1		61.3	26.3	26.2	21.9	11.6	23482	937
	65	6.0		50.0	26.8	33.5	14.3	13.3	23625	787
	70	5.6		52.5	24.8	17.5	22.2	12.4	24303	900
	2	5.3		67.5	20.0	32.0	6.9	13.7	20495	1187
	5	5.3		73.8	20.6	42.5	13.2	14.7	22036	1175
	10	5.4		66.3	20.9	21.3	12.0	19.1	23358	1137
	15	5.3		58.8	17.3	32.9	9.2	11.6	20172	950
	20	5.3		61.3	18.8	35.0	13.4	13.6	22400	1087
P3	25	5.3		60.0	18.8	27.5	14.1	15.1	22662	1487
	30	5.3		53.8	18.8	40.0	16.5	15.5	25075	1412
	35	5.3		53.8	21.9	35.4	25.5	14.5	26975	1937
	40	5.3		50.0	17.5	30.0	17.5	13.5	21781	1250
	45	5.5		48.8	17.5	30.7	22.2	11.6	25850	1375
	50	5.5		48.8	20.3	39.3	17.1	11.9	23100	1025
	55	5.2		60.0	20.0	23.7	21.4	13.5	29187	1262

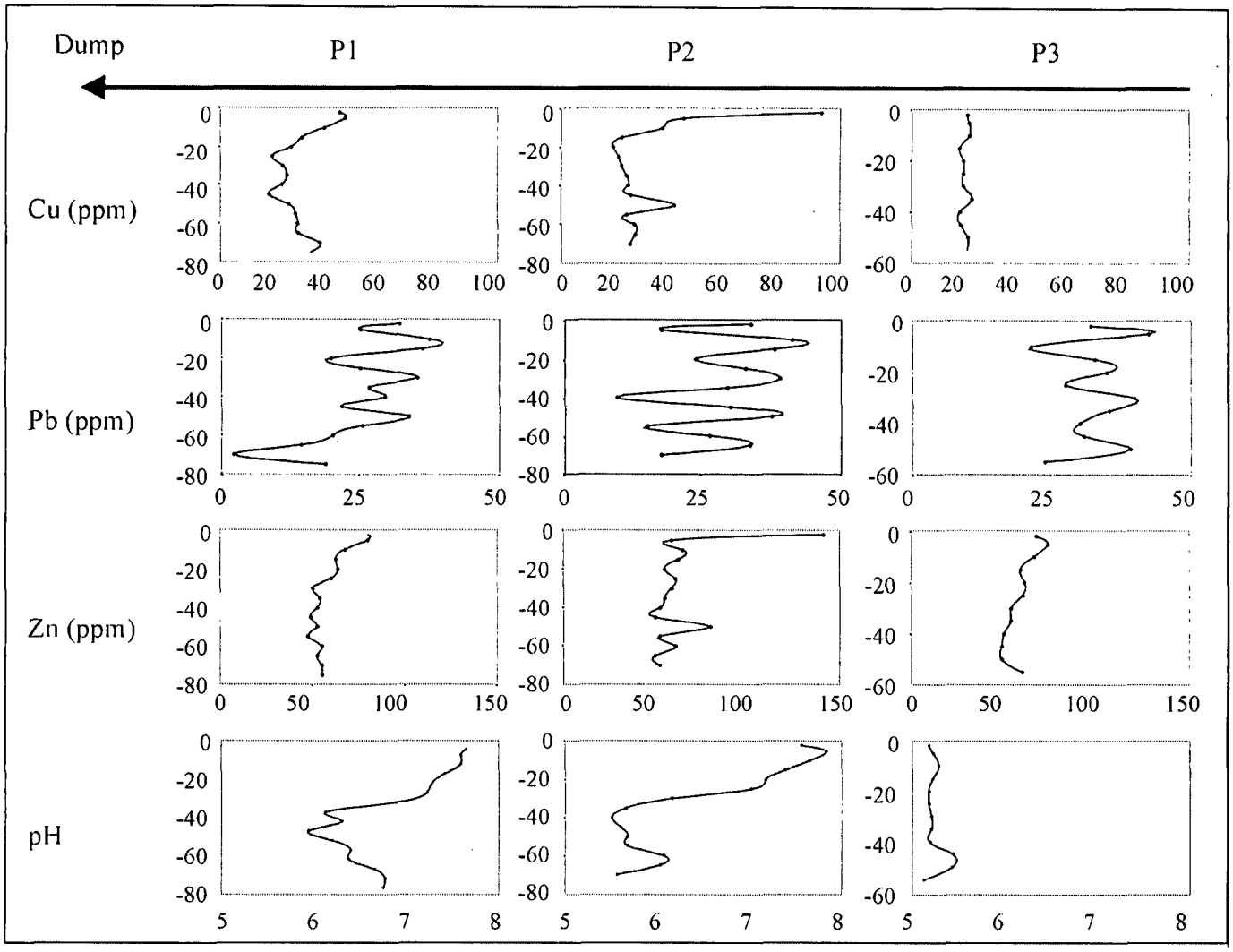

Fig. 5. Vertical variation of Zn, Pb, Cu and pH along the three profiles studied.

feldspar are the dominating phases, while below 2 μm phyllosilicates, over all kaolinite occurs as well. There is only a little detectable variation in the mineralogical composition among the three soil profiles; illite/smectite and chlorite appear exclusively in the P3 profile (Fig. 6). Calcite is present in P1 down to 40 cm, and also in P2 in the upper 20 cm. There is no detectable calcite in P3.

According to the semiquantitative XRF spectra Fe, Mn, Co and Ni reach their peak concentration in the >20 μm grain size fraction, while Cu, Zn and Pb are highest in the 5-10 μm interval.

Mathematical evaluation

In order to be able to compare the vertical variation of the metals and pH quantitatively, geostatistical calculations were made. Concentrations of most elements exhibit a clear dependence on depth as it is shown by their diverse accumulation behaviour. That is, why

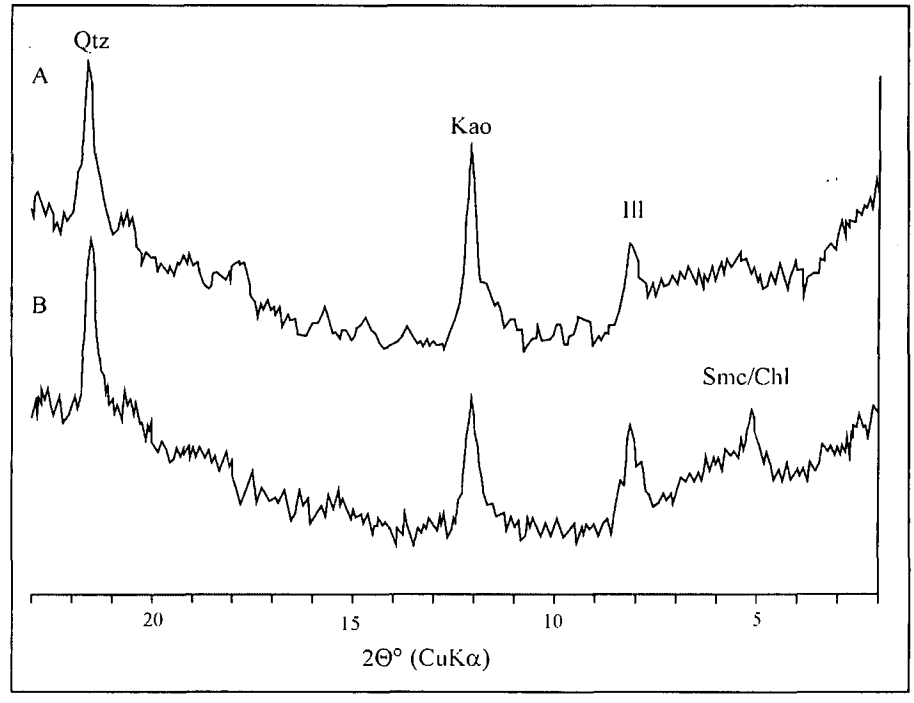

Fig. 6. Selected XRD spectra of settled soil preparates for a) P2, 45-50 cm; b) P3, 45-50 cm

Table 2. The factor score matrix of the three profiles. Significant values are highlighted.

	P1 profile			P2 profile			P3 profile		
Element	factor1	factor2	factor3	factor1	factor2	factor3	factor1	factor2	factor3
Zn	**.88**	-.13	-.22	-.21	**.87**	-.15	-.44	**.85**	.11
Cu	**.71**	.28	-.39	-.38	**.81**	-.29	.44	**.68**	.35
Pb	.35	**-.70**	.00	.54	**.69**	.29	.01	-.19	**.89**
Co	-.24	.01	**.90**	**.66**	-.59	-.14	**.92**	-.29	-.01
Ni	**.65**	.43	.01	**.90**	.01	-.15	.13	**.75**	-.19
Fe	.14	**.94**	-.11	**.89**	-.19	-.25	**.87**	.01	-.21
Mn	.01	-.46	**.83**	**.76**	-.54	-13	**.82**	.13	.12
Al	.34	**.71**	-.40	**.87**	-.22	.01	-.34	**.69**	-.01
pH	**.95**	.01	-.01	-.37	**.60**	.50	.01	-.49	.28
C_{org}	**.76**	-.51	-.04	-.14	-.15	**.84**	**-.62**	.41	.46

prior to variography (e.g. Cressie, 1991), trend functions had to be subtracted. In several cases (Fe, Co, Zn) linear trends were chosen, while in others (Ni, Cu, pH, Mn) a second power function fitted the best. Semivariogram for each variable is of a simple Gaussian type with ranges varying between 15 and 35 cm. Calcophile metals, which accumulate in the topsoil have similar range values for each profile (Zn ~ 23 cm, Cu ~ 21 cm, Ni ~ 18 cm), that is they have an influence down to around 18-23 cm depth. Pb and Mn are rather immobile (Pb ~ 15 cm, Mn ~ 14 cm) opposite to Fe (~ 27 cm) and Co (~ 26 cm). The largest vertical range value is typical for pH (~ 35 cm) in each case.

To emphasize the relationship between the behaviour of different variables, factor analysis (principal component method with varimax rotation) was performed independently for the three profiles. Results are collected in Table 2, where elements with correlation coefficient > 0.6 are pointed out. Calculations resulted in 3 factors in each case suggesting that groups of certain elements have a tendency to change together. Mn, Co and Fe, another one by Cu and Zn can define a group while Al, Pb and Ni alter their positions. Also the role of pH changes from P1 to P3; while for P1 pH has as high as r=0.9 correlation coefficient with Zn and Cu, it has no effect on the elements behaviour in the latter case (r<0.3).

Discussion

Comparison of the profiles

Based on the soil chemical and mineralogical data as well as the statistical results, the laws of the spatial distribution of the heavy metals around the studied dump in the Mátra Mts. can be understood. The three profiles represent different stages of the evolution. While P1 is under the strong influence of the dump material, P3 is almost identical with soils characteristic in other parts of the study area. In this latter case neither positive pH anomaly can be recognized, nor significant chalcophile element accumulation is present in the topsoil. All these values along the whole section are typical for brown earths of the study area. Elements that concentrate in the andesitic bedrock (Fe, Mn, Co) exhibit a clear increasing trend downwards, suggesting lithogene origin in the whole soil profile. The common origin of these elements is also confirmed by the factor analysis. The results show that in case of P3, the „lithogene" factor (Fe, Mn, Co, -C_{org}) has the largest eigen value, suggesting that it determines the chemical nature of the soil. The behaviour of the commonly most conservative Pb is independent of the other chalcophile elements, Cu, Zn and Ni, which have a common peak together with Al; they possibly are adsorbed on clay mineral surfaces. Although, in the whole study area kaolinite dominates the clay mineral fraction, in case of P3 also illite/smectite occurs (c.f. Fig. 6) and could serve as efficient trap for heavy metals because of its high adsorptive capacity (Allard et al., 1991; Lothenbach et al, 1998).

P1 profile, which represents the soil of the dump itself, shows different characteristics. There is a significant accumulation in the topsoil of metals, which redeposit from the dump material (Fig. 4B). Based on the results of the factor analysis, the most determining group of elements is the (Cu, Zn, Ni) concerning the whole profile. In this case also pH varies together with these metals with a very strong positive correlation coefficient. As decomposition of the sulphide ore minerals would significantly decrease pH, in this case another effect should be taken into account. Dissolution of calcite, which is an important constituent of the dump and is also present in the topsoil of P1 and P2, may be responsible for local increase of pH. Calcite disappears close to the bedrock and also pH reaches its normal value (5.5) confirming the above statement. Results of the variography show that pH has a significantly larger range than any metals studied. Although, there is a significant amount of metal on the surface, and in this case the characteristic clay mineral of the soil is kaolinite, which is unable to adsorb the pollution, the locally increased pH may hinder the mobility of Zn, Cu and Ni. As a consequence, the ranges of the metals in the case of P1 are analogous with those calculated in the case of P3.

P2, which lies between the two previous profiles geographically, shows intermediate features concerning the soil chemistry as well. Here, similarly to P3 the lithogene factor (Fe, Co, Mn) has the largest significance characterizing the soil chemistry. On the other hand, there still is a significant role of calcite redeposition and dissolution resulting in a tight connection between pH and the (Cu, Zn Ni) group. Complex behaviour of this profile proves that pH has a broad influence regime not only vertically (range > 30 cm in each case), but also horizontally.

Presence of carbonate minerals is rather strange in the volcanic rocks dominated surface; strictly speaking, they are pollutants around the dump. In the studied brown earth soils, however, which generally are characterized by low pH values and clay minerals of low cation adsorption capacity (kaolinite), calcite helps to diminish metal mobility through increasing pH locally. Data suggest that basically the pH-barrier balanced by calcite deposition and dissolution is

responsible for the fact that P3 profile 150 m far from the dump may chemically be unpolluted. Dudley et al. (1991) described similar sorption effect between natural calcareous soils and acid mine waste. The process essentially is the natural analogue of the crushed limestone barriers commonly applied to mitigate heavy metal migration via adsorption and metal-carbonate fixation (e.g. Artiole and Fuller, 1979). Behaviour of the studied dump also is in harmony with the observations of Tyler and Olsson (2001) who measured decreasing element mobility when adding extra $CaCO_3$ to different soils.

Regional consequences

To determine the sensibility of the soils to heavy metals in the whole catchment area, a buffer capacity map was constructed for each metal based on the values of pH, C_{org} and mechanical structure. Following the algorithm of Marks et al. (1989) buffer capacity can be coded with an integer between 1 and 5 (for details see Farsang, 1996b). In this calculation only those 150 soil samples, which are not under the influence of any dumps were involved. Maps for Ni, Cu and Cd, respectively are presented on Fig. 7. In its present state, the soils buffer Cu and Pb well in the whole catchment, while in the case of Ni and Zn also areas with lower buffer capacity exist. Areas with average or low buffer capacity are the most common in the case of Cd, also the dump studied is located in a region where Cd is buffered insufficiently. A theoretical model, in which we decrease pH values with 1.0 in each datum point, shows that buffer capacity maps would change significantly due to such a supposed environmental effect. In this case not only Cd, but also Ni and Zn would easily be mobilized making the dump possibly dangerous for its close surrounding. Cu and Pb, on the other hand, would not mobilize even in this extreme situation (Fig. 8).

Nevertheless, as we discussed previously, in addition to regional characteristics, the dump studied has its own mechanism to control the mobility of heavy metals. Because relatively large pH around the dump is set up by calcite, which phase deposits and dissolves from the dump material itself, there is no way to get such an acid soil which would be dangerous.

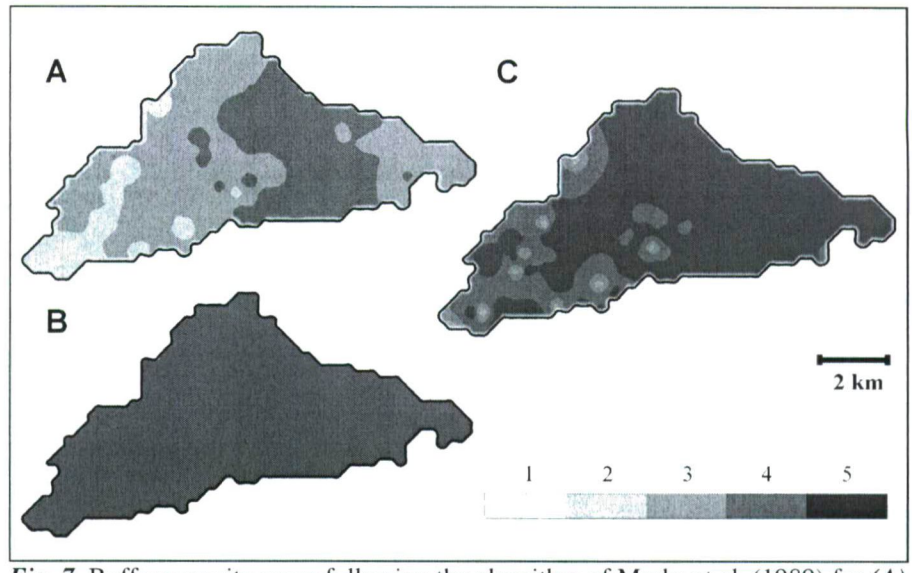

Fig. 7. Buffer capacity maps following the algorithm of Marks et al. (1989) for ***(A)*** Cd, ***(B)*** Cu, ***(C)*** Ni.

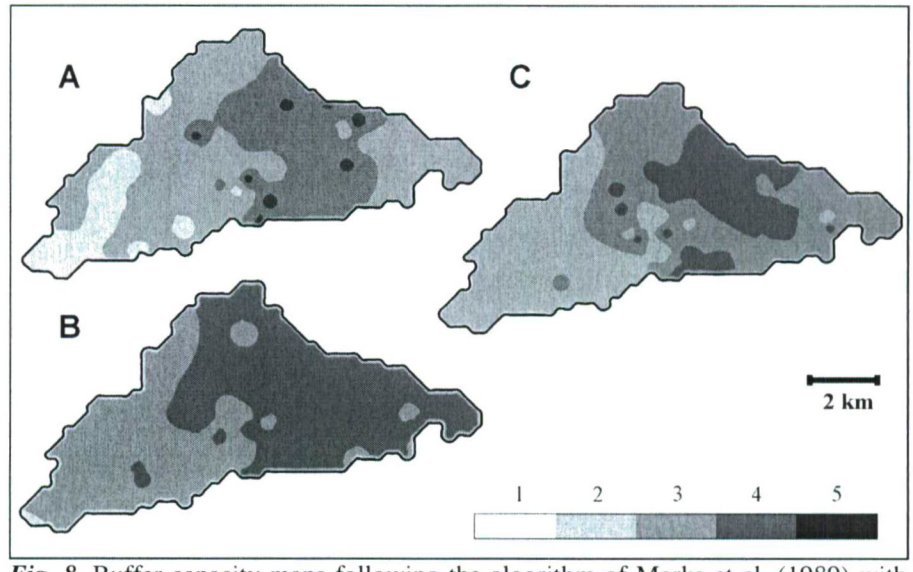

Fig. 8. Buffer capacity maps following the algorithm of Marks et al. (1989) with decreasing pH values by 1.0 for ***(A)*** Cd, ***(B)*** Cu, ***(C)*** Ni.

CONCLUSIONS

In conclusion we can state that

- due to resedimentation of the dump material as well as transportation with rain water, Zn and Cu accumulate in the upper horizon of the surrounding soils,
- local deposition and dissolution of calcite increases pH in the close surrounding of the dump,
- the vertical as well as the horizontal movement of Zn, Ni and Cu are hindered due mainly to intermediate pH value. Pb is buffered under each possible conditions well and remains immobile,
- the dump has no environmental risk at its present condition and under possible environmental changes.

ACKNOWLEDGMENTS

The Internationales Zentrum, Tübingen, sponsored researches of the second author at the University of Tübingen. Thanks to Prof. K.-H. Pfeffer for making the AAS measurements possible and to R. Beck for his sincere help. Thanks go to Bertalan Á. (Dept. Mineralogy, Geochemistry and Petrology., University of Szeged) for XRD and XRF measurements. The thorough reviews of Földessy J. and Sipos P. improved the manuscript significantly. Philip Glover is thanked for cleaning the English.

REFERENCES

ALLARD, B., HAKANSSON, K., KARLSSON, S., SIGAS, E. (1991): Field study of diffusion controlled migration of copper, zinc and cadmium in clay formations. Water, Air and Soil Pollution, **57-58**, 259-268.

ARTIOLE, J., FULLER, W. H. (1979): Effect of crushed limestone barriers on chromium attenuationin soils. Journal of Environmental Quality, **8**, 503-510.

BÁLDI, T. (1983): Magyarországi oligocén és alsómiocén formációk. Akadémiai Kiadó, p. 293.

BECK, R., BURGER, D., PFEFFER, K. H. (1995): Laborskript (Ein Handbuch für die Benutzer der Laboratorien der Physischen Geographie der Univesitat Tübingen). Selbstverlag des Geographisches Institut der Universität Tübingen.

CRESSIE, N. A. (1991): Statistics for spatial data. Wiley & Sons, New York.

DUDLEY, L. M., MCLEAN, B. L., FURST, T. H., JURINAK, J. J. (1991): Sorption of Cd and Cu from acid mine waste extract by two calcareous soils: column studies. Soil Science, **151**, 121-135.

FAO, (1974): FAO/Unesco Soil map of the World.

FARSANG, A. (1996a): Regionale Untersuchungen von Bodenschwermetallen (Kausalstudie in Mátra). Tübinger Geographische Studien - Interaktion von Ökologie und Umwelt mit Ökonomie und Raumplanung, Heft 116, 135-152

FARSANG, A. (1996b): Regional analysis of heavy metal content of soils on the NE pediment of the Mátra Mts. Acta Geographica Szegediensis, **33**, 65-81

GÄBLER, H, E., SCHNEIDER, J. (2000): Assesment of heavy-metal contamination of floodplain soils due to mining and mineral processing in the Harz Mountains, Germany. Environmental Geology, **39** (7), 774-782.

KLOKE, A. (1980): Richtwerte '80, Orientierungsdaten für tolerierbare Gesamtgehalte einiger Elemente in Kulturböden. Mitteilungen VDLUFA,Heft 1-3.

KORTE, N. E., SKOPP, J., FULLER, W. H., NIEBLA, E. E., ALSEII, B. A. (1976): Trace element movement in soil, influence of soil physical and chemical properties. Soil Sciences, **122**, 350-359.

LOTHENBACH, B., KREBS, R., FURRER, G., GUPTA, S. K., SCHULIN, R. (1998): Immobilization of Cd and Zn in soil by Al-montmorillonite and gravel sludge. European Journal of Soil Science, **49**, 141-148.

MARKS, R., MÜLLER, M. J., LESER, H., KLINK, H. J. (1989): Anleitung zur Bewertung des Leistungsvermögens des Landschaftshaftshaushaltes. Forschungen zur Deutschen Landeskunde, Band 229. Selbstverlag, Trier, p. 222

MASKALL, J., WHITEHEAD, K., THORNTON, I. (1995): Heavy metal migration in soils and rocks at historical smelting sites. Environ Geochem Health., **17**, 127-138

MERRINGTON, G., ALLOWAY, B. J. (1994): The flux of Cd, Cu, Pb and Zn in mining polluted soils. Water, air and soil pollution, **73**,

MEZŐSI, G., RAKONCZAI, J. (eds.) (1997): A geoökológiai térképezés elmélete és gyakorlata. (Theory and practice of geoecological mapping.) Department of Physical Geography, University of Szeged, Szeged. (in Hungarian)

SOMOGYI, S. (ed.) (1990): Magyarország kistájainak katasztere II. (Register of small landscapes in Hungary II.) MTA FKI, Budapest, 1023 p. (in Hungarian)

TYLER, G., OLSSON, T., (2001): Concentration of 60 elements in the soil solution as related to the soil acidity. European Journal of Soil Science, **52**, 151-165.

Received: August 10, 2003; accepted: October 29, 2003

2ND MID-EUROPEAN CLAY CONFERENCE
MECC'04, 20–24 September, 2004, Miskolc, Hungary

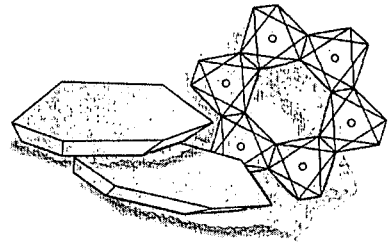

INTERNATIONAL WORKSHOP ON CURRENT KNOWLEDGE ON THE LAYER CHARGE OF CLAY MINERALS
LCCM'04, 18–19 September, 2004, Smolenice, Slovakia

GENERAL INFORMATION

The MECC is the joint conference of the national clay groups of Poland, Slovakia, Croatia and Hungary.

The plan of joint meetings of the Mid-European clay groups was decided during the EUROCLAY Meeting in Kraków, Poland in 1999, and supported by the European Clay Groups Association (ECGA). The aim of these tri-annual meetings is to promote co-operation and exchange of ideas among specialists of neighbouring countries. Participants from other countries of Europe and from other continents are welcomed.

The first conference MECC'01 was organised by the Slovak Clay Group in 2001 in Stará Lesná, Slovakia (114 participants from 18 European + 4 overseas countries). MECC'04 will be organised in Hungary.

CONFERENCE DATE AND PLACE:

September 20–24, 2004, Conference Centre of the University of Miskolc, Miskolc, Hungary

SCIENTIFIC PROGRAMME

Contributions from all fields of clay research are welcomed.

Key topics: Crystal chemistry and structure; Physical and chemical properties of clays; Colloidal properties and surface chemistry; Advanced instrumental techniques; Genesis and synthesis; Geology of clays; Clays in soils and weathering; Environmental application of clays; Clays in industry.

Special attention will be paid to themes of local interest such as: clay-organic reactions; phyllosilicates of very low-grade metamorphism; diagenesis, basin analysis, palaeosols and fossil weathering crusts; bentonite and illite deposits; iron in clay minerals; environmental and geotechnical applications etc.

REPRESENTATIVES OF THE LOCAL SCIENTIFIC COMMITTEE

Chairman: István Viczián, Hungary; Krzysztof Bahranowski, Poland, Goran Durn, Croatia, Peter Komadel, Slovakia

REPRESENTATIVES OF THE LOCAL ORGANISING COMMITTEE

Chairman: Tamás G. Weiszburg; University of Miskolc: József Bőhm, Hungarian Geological Society: Endre Dudich

ABSTRACTS

Participants are invited to submit contributions in the field of the scientific programme. The abstracts will be published in ***Acta Mineralogica-Petrographica, Abstract Series, Szeged***. For details please refer to the Second Circular.

IMPORTANT DATES

Deadline for returning the First Circular	**October 15, 2003**
Second Circular (only in electronic form, downloadable from the web site)	**November 15, 2003**
Deadline for grant applications	**February 29, 2004**
Deadline for abstracts and for paying normal registration fee	**May 31, 2004**

ORGANISERS

Faculty of Earth Science and Engineering, University of Miskolc, Hungary
Hungarian Geological Society
on behalf of the Clay Groups of Slovakia, Poland, Croatia and Hungary

SCIENTIFIC SPONSORS (PRELIMINARY LIST)

European Clay Groups Association (ECGA)
Commissions of HAS
on Geochemistry, Mineralogy and Petrology and on Colloids and Material Science
IUGS Hungarian National Committee

ADDRESSES FOR CORRESPONDENCE AND INFORMATION

MECC'04
c/o Department of Mineralogy and Petrology
University of Miskolc
H-3515 Miskolc, Egyetemváros, HUNGARY
Fax: +36-46-563 465
e-mail: mecc04@gold.uni-miskolc.hu
http://www.uni-miskolc.hu/mecc04

LCCM'04
Institute of Inorganic Chemistry, SAS
SK-845 36 Bratislava, SLOVAKIA
e-mail: uachlach@savba.sk
http://www.lach.sav.sk

*Acta Mineralogica-Petrographica, Szeged 2003, Vol. **44**, pp. 31-34*

ACTA
Mineralogica
Petrographica

MINERALS OF THE CARPATHIANS: FIRST UPDATE

BOGDAN P. ONAC

Department of Mineralogy, Babeş-Bolyai University, Kogalniceanu 1
Emil Racoviţă Institute of Speleology, Clinicilor 5
3400 Cluj-Napoca, Romania
e-mail: bonac@bioge.ubbcluj.ro

ABSTRACT

A number of rare minerals were recently discovered in different caves from Romania. Fifteen of them were identified for the first time in the Carpathians. The aim of this paper is to briefly summarize data on those mineral species published in various journals as an update to the recently published topographical mineralogical handbook of the Carpathians. Chemical and mineralogical characterization of these minerals was undertaken by X-ray powder diffraction and fluorescence analyses, energy-dispersive, atomic absorption, infrared spectrometry, thermal and electron-microprobe analyses, optical, transmission, and scanning electron microscope observations.

Key words: Cave minerals, Romania, secondary minerals, topographical mineralogy.

INTRODUCTION

Over 1000 mineral species were recently compiled in a comprehensive handbook on the Minerals of the Carpathians (Szakáll, 2002). The core of the book consists of a systematic description of 1000 valid mineral species following Dana's system of classification. Each entry describes the more important occurrences and the most interesting forms of the given mineral. Also included with the description are the size of the mineral and its color, presence of twins, and accompanying minerals. Crystallographic system and ideal formula of the mineral is given in the heading of the entry.

The following descriptive article follows the pattern of the book, providing the first update to Szakáll's book on the mineralogy of the Carpathians. The entries listed in this paper (except for jokokuite) consist of new species described from various caves in Romania. Since the fifteen minerals presented in this paper have been characterized in detail in several published articles, we are now beginning to integrate the information concerning them. By doing this, it is our hope to help the editor of the next edition of the Minerals of the Carpathians by providing quick access to this mineralogical information. The specimens discussed in this article are deposited in the Mineralogical Museum of the „Babeş-Bolyai" University and at the „Emil Racoviţă" Institute of Speleology in Cluj-Napoca and Bucharest, Romania.

MINERALS DISCOVERED BEFORE 2002

Monohydrocalcite, $CaCO_3 \cdot H_2O$ (hexagonal), was reported to occur in the composition of white hydrated moonmilk in Humpleu and Lucia Mică caves (Bihor Mts.) (Onac and Ghergari, 1993). This mineral was identified by means of X-ray powder diffraction (XRD) and transmission electron microscope (TEM). TEM analyses revealed partial pseudomorphs of calcite after monohydrocalcite (Fig. 1).

Darapskite, $Na_3(SO_4)(NO_3) \cdot H_2O$ (monoclinic) and *nitratine*, $NaNO_3$ (trigonal) were found closely associated in a thin layer (~50 cm) just below a guano horizon and overlying some gravels and clays that accumulated on the floor of Şălitrari Cave (Cerna Mts.) (Diaconu and Lascu, 1999). No further information on the appearance (color, morphology etc.) of these nitrates was given. The authors suspect that the two minerals formed due to the thermomineral water activity upon guano deposits under a warm and dry cave environment.

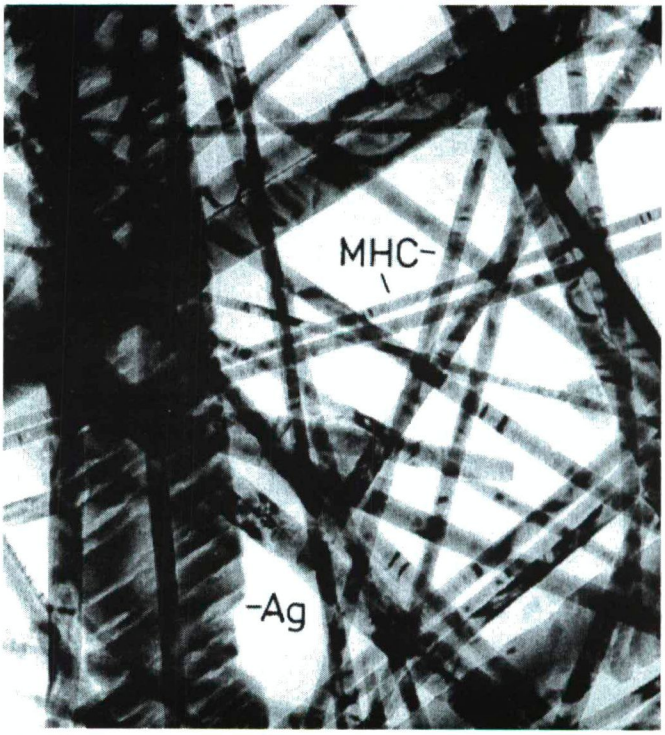

Fig. 1. Partial pseudomorphs of calcite after monohydrocalcite (Ag = aragonite; MHC = monohydrocalcite).

MINERAL SPECIES DESCRIBED DURING 2002-2003

Carbonates

Burbankite, $(Na,Ca)_3(Sr,Ba,Ce)_3(CO_3)_5$ (hexagonal) appears as a thin crust composed of sub-millimeter yellow grayish anhedral crystals. This rare anhydrous carbonate was found in association with colorless or milky white needle-like brushite and gypsum crystals in Cioclovina Cave, Şureanu Mts. (Onac et al., 2002). Its identification relies on XRD and energy dispersive spectrometry. Burbankite was precipitated under dry and either poor or no drainage conditions from alkali-rich carbonate solutions.

Glaukosphaerite, $(Cu,Ni)_2(CO_3)(OH)_2$ (monoclinic) occurs in the Water Cave (Peştera cu Apă) from Codreanu mine (Băiţa, Bihor county) as thin coatings of deep green color in association with malachite and rosasite (Onac, 2002). The diffraction data for glaukosphaerite and rosasite differ significantly, allowing them to be easily distinguish where they coexist. The calculated unit cell parameter corresponds closely to those values reported in PDF 27-178, which supports the stoichiometry. In thin section glaukosphaerite displays fibrous green spherulites and is biaxial negative.

Lansfordite, $MgCO_3 \cdot 5H_2O$ (monoclinic) was first described as a cave mineral from Valea Rea Cave (Bihor Mts.) where it appears as fine white powdery masses associated with hydromagnesite (Onac and Feier in prep.). Lansfordite seems to have precipitated from CO_3^{2-}-depleted and HCO_3^--rich magnesium solutions at temperature below 8°C.

Norsethite, $BaMg(CO_3)_2$ (trigonal) appears as sub-millimeter well-crystallized milky white nodular aggregates on the walls of two skarn-hosted caves: Crystal (Peştera cu Cristale) and Surprise (Peştera Surpriză) in the Băiţa metallogenic district (Bihor county). The chemical composition of norsethite was obtained by atomic absorption spectroscopy (AAS) and its corresponding structural formula was found to be $BaMgFe_{0.01}(CO_3)_{1.99}$. There is no information on the way this mineral was precipitated in the cave environment (Onac, 2002).

Sulfates

Cesanite, $Na_3Ca_2(SO_4)_3(OH)$ (hexagonal) was found closely associated with hydroxylapatite as ochre to red-brown crusts along the walls in Măgurici Cave (Someş Plateau). Cesanite is a rare sulfate and so far documented only from a single cave location (Onac et al., 2001). This hydroxylated double salt is isostructural with hydroxylapatite, with three Ca^{2+} replaced by three Na^+ and three PO_4^{3-} replaced by three SO_4^{2-}, maintaining charge balance within the structure (Onac and Vereş, 2003). Hence, the close association of the two minerals in some of the investigated samples is expected. We assume, in the absence of any data on cesanite stability at low temperature that the crystallization sequence is as follows: first to precipitate is hydroxylapatite and then cesanite from the Ca-depleted, Na- and SO_4^{2-}-enriched solutions. The presence of both gypsum and mirabilite in Măgurici Cave may have been crucial to cesanite precipitation.

Jokokuite, $Mn^{2+}SO_4 \cdot 5H_2O$ (triclinic), is a member of the chalcanthite group and forms pale pink, rosette-like aggregates (2-3 cm in diameter) intimately associated with rozenite (Fig. 2). The jokokuite crystals have a vitreous luster

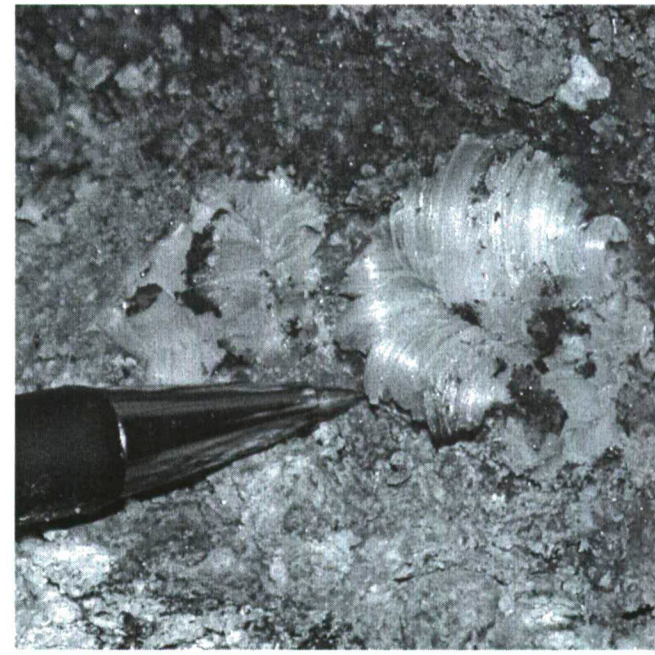

Fig. 2. Rosette-like aggregates of rozenite and jokokuite in an old adit from Roşia Montană.

and show no cleavage (Onac et al., 2003). The energy-dispersive analyses (EDS) of the pink rosette-like crystals revealed Mn, S, and O to be the major elements with Fe appearing as a minor constituent. The average cell parameters obtained on the basis of 24 X-ray powder reflections are a = 6.36(5) Å, b = 10.75(9) Å, c = 6.12(2) Å, α = 98.93(1)°, β = 109.96(5)°, γ = 75.11(9)°, and V = 379.81(1) Å^3. These values are nearly identical to those from PDF 31-836 suggesting a pure compound.

Phosphates

Berlinite, $AlPO_4$ (hexagonal) was found as grayish or colorless fine crystals in vacuoles and along cracks in well-cemented clay or impregnated in the body of this clay in Cioclovina Cave (Onac et al., 2002) (Fig. 3). The XRD pattern and the hexagonal unit-cell of the Cioclovina berlinite

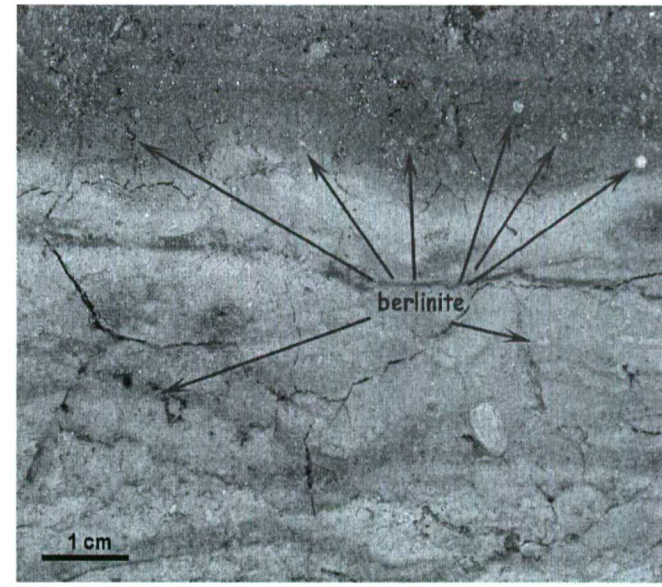

Fig. 3. Berlinite crystals within phosphate-rich sediments from Cioclovina Cave.

specimen compare well with other published determinations. The lattice parameters are a = 4.94(4) Å, c = 10.87(1) Å, V = 230.1(3) Å^3. Microprobe analyses confirmed a nearly ideal formula for berlinite. In situ guano combustion (temperature around 550°C) is responsible for the transformation of taranakite and for the dehydration of variscite into berlinite (Onac and White, 2003).

Collinsite, $Ca_2(Mg,Fe^{2+})(PO_4)_2 \cdot 2H_2O$ (triclinic) appears as translucent millimeter thin-walled hollow spherules lining dissolution cavities within a thick hydroxylapatite crust collected from Cioclovina Cave. The mineral was identified by means of XRD and is believed to have precipitated from bat guano in damp, near-neutral pH environment (Onac et al., 2002).

Foggite, $CaAl(PO_4)(OH)_2 \cdot H_2O$ (orthorhombic) occurs within black aggregates having earthy consistence that were collected from below brown-reddish crandallite-rich clays in Cioclovina Cave (Onac et al., 2002). XRD was used to identify the mineral. Foggite seems to be the result of partial decomposition of crandallite. More investigations are planned to shed light on the presence of this mineral in the cave environment.

Francoanellite, $H_6(K,Na)_3(Al, Fe^{3+})_5(PO_4)_8 \cdot 13H_2O$ (trigonal) forms soft and unctuous to the touch, white nodular aggregates (3 to 50 mm in diameter) and earthy masses in the lower part of the fresh guano that overlies the argillaceous floor deposits in Măgurici Cave. XRD indicated that the mineral is francoanellite. Its XRD patterns exhibit similar d-values with taranakite except at the initial part of the diffraction spectra ($2\theta < 20°$). The difference in water content between the two hydrated phosphates leads to a noticeable variation of the c value (97.6 Å for taranakite and 83.2 Å for francoanellite). The a values, however, are identical (8.70 Å) for both minerals (Onac and Vereş, 2003). All francoanellite samples inspected by means of SEM revealed the presence of thousands of pseudohexagonal crystals (Fig. 4). The partial dehydration of taranakite has resulted in the precipitation of francoanellite.

Leucophosphite, $KFe_2^{3+}(PO_4)_2(OH) \cdot 2H_2O$ (monoclinic) forms thin pale yellowish-brown crusts (less than 1 mm thick) within white taranakite veins in a section below the Bivouac Room, Cioclovina Cave (Onac et al., 2002). XRD was used to identify the mineral. Leucophosphite may be the final product of the reaction between H_3PO_4 (derived from the leached guano) and illite in the presence of iron hydroxides.

Phosphammite, $(NH_4)_2HPO_4$ (monoclinic?) occurs as sparse, colorless, and transparent anhedral crystals (0.5 mm in size) in the lower part of a dry decomposed guano deposit hosted in Măgurici Cave (Onac and Vereş, 2003). The XRD data and the unit cell of the Măgurici specimen showed a striking similarity to that of artificial phosphammite as recorded in the PDF 29-111. This similarity indicates an almost pure compound. As in the other known occurrence (Bridge, 1973), phosphammite was precipitated in an early stage from the liquid fraction of guano. This unusual occurrence of phosphammite in a cave from a temperate region provides evidence that the highly soluble phosphate mineral may persist even in relatively moist environments as long as the temperature "within" the dry fossil guano deposit is almost twice the annual average within the cave.

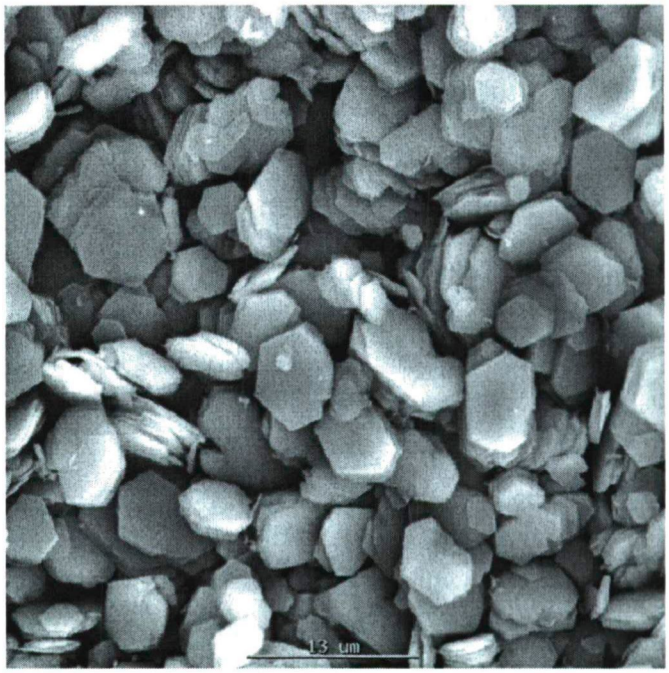

Fig. 4. SEM image of pseudohexagonal crystals of francoanellite from Măgurici Cave.

Tinsleyite, $KAl_2(PO_4)(OH) \cdot 2H_2O$ (monoclinic) appears as an early diagenetic mineral, in small quantities, as composite aggregates in the bat guano deposit in Cioclovina Cave. The mineral association (tinsleyite, quartz, and K-bearing clay minerals) suggests that highly concentrated phosphoric acid solutions from guano reacted with illite to form quartz and tinsleyite (Marincea et al., 2002).

ACKNOWLEDGEMENTS

This paper is part of the CNCSIS grant #1696 to B. P. Onac. The author thanks Joe Kearns for critically reading an early version of the manuscript.

REFERENCES

BRIDGE, P. J. (1973): List of cave minerals in the Simpson and Mineral Division collections of the Western Australian Government Chemical Laboratories: II. The Western Caver, **13**, 193-197.

DIACONU, G., LASCU, C. (1999): Preliminary data about nitrates in "Peştera Mare de la Şălitrari", Cerna Mountains, Romania. Theoretical and Applied Karstology, **11-12**, 47-52.

MARINCEA, Ş., DUMITRAŞ, D., GIBERT, R. (2002): Tinsleyite in the "dry" Cioclovina Cave (Sureanu Mountains, Romania). European Journal of Mineralogy, **14**, 157-164.

ONAC, B. P., MYLROIE, J. E., WHITE, W. B. (2001): Mineralogy of cave deposits on San Salvador Island, Bahamas. Carbonates and Evaporites, **16**, 8-16.

ONAC, B. P. (2002): Caves formed within Upper Cretaceous skarns at Băiţa, Bihor County, Romania: mineral deposition and speleogenesis. The Canadian Mineralogist, **40**, 1551-1561.

ONAC, B. P., BREBAN, R., KEARNS, J., TĂMAŞ, T. (2002): Unusual minerals related to phosphate deposits in Cioclovina Cave, Şureanu Mts. (Romania). Theoretical and Applied Karstology, **15**, 27-34.

ONAC, B. P., GHERGARI, L. (1993): Moonmilk mineralogy in some Romanian and Norwegian caves. Cave Science, **20**, 107-111.

ONAC. B. P., VEREŞ, D. Ş. (2003): Sequence of secondary phosphates deposition in a karst environment: evidence from Măgurici Cave (Romania). European Journal of Mineralogy, **15**, 741-745.

ONAC, B. P., VEREŞ, D. Ş., KEARNS, J., CHIRIENCO, M., MINUŢ, A., BREBAN, R. (2003): Secondary sulfates in an old adit from Roşia Montană, Romania. Studia Universitatis Babeş-Bolyai, Geologia, **XLVIII**, 29-44.

ONAC, B. P., WHITE, W. B. (2003): First reported sedimentary occurrence of berlinite ($AlPO_4$) in phosphate-bearing sediments from Cioclovina Cave, Romania. American Mineralogist, **88**, 1395-1397.

SZAKÁLL, S. (ed.) (2002): Minerals of the Carpathians. Granit, Prague, 480 p.

Received: June 10, 2003; accepted: October16, 2003

*Acta Mineralogica-Petrographica, Szeged 2003, Vol. **44**, pp. 35-41*

ACTA Mineralogica Petrographica

THE HYDROGEOLOGICAL ASPECTS OF LAKE FEHÉR, KARDOSKÚT, SOUTHERN HUNGARY

BERTALAN BUSA-FEKETE[1], RÓBERT HEGYI[1], JÁNOS SZANYI[2]

[1] Department of Mineralogy, Geochemistry and Petrology, University of Szeged
H-6701 Szeged, P. O. Box 651, Hungary
[2] Hungarian Geological Survey Szeged Office
H-6721 Szeged, Sóhordó u. 20, Hungary
e-mail: szanyi@iif.u-szeged.hu

ABSTRACT

The Lake Fehér near Kardoskút village (Békés County, S Hungary) is a highly protected area of the Körös-Maros National Park (Fig. 1). The regular desiccation of the lake violates the habitat of the migrating birds. In order to understand the mechanisms of the water supply of the lake, six groundwater-monitoring wells and two water gauges were made in the area. Data were evaluated by geostatistical methods. Water levels in the two automatically measured monitoring wells changed differently with precipitation. One, which was located in the southern margin of the lake, responded to precipitation immediately and also with a twelve-day delay. While the other one, situated between the lake and the canal, had not any significant reactions. Groundwater flow direction is towards the canal (Fig. 3) every time, independently of the season. The canal, depending on water level in it, disturbs groundwater flow. Based on pressure-elevation profiles [p(z)], upward flow from deeper layers was established. Chemical data supported upward flow too.

Key words: groundwater flow, discharge area, water chemistry, pressure-elevation profile [p(z)]

INTRODUCTION

The Lake Fehér near the village of Kardoskút, is the largest lake in the Körös-Maros Interfluves, located about 12 km southwestward from the town of Orosháza (Fig. 1). The East-West extension of its basin is 3,6 km, divided by an artificial dam. The widest north-south extension of its western part is 500 m, however, that of its eastern part is less than 100 m in many places. The area belongs to the small landscape called the Csongrád Plain. There are no significant differences in the relief. Its value is ranging between 85 to 88 m a.s.l.. The lake is the largest highly protected area of the Körös-Maros National Park. Year by year, it serves as a resting place for some hundred thousands of birds of passage, therefore, it is protected by the Ramsari Convention. The lake, as it is common for salt lakes, dries out in every summer. Arid climatic conditions, characteristic for the last one and a half decade have caused serious problems in the water balance of the lake. Therefore, understanding the mechanisms of water recharge is of crucial importance.

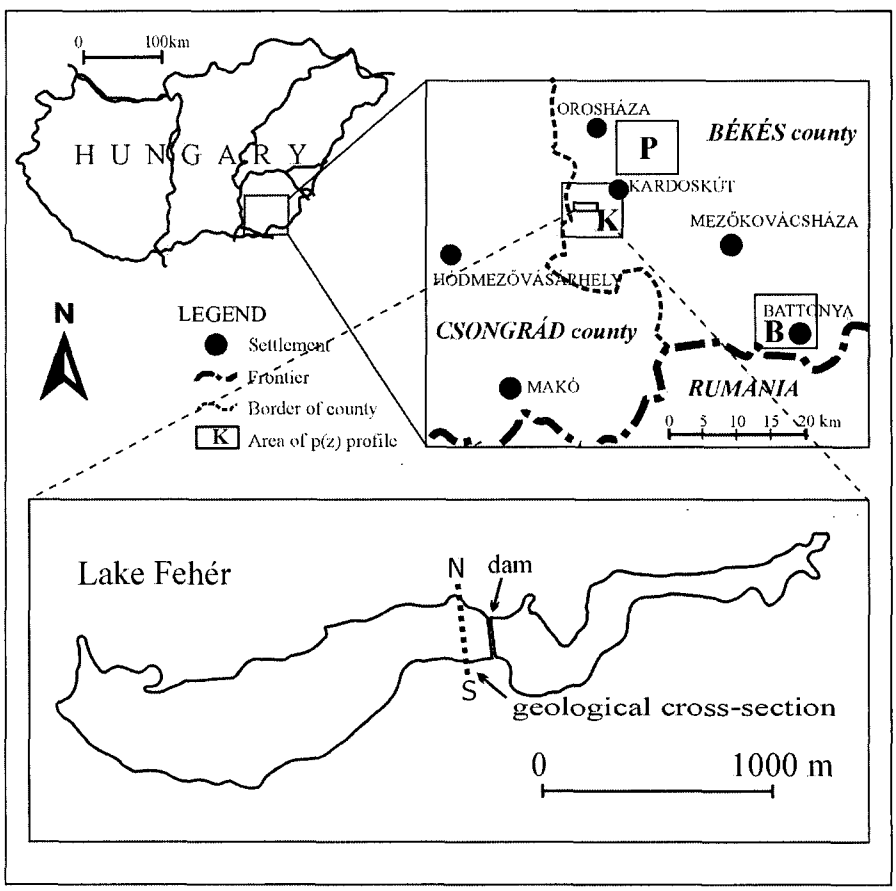

Fig. 1. Location of the Study area.

This study intends to justify the significant role of groundwater in the water recharge of the lake. The major aim of this study is to establish the character of the hydrogeological regime in the environment of the lake.

GEOLOGICAL AND ENVIRONMENTAL SETTINGS

There are several theories about the origin of the lake. The lake basin is regarded as a cut-off channel of the ancient River Maros. The basin was developed in a Pleistocene depression during the beginning of the Upper Würmian (Molnár and Mucsi, 1966; Sümegi, 1999). The region is located between two sub-basins – the area of the Rivers Körös and the mouth of the River Maros. The environment is built up from alluvial sediments and loess, which were deposited at the end of the Pleistocene on sandy layers of some meters thick.

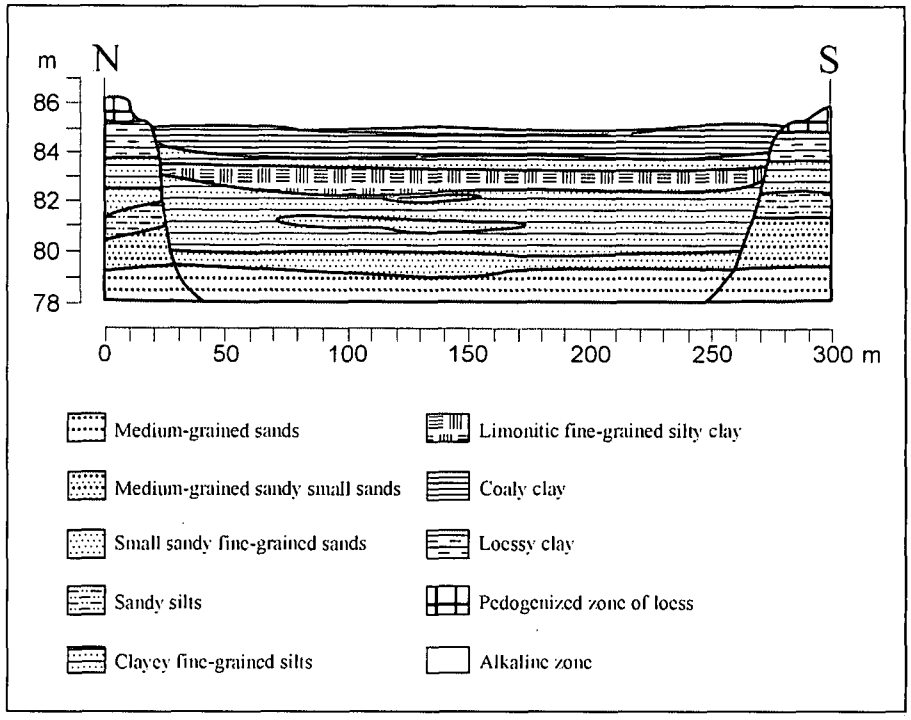

Fig. 2. N-S Geological cross-section of Lake Fehér (after Sümegi et al. 1999).

On the basis of litho- and biofacies analyses, these sediments must have been deposited in a slowly moving or stagnant aquatic environment characterized by rich palustrine vegetation (Sümegi et al., 1999). Due to groundwater fluctuations, salty layers could have formed in the near-surface layers of the loess-like sediments of high clay and carbonate content within a relatively short time. The Quaternary history of the area was basically determined by the formation and transformation of a river system in the southern part of the Great Hungarian Plain. Alluvial fan was dominantly influenced by small local subsidence and uplift (Sümegi et al., 1999). The Orosháza Plain extending as far as the Apuseni Mountains is situated between depressions. The area of this alluvial fan was formed by the River Maros. The lake can be found at the margin of this alluvial plain (Molnár and Mucsi, 1966).

According to Sümegi et al. (1999) the overburden is made up of medium-grained sands indicating fluvial environment. Going upwards silt becomes dominant with sporadic appearance of fine-grained sand lenses and bands within the layers. These lenses denote a progressive formation of an abandoned meander, where connections to the river may have been restored from time to time. Clayey sediments representing lacustrine conditions follow these layers. The coarse-grained silts appearing in the beds must have come from the loess on the banks. Finally, a salty layer of several cm precipitated on the top of the lacustrine sediments (Fig. 2).

The presences of water upwelling in the area of the Lake Fehér are well known. Changes in the vegetation clearly mark these sites (Kiss, 1962). On the basis of his observations, Kiss (1962) concluded that high groundwater levels and inland waters are not always connected to precipitation. When the soaked surficial loessy sediments subside, the salty surface becomes impermeable because of the salt remaining on the surface, which also inhibits water infiltration. During the past decades inland waters (every 14-16th year) caused serious problems on the plain, however, in the deeper flood plain of the River Maros inland waters do not even appear, in general.

The first botanical study of the area was making by Kiss (1963). Molnár and Bíró (1997) performed ecological investigations in 1995 and 1997. The long period of arid climate significantly modified the vegetation: xerophilous weeds appeared to the detriment of the palustrine plants. The humid interval from 1995 to 1997 temporarily reversed this process (Molnár and Bíró, 1997).

CLIMATIC CONDITIONS

The climate of the area is continental and the aridity index is lower than one. Regarding the annual pattern of precipitation, climatic influences characteristic for the Carpathian Basin are effective. In May and June the maximum of precipitation is the result of a superposition of the dominant arid continental climate and an oceanic influence. Because of a mediterranean effect, a secondary maximum of precipitation occurs in October and November, too. The least humid months are February and September. Precipitation of high intensity is frequent in the summer. The duration of snow-cover is 30 days. Long dry periods, mainly in summer, may last as long as 45-50 days. The lowest and highest rates of the annual amount of precipitation are 300 and 900 mm, respectively. On the basis of the 100 years data series of the precipitation monitoring station in Orosháza, the average annual precipitation is 550 mm. Using temperature, precipitation and evaporation data, the calculated average potential evaporation of several years is 882 mm per annum in the area. The value of the estimated water deficit is 140 mm per annum.

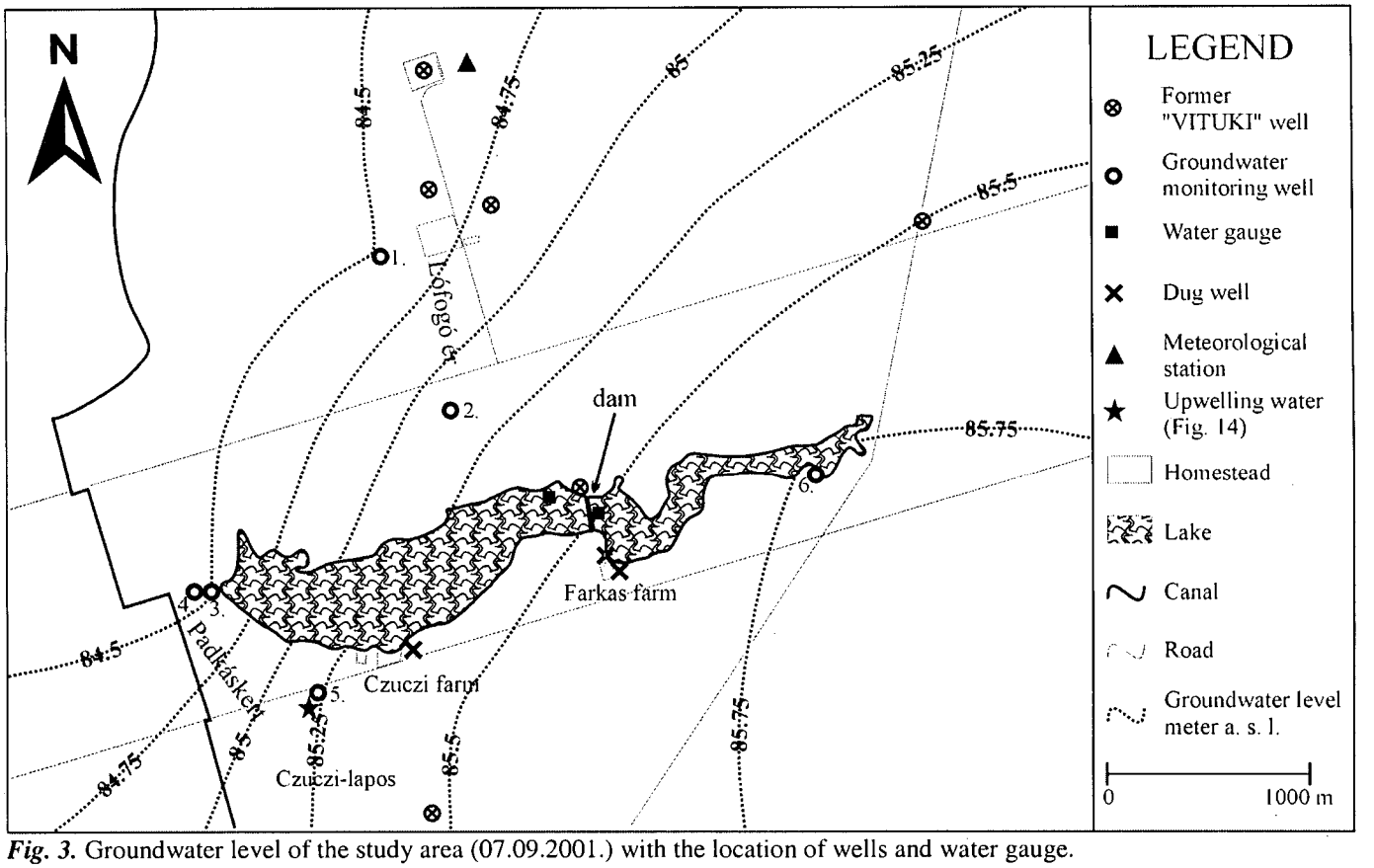

Fig. 3. Groundwater level of the study area (07.09.2001.) with the location of wells and water gauge.

METHODS

Data

No systematically collected hydrogeological data were available from the area of the Lake Fehér until 1998. Systematic observations of the lake and its environment have been carried out since 1999. In the summer of 2001 five 10 m and one 5 m deep groundwater monitoring wells were deepened, and two water gauges were placed in the wells located at the eastern and western basin of the lake (Fig. 3). Ott Thalimedes type automatic water level registration equipments have been working in two wells (No. 4 called as "western" and No. 5 called as "Czuczi") since March 2001, taking measurements every 12 hours. Data from these wells could have been downloaded and processed with the help of a computer. In December 2002 an automatic meteorological station (Fig. 3) was put into operation in the area under investigation. Besides the water level and precipitation data coming from these equipments, former precipitation and well data were also utilized in our work.

On the basis of the well data from Hungarian Inventory of Wells, pressure-elevation [p(z)] profiles of the Kardoskút, Pusztaföldvár and Battonya area were constructed, and fluid potential was given in graphical way (Tóth and Almási, 2001).

Theory

Driving forces of flows in sedimentary basins can be derived from gravitation, sediment compaction, osmosis, tectonic compression, and thermal convection (Tóth, 1995). From a hydrogeological point of view groundwater flows driven by gravitation are the most important. Their geometry can be described by mathematical and physical equations in an exact way. A uniformly sloping groundwater table results one flow system in a homogeneous basin. In fact, the different topographic conditions modify the groundwater relief, thus flow systems of different order (local, intermediate, regional) are formed (Tóth, 1963) (Fig. 4).

Hydraulic head (h) is the elevation of the standing level measured in a well from the datum level (z=0) in meters. Its value can be expressed as the sum of the pressure head (φ) and the height of the measuring point above the datum level (z) [m]:

$$h = \varphi + z.$$

The regional system revealed by this method serves as a basis for the evaluation of the distribution of the fluid potential and its gradient, the driving force of the water.

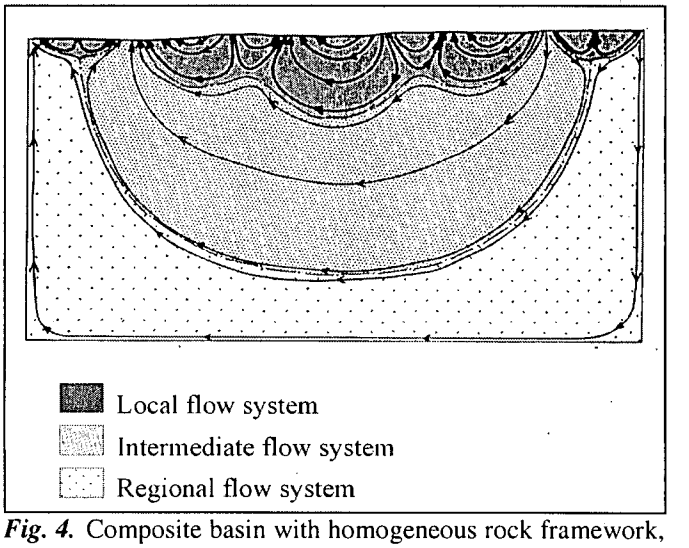

Fig. 4. Composite basin with homogeneous rock framework, showing flow-system types (Tóth, 1963).

Flow direction corresponds to the direction of the decreasing hydraulic head because it is directly proportional to the fluid's potential energy (Φ) [m^2/s^2]:

$$h = \Phi / g$$

where g is the gravitational acceleration [m/s^2]. Then the energy content per unit mass (Hubbert's energy equation) can be calculated with the following equation:

$$\Phi = gz + \frac{p}{\rho}$$

and

$$h = z + \frac{p}{\rho g} = z + \frac{\rho}{\gamma}$$

where z is the elevation of the measuring point above the datum level (sea level, in general), p is pore pressure [Mpa], ρ is water density [kg/m^3]; thus, every component of h is measurable. If the estimated dynamic pressure gradient is larger than the static gradient (9,8067 MPa), then the vertical component of the groundwater flow points upwards. Conversely, this component points downwards.

In order to reveal the effects of precipitation on the groundwater, geostatistical analyses were performed. The software Stratigraphics was used for cross-correlation analysis of daily precipitation and groundwater level data.

To perform hydrochemical analyses two series of samples were collected from both the newly deepened groundwater monitoring wells and the former "VITUKI" wells (Fig. 3). Hydrochemical analyses of the samples have been carried out in the laboratory of the Natural Protection Survey of the Lower Tisza Region. The analyses of stable isotopes have been made at the Department of Earth and Atmospheric Sciences of the University of Alberta, Edmonton Canada.

Results and Discussion

Field observations

One of the most interesting phenomena is the overflowing water in the dug wells in springtime, despite the fact that the level of groundwater did not reach the surface in the surroundings of the well (Fig. 14). Most of these wells can be found in the farms situated on the southern banks of the lake.

1. Dug well in the Farkas farm. There were two wells on the yard of the farm, and the overflowing one was closer to the lake. Now, only the latter one is available next to the ruins of the farmhouse. Its depth is 2.8 m, the upper part is bricked, and the lower is boarded. Boarding was mainly used at wells abounding in water. This bed is penetrated by an iron tube of 2 inches in diameter (its length is unknown), probably for eliminating the aquitard (clayey layers). This well was dug around 1910, providing artificial water inflow to the lake every spring since then. On the 7th of July 2001 the well was dewatered in order to measure its re-fill: it proved to be 450 l/hour.

2. Dug well in the Czuczi farm. The well was dug in 1904. Later it was partially infilled with debris as it flooded the yard. Its recent depth is 2.8 m the original value is unknown. The upper part is bricked, and the lower is boarded.

The appearance of wet areas in the basin after desiccation is quite a fascinating phenomenon. Remnant waters could not have played a role here as wet areas generally develop only after the basin is fully dried out. According to our findings, the upper 15 cm zones of these areas are totally saturated. However, profiles are dry under this zone down to the groundwater table (it may exceed a depth of 120 cm). The wet areas are circular with about 1,5 meter diameter having green vegetation cover even in the arid periods. Most of them are on the southern bank of the lake. They are in sharp contrast with the background. Piercing the "flexible layers" found in the areas covered by inner waters behind the Czuczi farm, we managed to observe intensive upwelling in three sites. The versatility of the vegetation also indicates a possible subsurface water source, as the vegetation receiving moisture only from the precipitation is quite uniform (Zsemle, 2000).

The horizontal direction of shallow groundwater flow has been defined by the water level data (Fig. 3). Defined flow direction occurred towards the canal every time, independently of the season (apprehensive time: September 2001, March 2002, August 2002). In our assumption, the canal disturbed the motion of the shallow groundwater flow, because of its bed was situated deeper than the lake bottom.

Hydrogeological conditions

Flow systems of the Great Hungarian Plains were hydraulically studying by many hydrogeologists (Erdélyi, 1975; Halász, 1975; Marton, 1982; Tóth and Almási, 2001). Tóth and Almási (2001) concluded that there are two principal driving forces in the basin: gravitation and compression. The two flow regimes are vertically separated from each other, the lower compression province influences the geometry of the upper gravitational system as it were perched by the lower one. Gravitational flow systems are divided into regimes (recharge area, flow area, discharge area) on the basis of their place in the flow system and other diagnostical hydraulic parameters as the vertical component of the flow direction.

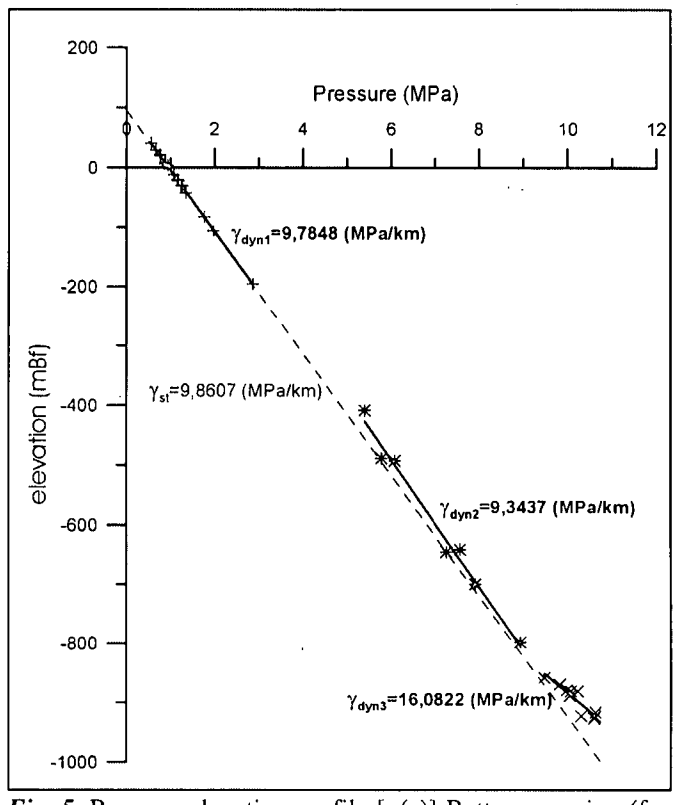

Fig. 5. Pressure-elevation profile [p(z)] Battonya region (for location, see Fig. 1).

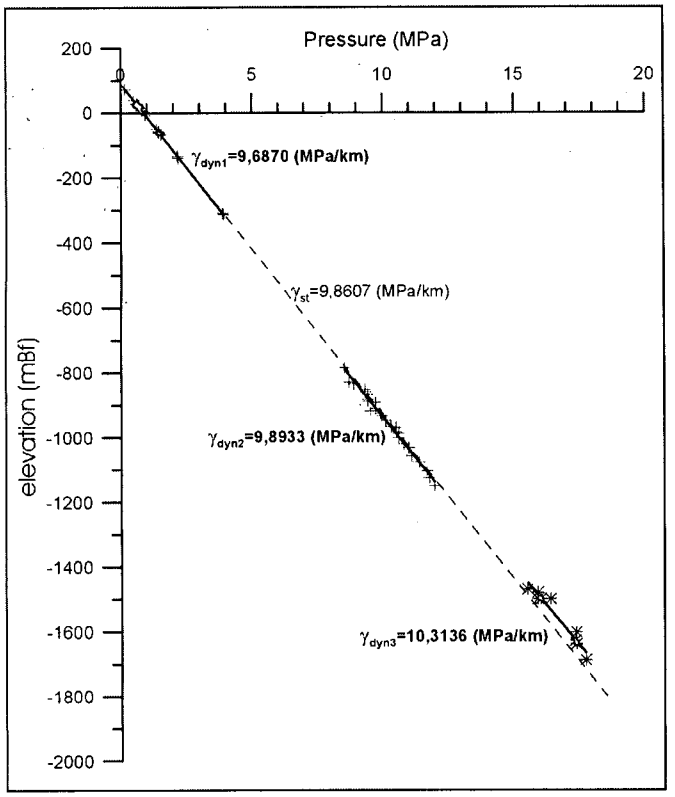

Fig. 6. Pressure-elevation profile [p(z)] Pusztaföldvár region (for location, see Fig. 1).

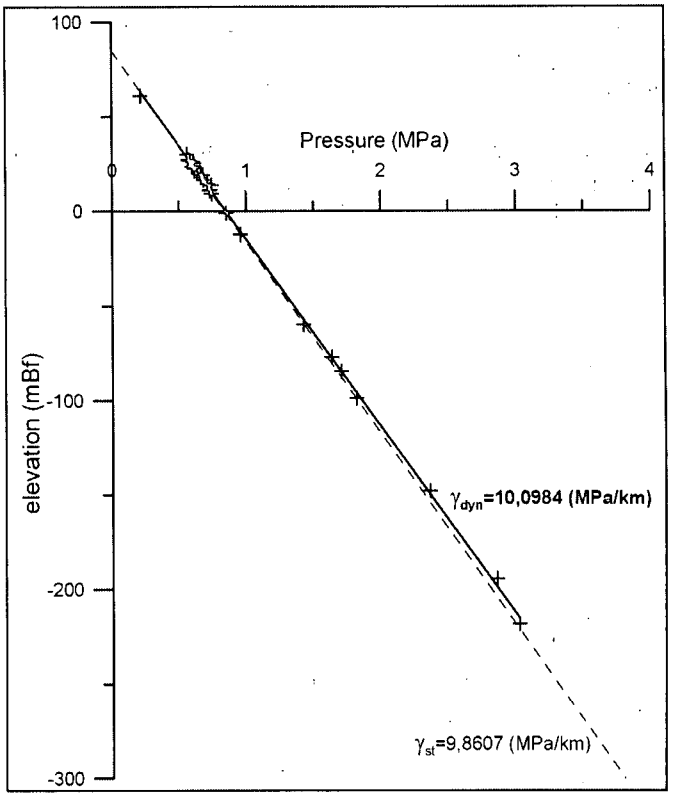

Fig. 7. Pressure-elevation profile [p(z)] Kardoskút region (for location, see Fig. 1).

Since in the case of the Lake Fehér the gravitational system could be supplied from NNE or SE, around Kardoskút because of relief, so [p(z)] profiles have been constructed for Battonya and the Pusztaföldvár-Orosháza regions beside Kardoskút as well. (Elevation is 110 and 95 m over the Baltic Sea level, respectively.)

The most time-consuming part of the building-up of a pressure-elevation profile is data collection. Data from more than one thousand wells are available, but they are incomplete, so 28 wells near Kardoskút, 40 wells near Battonya, 63 wells near Pusztaföldvár were used for further implementation. (Wells having incomplete data or filtered at two or more places were ignored in our analysis.) The most significant parameters determining the usability of the data were the initial piezometric levels, the depths of the wells, and the elevations of the area above sea level.

According to the pressure-elevation profile of the Battonya region (Fig. 5) the gradient was lower than the hydrostatic gradient from the surface to a depth of 850 m. Therefore, this can be regarded as a recharge area down to this depth. Below 850 m the gradient is much higher than the hydrostatic one, thus the vertical movement of the water is upward in the low zone.

The pressure-elevation profile of Pusztaföldvár-Orosháza (Fig. 6) indicates a recharge for the upper 300 m, intermediate (only horizontal flow component) from the depth of 800-1200 m and a discharge from the next measured depth (1500 m), however, the gradient is much lower than in the case of the previous figure.

In the case of Kardoskút, data were available for the upper 300 m (Fig. 7). The curve is over the hydrostatic pressure-line with a gradient higher than the hydrostatic gradient, i.e., the deeper wells have higher initial hydraulic heads. This fact obviously refers to a discharge area.

Almási (2001) divided the Great Hungarian Plain into recharge, discharge, and intermediate areas according to the character of the regime of the upper 400 m. (This analogize with other authors classification, for example Erdélyi, 1975.) He classified the Kardoskút area as a discharge province adjacent to the intermediate flow zone situated in the western margin of the Battonya-Pusztaföldvár plain (Fig. 8).

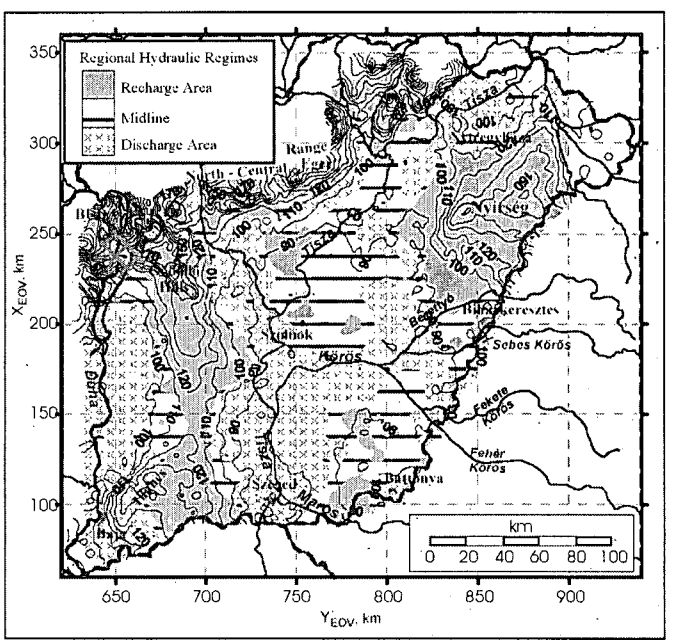

Fig. 8. Calculated distribution of regional groundwater regimes in eastern Hungary inferred from fluid-potential maps between the land surface (z_0) and z=-300m elevation, and from p(z) profiles. Topographic elevation contours are in meters (Almási, 2001).

Statistical analysis

Comparing the daily data series of groundwater level in the well No. 4 (western) and No. 5 (Czuczi), which are located at a distance of 800 m apart, surprising conclusions can be drawn (Fig. 9). Although the elevation of the wells is almost absolutely the same, the ground water level in the well next to the upwelling (Czuczi) is more than 1 m higher than that of the other. Variation of the levels in the two wells is totally opposite in the first 50 days.

Reactions of the two wells to the precipitation were analyzed by cross-correlation (Fig. 10 and Fig. 11). Daily measurement data from the precipitation monitoring station in Orosháza were used. The essence of this method is that aquitard delayed effects, or even the degree of retardation can be numerically expressed.

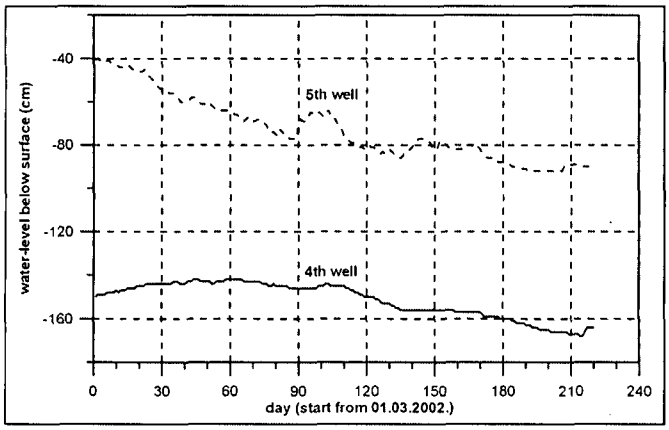

Fig. 9. Water level in two monitoring wells versus elapsed time.

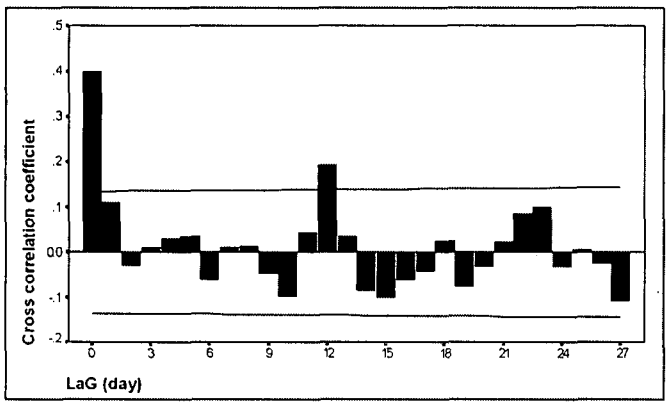

Fig. 10. Cross-correlation coefficient between water level and precipitation, well N° 5.

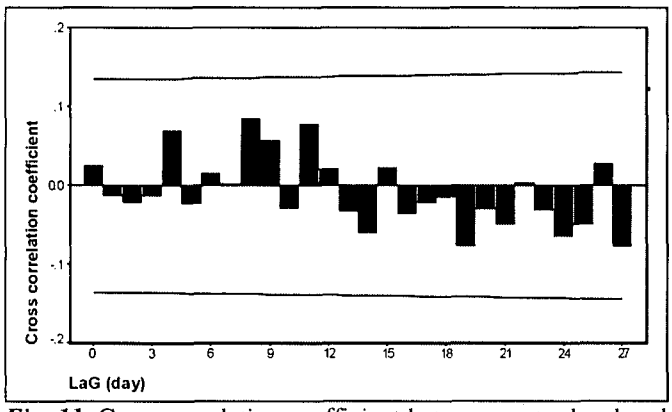

Fig. 11. Cross-correlation coefficient between water level and precipitation, well N° 4.

As Fig. 10. shows, well No. 5 situated in the southern margin of the lake responded to changes in precipitation immediately and with a 12-day delay, i.e. precipitation raises the water level in this well immediately and with a 12-day delay. It is supposed that the beds near the well allow for the quick infiltration of precipitation into the soil, and the pressure front of the upstream water increases the piezometric level 12 days afterwards. In case of the well No. 4 there is no significant connection between the precipitation and the daily regime of the groundwater (Fig. 11). The upper 8 m is built up by clayey beds in the environment of the well (the western end of the lake), therefore, immediate infiltration of the precipitation is not possible. No groundwater pressure wave can be observed which suggests that the water supply of this well is totally different from that of the well No. 5. Moreover, well No. 4 has a special chemical character.

Hydrochemistry

Twelve samples were collected from the Kardoskút area from 9 m up to 150 m below surface. The chemical composition of groundwater is quite uniform to a depth of about 15 m. Concentrations and spatial distributions of the chemical components suggest the presence of upstream in the area. According to the uniform water quality the rate of local chemical reactions is lower than the speed of the water movement. Waters coming from a depth of less than 15 m are not uniform chemically. There are local differences, which are increasing towards the surface. The largest differences in the chemical compositions of the water samples can be found in the shallowest zone (9 m depth). The lack of homogeneity indicates that local factors control the chemical composition of water in the near surface layers (Fig. 12 and Fig. 13).

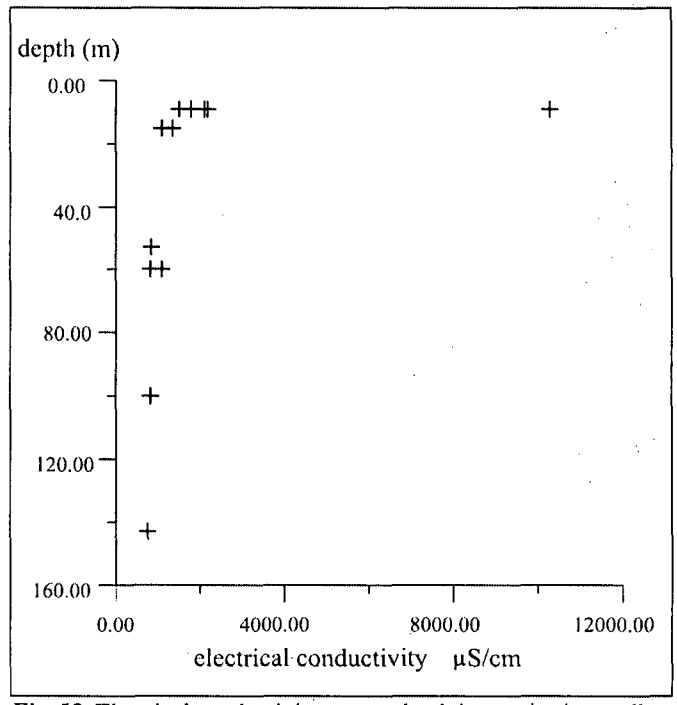

Fig. 12. Electrical conductivity versus depth in monitoring wells.

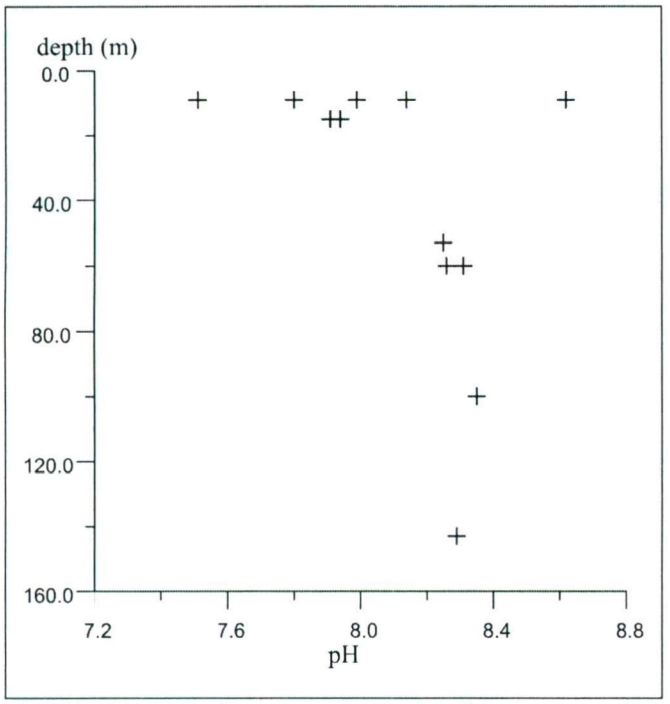

Fig. 13. pH versus depth in monitoring wells.

Conclusions

The environment of the Lake Fehér near Kardoskút village is hydrogeologically a unique area. According to the former observations and our studies it can be regarded as a discharge area of a regional flow system (Fig. 14). Special variations of the automatically registered piezometric level of two wells as well as upwelling also seem to justify this hypothesis. Upwelling is also underlined by the results of the chemical analysis of the ground water.

In our opinion the canal must have an effect on the water balance of the lake as well. The measured groundwater levels indicate a water-flow to the direction of the canal (Fig. 3), so the lake is depleted by the canal. Furthermore, the water level in the well near the canal does not show any dependence on the precipitation.

Fig. 14. Upwelling water near bank of Lake Fehér (10. 03. 1999.).

The best alternative to enhance the water balance would be to store the spring precipitation in the area so it can infiltrate into the soil, and reflow it a few months later to the surface.

A detailed study and a small-scale description of the stream require further registration data series of 3-4 years. With data series and the results of the stable isotope analyses, presently in progress, at hand, we will be able to calculate and plan the recharge mechanisms.

Acknowledgements

The authors would like to thank Dr. Irén Varsányi for doing parts of the hydrochemical analyzes and interpretation. This work has been supported by the Körös-Maros Natinal Park.

References

Almási, I. (2001): Petroleum hydrogeology of the Great Hungarian Plain, Eastern Pannonian Basin, Hungary. PhD thesis, University of Alberta, US.

Erdélyi, M. (1975): A Magyar Medence hidrodinamikája. Hidrológiai Közlöny, **55/4**, 147-156. (in Hungarian)

Halász, B. (1975): A rétegzett hidrogeológiai rendszerek sajátosságai. Hidrológiai Közlöny, **11**, 505-507.

Kiss, I. (1963): Vízfeltörések vizsgálata az Orosháza környéki szikes területeken, különös tekintettel a talajállapot és a növényzet változására, A Szegedi Tanárképző Főiskola Tudományos közleményei, **2**, 43-78. (in Hungarian)

Magyarország mélyfúrású kútjainak katasztere, Vízkészletgazdálkodási és Vízvédelmi Iroda, Felszínalatti Vízkészletgazdálkodási Osztály.

Marton, L. (1982): Izotóphidrológiai modellek és számítási eljárások a felszín alatti vizek mozgásának tanulmányozásához. Hidrológiai Közlöny, **12**, 525-533. (in Hungarian)

Molnár, B., Mucsi, M. (1966): A kardoskúti Fehér-tó vízföldtani viszonyai. Hidrológiai közlöny, **9**, 413-420. (in Hungarian)

Molnár, Zs., Bíró, M. (1997): A kardoskúti Fehér-tó kezelési tervet alapozó botanikai felmérése és az utóbbi évek változásainak elemzése. Körös-Maros Nemzeti Park, manuscript (in Hungarian)

Sümegi, P., Magyari, E., Dániel, P., Hertelendi, E., Rudner, E. (1999): A Kardoskúti Fehér-tó negyedidőszaki fejlődéstörténetének rekonstrukciója. Földtani Közlöny, **129/4**, 479-521. (in Hungarian)

Sümegi, P., Molnár, A., Szilágyi, G. (2000): Szikesedés a Hortobágyon. Természet Világa 2000, 213-216. (in Hungarian)

Sümegi, P. (2001): A negyedidőszak földtani és őskörnyezettani alapjai. JATEPRESS, Szeged, Hungary, 220-247. (in Hungarian)

Tóth, J. (1963): A theoretical analysis of groundwater flow in small drainage basins. Journal of Geophysical Research, **67**, 4375-4387.

Tóth, J. (1995): Hydraulic continuity in large sedimentary basins. Hydrogeology Journal, **3/4**, 4-16.

Tóth, J., Almási, I. (2001): Interpretation of abserved fluid potential patterns in a deep sedimentary basin under tectonic compression: Hungarian Great Plain, Pannonian Basin. Geofluids **1**, 11-36.

Zsemle, F., Mádlné Szőnyi, J., Angelus, B. (2000): Felszíni hidraulikai rezsimjelleg térképezése az Izsáki Kolon-tó környezetében. Hidrológiai Közlöny, 82/2, 110-119. (in Hungarian)

Received: May 18, 2003; accepted: September 28, 2003

Acta Mineralogica-Petrographica, Szeged 2003, Vol. 44, pp. 43-50

ACTA
Mineralogica
Petrographica

DISTRIBUTION OF CU, NI, PB, AND ZN IN NATURAL BROWN FOREST SOIL PROFILES FROM THE CSERHÁT MTS., NE HUNGARY

PÉTER SIPOS

Laboratory for Geochemical Research, Hungarian Academy of Sciences
Budaörsi út 45, H-1112, Budapest, Hungary
e-mail: sipos@geochem.hu

ABSTRACT

Distributions of total and bioavailable amounts of heavy metals (Cu, Ni, Pb, Zn) were studied in four brown forest soil profiles developed on different types of bedrock. In the study area (Cserhát Mts., NE Hungary) facilities are provided to recognize the role of bedrock and pedogenic processes in the distribution of heavy metals in soils characterized by natural background level of heavy metals.

Distribution of total and soluble metal concentrations are generally similar in the studied profiles, differences were observed only in case of zinc. Among the studied metals the following bioavailability sequence was observed: Pb (25% of total Pb) > Cu (20% of total Cu) > Ni (10% of total Ni) > Zn (2.5% of total Zn).

The obvious effect of organic matter on trace metal distribution is supported by its influence on the distributions of Pb and Zn. Distributions of Cu and Zn is determined by the presence of amorphous Al and Fe oxides. The stronger retention of trace metals by clay minerals is suggested by the good negative correlation of clay mineral and available Pb, Ni, and Zn contents of soils. Clay minerals and organic matter have contrary effect on heavy metal retention in soils.

There are factors dependent (e.g. clay minerals) on and independent (e.g. organic matter) of bedrock, of which common effect forms the actual distribution of heavy metals in soils.

Key words: soil geochemistry, heavy metal distribution, bedrock effect, brown forest soils.

INTRODUCTION

Soils formed under different pedogeneses show considerably different trace element distribution in their profiles. However, different soil types showing similar trace element distribution may differ in vertical metal distribution as a result of differences in metal extractability (Fujikawa et al., 2000). Parent material composition largely influences the contents of heavy metals in most of soils (Pasieczna and Lis, 1999; Davies et al., 1999), except e.g. by that carbonate free soil types, which are markedly enriched in heavy metals with respect to the underlying calcareous rock types. Heavy metal enrichment in these soils is associated with the formation of Fe-Mn oxides and clay accumulation (Palumbo et al., 2000). Besides amorphous oxides and clay minerals, organic matter is of important role in heavy metal retention in surface soil horizons (Tack et al., 1997). In addition, the anthropogenic contamination also enhances the amount of heavy metals in the topsoil (Baize and Streckeman, 2001).

De Matos et al. (2001) found that soil types and soil horizons influence the metal retardation in soils which, in turn, correlates better with the chemical than the mineralogical characteristics of soils. These chemical characteristics are greatly influenced by soil pH, which has important effect on behavior of metals in soils (Maskall and Thornton, 1996). The alkalising effect of carbonates may also influence the mobility and retention of some heavy metals through precipitation (Echeverría et al., 1998). Gomes et al. (2001) observed that soil characteristics that may have affected the adsorption of heavy metals were organic carbon, clay and gibbsite contents for Cu, pH and cation exchange capacity for Ni and Pb, as well as iron oxides for Zn.

In this paper we study the distribution of Cu, Ni, Pb, and Zn in natural forest soils from the Cserhát Mountains, NE Hungary. The study area is characterized by various geological formations (Neogene volcanics and molasses sediments) which are covered by forest soil types, such as brown forest soils (60%), brown earths (30%), as well as stony soils (10%). They have mostly loam texture and low hydraulic conductivity (Marosi and Somogyi, 1990). These soils are often characterized by the same pedogenic process, such as clay illuviation (Stefanovits, 1971). The study area is almost free of anthropogenic contamination, it is far from the main roads and industrial activities. These facts provide facilities to recognize the role of soil parent material and the pedogenic processes in the distribution of heavy metals in soils characterized by the natural background level of heavy metals.

MATERIALS AND METHODS

Four forest soil profiles developed on siltstone (P09), sandstone (P14), limestone (P15), and andesite (P16) were studied with respect to heavy metal distribution (Fig. 1). Samples were collected by hand drill for laboratory analyses. Air dried samples were passed through a 2 mm sieve. The clay fractions of samples were separated by sedimentation from aqueous suspensions.

Soil particle size was determined by a simplified pipette method after Kettler et al. (2001). Soil pH was measured potentiometrically in 1:2.5 suspension (soil:distilled water). The analysis of organic carbon was performed using the Rock-Eval method. Mineralogical composition of samples was identified by powder X-ray diffraction (Philips PW1710). Major elements were determined by X-ray

fluorescence spectrometry (Philips PW1410), while total and bioavailable heavy metal concentrations were measured by atomic absorption spectrometry (Perklin-Elmer AAnalyst 300). Total element concentrations were dissolved using the mixture of nitric-acid and hydrogen-peroxide with microwave digestion system, while bioavailable amounts of heavy metals were digested using the Lakanen-Erviö method (mixture of EDTA, acetic-acid and ammonium-hydroxide) according to the Hungarian standard methods (MSZ 21470-50: 1998).

RESULTS AND DISCUSSION

Soil composition

Characteristics of the studied soil profiles are summarised in Table 1. Soil P14 is a Cambisol with loam texture, while the other ones are Luvisols having silt loam texture (Driessen et al., 2001). Soil on siltstone is characterized by the highest organic matter content (up to 6.74%), the other profiles contain maximum half of this amount. The organic matter content in the B horizons exceeds 1% only in one case (soil P15).

The mineralogical compositions of the studied profiles are dominated by inherited minerals, such as quartz (50-80%) and feldspars (up to 20%). In some cases (P14 and P16) pyroxene and amphibole appear in traces. Significant amounts of calcite were found in the subsoil of profiles on siltstone and on limestone (up to 30% and 50%, respectively).

Although most of the studied profiles (P09, P15, P16) are characterized by an argic horizon (Driessen et al., 2001), their clay mineralogical compositions are largely different. These profiles contain similar quantities of clay minerals (up to 25%), which have a maximum in B horizon (P09 and P15), or their amounts increase with depth (P14 and P16).

In soil on siltstone there are vermiculite and chlorite/vermiculite intergrade mineral species with increasing chlorite component downward, and a small amount of illite. In soil on sandstone besides the dominating low charge montmorillonite, discrete illite and illite/smectite mixed layer species appear in the topsoil. In the upper part of soil on limestone the "poorly crystallized" low charge montmorillonite dominates, while below 70 cm high charge montmorillonite enters in its place. In the top of soil on andesite vermiculite and illite are the dominating species, while below 40 cm the low charge montmorillonite dominates.

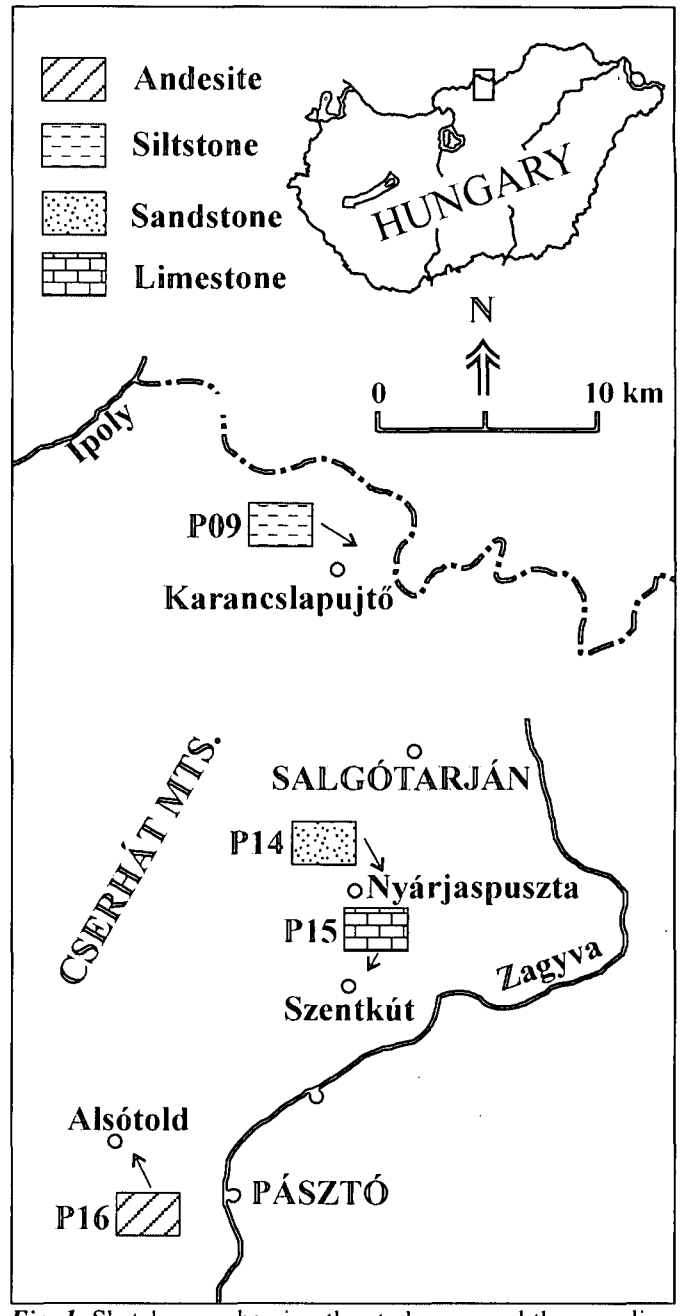

Fig. 1. Sketch map showing the study area and the sampling sites.

Soil chemistry

Three of the studied profiles (P09, P14, and P15) are characterized by acidic topsoil and alkaline subsoil, and an abrupt change in soil pH below the B horizons. Soil on andesite has an acidic pH increasing with depth within a narrow range (Table 1).

Total and bioavailable heavy metal concentrations of soils are shown in Table 2. The lowest values of heavy metals are found in soil on sandstone and on limestone. However, in case of soil on limestone the amount of lead is the highest. The highest values are generally measured in soil on andesite. Soil on siltstone contains higher amount of Ni and Zn, and lower amount of Pb and Cu as compared to the other profiles. All of four elements were within the range reported as typical average concentrations in soils (Adriano, 1986).

The most easily extractable metal is lead, its 25% is available for plants, while only 2.5% of total zinc is soluble. The copper and nickel are characterized medium bioavailability, 20% and 10% of their total amount is available for plants, respectively. Soil on siltstone is characterized by the lowest extractability, except in case of Pb, which is at least available metal in soil on andesite. According to Fujikawa and Fukui (2001) the binding of Cu, Ni, Pb and Zn to soil organic matter in forest soils is higher than in other soil types causing higher availability. The bioavailabilities of heavy metals are shown in Table 3 and Table 4.

Characterization of Al, Fe, and Mn distribution is also necessary, because of their significant effect on trace metal retention in soils. The distribution of Al and Fe is very similar in all of the studied profiles, these two elements correlate well with each other (r = 0.90). They have a

Table 1. Some physico-chemical properties of the studied soil profiles.

P	H	Depth cm	Sample No.	Depth cm	Colour	PH_{H2}	Texture (%) Sand	Silt	Clay	TOC %	Carb %	Relative amounts of CM in clay fractions (%) Montm	Verm	Ill	Chl	Kao
P09	A	0-10	911	5	10YR 3/4	5.66	41	51	8	6.74			65	35		
	B	10-40	912	15	7.5YR 5/8	6.39	28	60	12	0.92			75	25		
			913	35	10YR 5/8	6.85	26	63	11	0.39			80	20		
	BC	40-60	914	50	10YR 6/8	8.08	37	54	9	<0.10	15			20	80	
	C	60-75	915	70	2.5YR 6/4	8.41	43	50	7	<0.10	30			25	75	
P14	A	0-40	1411	5	10YR 4/2	5.33	40	49	11	2.90		50		35		15
			1412	30	10YR 4/4	5.88				0.62		70		20		10
	B	40-200	1413	60	10YR 5/6	5.59	41	48	11	0.25		80		15		5
			1414	80		5.59				0.20		75		20		5
			1415	100	10YR 5/6	5.67	46	45	9	0.11		75		20		5
			1416	140		6.30				<0.10		75		20		5
			1417	180	10YR 5/6	6.81	57	36	6	<0.10		70		25		5
	C	200-240	1418	210		8.68				<0.10	1	80		15		5
			1419	230	2.5YR 6/4	8.77	50	44	6	<0.10	2	65		30		5
P15	A	0-20	1511	5	10YR 3/3	5.27	29	61	11	3.48		55		35		10
			1512	15	10YR 6/3	5.60				2.59		55		30		15
	B	20-100	1513	40	10YR 4/4	5.27	9	76	14	1.06		70		20		10
			1514	60		5.39				0.95		70		20		10
			1515	80	10YR 5/4	5.67	8	76	17	0.78		60		30		10
			1516	100		6.17				0.80		70		20		10
	C	10-120	1517	110	10YR 6/4	7.84	32	60	9	0.75	50	70		20		10
P16	A	0-40	1611	5	10YR 3/3	5.84	24	67	9	2.29		15	40	30		15
			1612	15	10YR 3/2	6.07				1.80		10	40	30		20
			1613	35	10YR 3/2	6.30	5	87	9	1.66		10	35	35		20
	B	40-130	1614	50		6.30				1.05		15	35	35		15
			1615	70	7.5YR 4/2	6.28	4	82	13	0.60		40	20	30		10
			1616	90		6.10				0.35		60	10	15		15
			1617	110	10YR 5/6	6.03	7	80	13	0.32		65	5	20		10
			1618	120		5.91				0.25		60	5	20		15
	C	130-150	1619	140	2.5YR 5/4	6.12	6	82	12	0.35		65	0	20		15
			16110	150		6.42				0.25		80	0	15		5

P = profile, H = horizon, TOC = total organic carbon, Carb = carbonate minerals, CM = clay minerals, Montm = montmorillonite, Verm = vermiculite, Ill = illite, Chl = chlorite, Kaol = kaolinite.

Table 2. Concentrations of Al, Fe, Mn, and Cu,. Ni, Pb, Zn, as well as the available amounts of trace metals in the studied profiles.

Profile	Sample No.	Depth cm	AL_2O_3	Fe_2O_3	Mn	Cu	Cu_A	Ni	Ni_A	Pb	Pb_A	Zn	Zn_A
			Wt. %		ppm								
P09	911	5	12.33	4.66	469	13	1.7	28	2.1	27	15.1	87	8.0
	912	15	16.45	6.39	330	15	1.1	36	1.0	21	3.5	92	<1.0
	913	35	16.30	6.76	444	16	2.6	42	1.5	15	<1.0	94	<1.0
	914	50	13.72	5.03	333	8	1.1	35	3.2	5	<1.0	76	1.7
	915	70	10.09	3.40	203	7	<1.0	26	1.1	3	<1.0	59	<1.0
P14	1411	5	9.82	2.90	602	6	1.9	22	2.9	22	10.1	42	3.5
	1412	30	12.28	4.02	248	5	<1.0	25	1.2	18	4.5	47	<1.0
	1413	60	12.24	4.69	184	6		27		20		54	
	1414	80	10.88	4.11	249	4	<1.0	24	<1.0	18	3.2	43	<1.0
	1415	100	10.97	3.79	289	4		25		19		42	
	1416	140	11.16	3.88	437	4	<1.0	28	1.8	12	3.0	47	<1.0
	1417	180	9.84	3.33	389	3	<1.0	31	3.5	8	2.9	42	<1.0
	1418	210	10.47	3.43	501	2	<1.0	27	5.8	12	3.8	40	<1.0
	1419	230	10.64	3.55	498	4		27		15		47	
P15	1511	5	13.15	4.84	1142	12	3.3	21	2.9	37	14.1	71	3.3
	1512	15	13.94	5.11	1043	13	3.0	23	2.3	30	9.3	69	2.4
	1513	40	14.72	5.77	451	13	4.8	24	2.3	24	5.9	70	1.5
	1514	60	14.79	5.75	525	14		25		21		69	
	1515	80	15.47	6.03	624	14	2.3	27	1.6	20	4.9	67	<1.0
	1516	100	15.34	6.14	434	16		30		21		66	
	1517	110	10.40	3.09	277	11	1.2	26	1.2	19	5.4	49	<1.0
P16	1611	5	13.10	6.49	1683	25	5.6	24	4.6	32	4.4	67	5.3
	1612	15	13.11	5.99	1781	23		24		32		66	
	1613	35	12.05	5.10	2021	19	5.0	26	7.6	27	7.3	62	3.3
	1614	50	13.98	5.86	1414	20		26		23		68	
	1615	70	15.13	6.85	868	22		26		20		72	
	1616	90	15.83	7.44	386	25	3.0	24	<1.0	19	<1.0	72	<1.0
	1617	110	15.48	7.28	428	25		24		21		71	
	1618	120	15.13	7.04	405	26		22		20		69	
	1619	140	15.05	7.38	997	29	7.9	28	<1.0	21	<1.0	72	0.0
	16110	150	16.47	9.90	1323	60		61		23		80	
Range			9.82-16.47	2.90-9.90	184-2021	2-60	0.4-7.9	21-61	0.6-7.6	3-37	0.8-15.1	40-94	0-8.0
Average			13.24	5.36	677	15	2.4	28	2.4	20	5.1	63	1.6
Median			13.15	5.11	451	13	1.8	26	2.0	20	4.1	67	0.7

Table 3. Relative extractability (in brackets in %) of Cu, Ni, Pb, and Zn in the studied soils by the Lakanen-Erviö digestion. R. E. = relative extractability.

Profile	P09			P14			P15			P16		
Horizon	A	B	C	A	B	C	A	B	C	A	B	C
Very High (>50%)	Pb (56)											
High (25-50%)			Pb (27)	Pb (36)		Pb (43)	Pb (35) Cu (26)	Pb (25)	Pb (28)			Cu (27)
Medium (10-25%)	Cu (13)	Pb (17) Cu (12)	Cu (13)	Cu (124)	Pb (22) Cu (15)	Cu (19) Ni (16)	Ni (12)	Cu (16)	Cu (11)	Cu (24) Ni (24) Pb (21)	Cu (12)	
Low (1-10%)	Ni (7.5) Zn (9.2)	Ni (3.2)	Ni (4.2) Zn (1.6)	Ni (8.9) Zn (4.5)	Ni (4.7)		Zn (4.1)	Ni (5.9)	Ni (4.6)	Zn (6.6)	Pb (4.2) Ni (2.5)	Pb (3.8) Ni (2.5)
Very low (<1%)		Zn (0.43)			Zn (0.22)	Zn (0.29)		Zn (0.15)	Zn (0.20)		Zn (0.92)	Zn (0.04)

maximum in the top of B horizon (P09 and P14), or their amount decreases with depth, and there is a significant change at the boundary of soil and its parent material. The amounts of these two elements depleted in soil on andesite, contrarily, they increased in soil on limestone, as compared to the parent materials. In the latter two profiles, Mn is distributed similarly to the previous elements, while in the other profiles uniformly.

Distribution of heavy metals in soil profiles

Copper

Copper is retained in soils through ion exchange and specific adsorption mechanisms. Cavallaro and McBride (1978) suggested that a clay mineral exchange phase may serve as a sink for Cu in noncalcareous soils. In calcareous soils, specific adsorption of Cu on $CaCO_3$ surfaces may control Cu concentration in solution. Copper also has a high affinity for soluble organic ligands and the formation of these complexes may greatly increase Cu mobility in soils (Dudley et al., 1991).

Distributions of the studied elements are shown in Fig. 2. Correlation between the different total and extractable metal concentrations and some physico-chemical properties of studied soils are presented in Table 4. In general, the distribution of copper in the studied profiles is uniform, except in soil on siltstone where this element shows a slight maximum in the B horizon. In case of profiles developed on carbonate containing rocks Cu significantly concentrates in the soil as compared to the parent material, while in case of soil formed on andesite there is a strong depletion of Cu in the soil.

Copper usually correlates well with Al and Fe in the studied profiles, except in case of soil on sandstone, where no relation was found among the different element distributions. In some cases (P09 and P16) its distribution is very similar to zinc and nickel. In general, the amount of copper slightly increases with the increasing clay mineral content of the studied samples. In soil on siltstone the copper content decreases as its carbonate content increases.

Table 4. Average relative extractability of Cu, Ni, Pb and Zn in the studied profiles by the Lakanen-Erviö digestion

	P09	P14	P15	P16
Cu	12	21	20	22
Ni	4.5	9.6	8.6	13
Pb	26	32	31	12
Zn	2.9	2.4	2.1	3.5

The amount of bioavailable Cu ranges between 7 and 37% of total copper content in the studied soils. The distribution of total and soluble copper contents is similar to each other within the profiles. The composition of soils has no effect on the available copper contents of soils.

Lead

Soluble lead added to the soil reacts with clays, phosphates, sulphates, carbonates, hydroxides, and organic matter, such that Pb solubility is greatly reduced due to adsorption as well as precipitation (McLean and Bledsoe, 1992). At pH values above 6, lead is either adsorbed on clay surfaces or forms lead carbonate. Puls et al. (1991) have demonstrated decrease sorption of Pb in the presence of complexing ligands and competing cations. Lead has a strong affinity for organic ligands and the formation of such complexes may greatly increase the mobility of Pb in soil.

The amount of lead in the studied profiles always decreases with depth independent of mineralogical composition of soils. Its amount correlates well with the total organic matter content of soil in all profiles: least of all in soil on sandstone, and most of all in soil on limestone. The lead does not correlates with one of the studied elements in these soil profiles, and it does not show correlation with the amount of clay minerals in the studied profiles either. In soil on siltstone the amount of lead increases as its calcite content decreases.

Among the studied metals lead is the most easily available metal for plants: up to 56% of total lead content of soils is extractable by the Lakanen-Erviö digest. The high amount of soluble lead in the upper part of profile P09 is due to the fact that there is a significant amount of lead bound to organic matter. This soil horizon is characterized by the highest organic matter content, which can accumulate lead from different sources (natural and atmospheric fallout). The amount of soluble lead decreases with depth within the soil profiles, and increases with organic matter content of soils, because the lead bound to organic mater can be easily desorbed by chelating agents (like EDTA in the Lakanen-Erviö solution). However, in most of studied profiles (P14, P15, P16) its amount decreases with increasing clay mineral content, suggesting the stronger binding of lead to clay minerals as compared to soil organic matter, showing that these two compounds have contrary effect on the available amount of lead in soils.

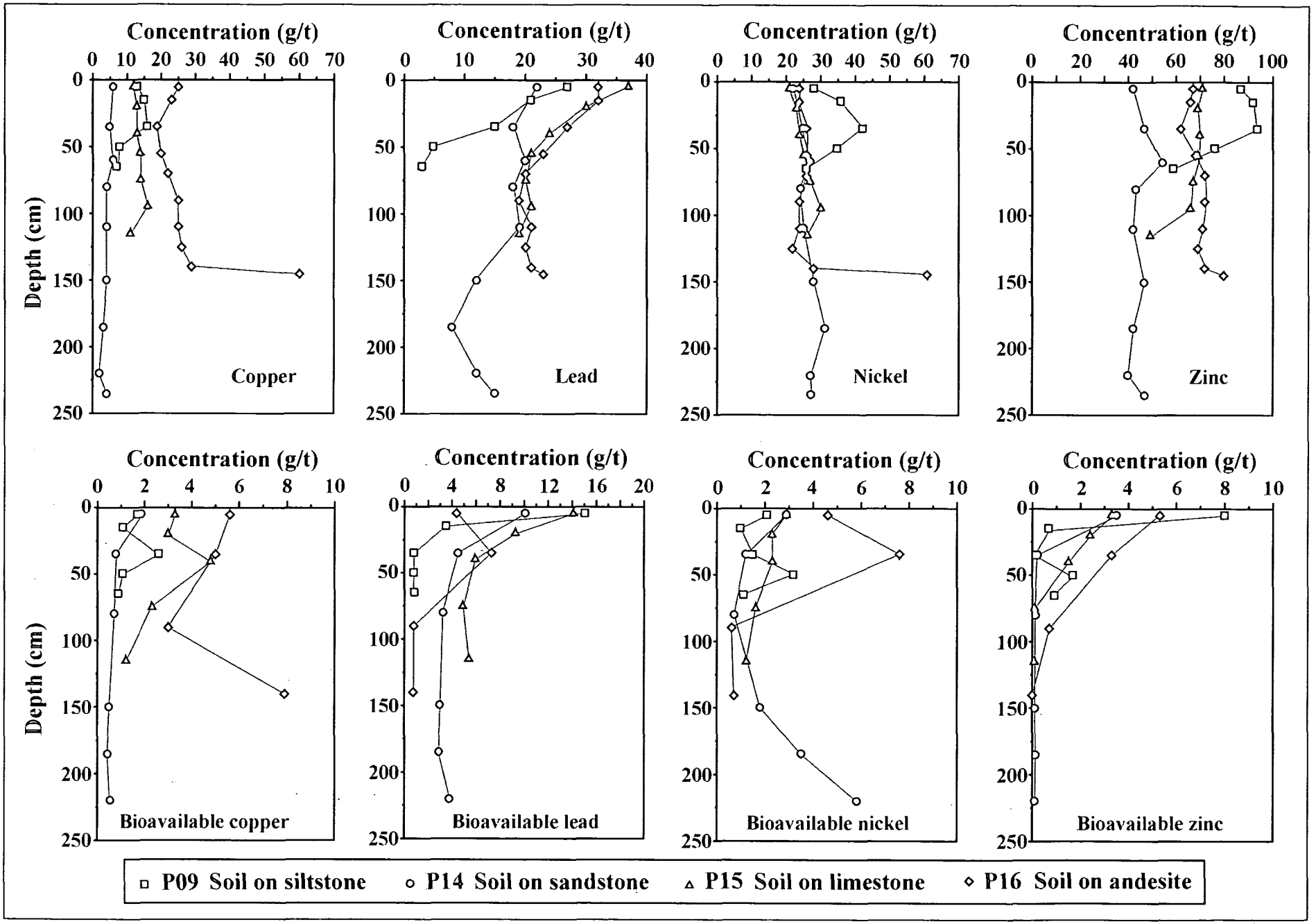

Fig. 2. Distribution of total and available amounts of Cu, Ni, Pb, and Zn in the studied profiles.

Nickel

Nickel does not form insoluble precipitates in unpolluted soils, therefore, the retention of Ni is proceeded exclusively through adsorption mechanisms. Nickel will adsorb to clays, iron and manganese oxides, and organic matter and it is thus removed from the soil solution. The formation of complexes of Ni with both inorganic and organic ligands will increase Ni mobility in soils (McLean and Bledsoe, 1992).

The distribution of nickel is very similar to that of copper, but in soil on siltstone Ni enriches significantly in the B horizon. The amount of Ni is near twofold in this horizon as compared to the other ones. In profiles formed on carbonate containing rocks nickel significantly enriches in the soil, while in case of soil on andesite there is a strong depletion of Ni as compared to the parent material.

In two profiles (P14 and P15) significant negative correlation between the nickel concentration and organic matter content of soils was found. The amount of nickel follows the distribution of Al and Fe, but less close as the amount of copper or zinc does. The amount of nickel shows slight increase with increasing clay mineral content, and their correlation are better in cases of soil developed on siltstone and on limestone.

The amount of soluble nickel (3-29% of total lead) does not correlate with the total nickel contents of soils, its distribution is usually uniform. There are no general rules determining the distribution of bioavailable nickel content of studied soils. In soils on limestone and on andesite the role of organic matter, in soil on andesite the role of clay minerals should be noted from this point of view.

Zinc

Zinc is readily adsorbed by clay minerals, carbonates, or hydrous oxides, while the precipitation is not a major mechanism for retention of Zn in soils because of high solubility of Zn compounds. In alkaline medium Zn hydrolyses, and its hydrolysed species are strongly adsorbed to soil surfaces. Zinc forms complexes with inorganic and organic ligands that will affect its adsorption reactions with the soil surface (McLean and Bledsoe, 1992).

Table 4. Correlation between the different element concentrations and some physico-chemical properties of the studied soils. A = (bio)available; $M:M_A$ = correlation between the concentration of a given trace metal and its bioavailable amount.

Profile	pH	TOC	CM	Al	Fe	Mn	$M:M_A$
All							
Cu	-0,20	0,02	0,23	0,68	**0,90**	0,51	**0,84**
Cu_A	-0,39	0,13	0,10	0,45	0,67	0,70	**0,84**
Ni	0,2	-0,14	0,18	0,37	0,48	0,05	-0,11
Ni_A	0,19	0,08	-0,22	-0,30	-0,19	0,67	-0,11
Pb	-0,64	0,57	-0,27	0,29	0,33	0,64	0,71
Pb_A	-0,41	**0,85**	-0,54	-0,18	-0,25	0,31	0,71
Zn	-0,20	0,40	-0,02	**0,83**	0,73	0,22	0,30
Zn_A	-0,24	**0,88**	-0,60	-0,08	0,01	0,46	0,30
P09							
Cu	**-0,88**	0,28	0,26	**0,80**	**0,85**	0,72	0,70
Cu_A	-0,32	0,25	0,66	0,49	0,61	0,78	0,70
Ni	-0,34	-0,36	**0,82**	**0,91**	**0,92**	0,43	0,05
Ni_A	0,35	0,19	0,45	-0,08	-0,11	0,27	0,05
Pb	**-0,90**	0,77	-0,20	0,39	0,43	0,75	0,79
Pb_A	-0,48	**0,99**	-0,42	-0,20	-0,16	0,59	0,79
Zn	**-0,86**	0,33	0,40	**0,86**	**0,90**	**0,82**	0,11
Zn_A	-0,24	**0,97**	-0,37	-0,37	-0,33	0,52	0,11
P14							
Cu	-0,68	0,69	-0,60	0,41	0,28	-0,22	**0,81**
Cu_A	-0,56	**1,00**	**-0,89**	-0,28	-0,57	0,51	**0,81**
Ni	0,46	-0,75	0,56	-0,07	0,09	-0,07	0,34
Ni_A	**0,85**	-0,19	0,27	-0,54	-0,63	0,65	0,34
Pb	-0,60	0,68	-0,57	0,35	0,23	-0,22	0,74
Pb_A	-0,42	**0,97**	**-0,87**	-0,34	-0,68	0,63	0,74
Zn	-0,20	-0,13	0,15	0,76	0,75	-0,50	-0,24
Zn_A	-0,45	**0,95**	**-0,85**	-0,46	-0,73	0,68	-0,24
P15							
Cu	-0,36	-0,23	0,71	**0,85**	**0,85**	-0,17	0,40
Cu_A	**-0,81**	0,12	-0,02	0,61	0,66	0,25	0,40
Ni	0,41	-0,72	0,76	0,29	0,28	-0,71	**-0,92**
Ni_A	**-0,80**	**0,73**	-0,53	0,36	0,40	**0,80**	**-0,92**
Pb	-0,50	**0,94**	-0,76	-0,08	-0,06	**0,91**	**0,98**
Pb_A	-0,43	**0,90**	**-0,80**	-0,07	-0,04	**0,86**	**0,98**
Zn	**-0,99**	0,37	0,12	0,78	0,79	0,59	0,66
Zn_A	-0,62	**0,87**	**-0,74**	0,12	0,16	0,85	0,66
P16							
Cu	0,38	-0,44	0,41	0,60	**0,90**	-0,03	0,49
Cu_A	-0,07	0,05	0,23	-0,11	0,08	0,28	0,49
Ni	0,61	-0,31	0,25	0,46	0,79	0,16	-0,12
Ni_A	0,25	**0,86**	**-0,96**	**-0,98**	**-0,98**	**0,93**	-0,12
Pb	-0,24	**0,89**	**-0,86**	-0,77	-0,41	**0,83**	0,73
Pb_A	0,26	**0,85**	**-0,96**	**-0,97**	**-0,99**	**0,92**	0,73
Zn	0,33	-0,73	0,73	**0,91**	**0,96**	-0,47	-0,71
Zn_A	-0,45	**0,97**	**-0,87**	-0,79	-0,63	0,76	-0,71

The distribution of zinc is very similar to that of copper and in some cases to nickel. Its amount does not change in the soil profiles with depth, but in soil on siltstone zinc also accumulates in the B horizon following the distribution of Fe and Al. Similarly to Cu and Ni its amount increases in soil formed on calcareous rocks, and decreases in soil developed on andesite as compared to the parent material.

Similarly to the copper, zinc correlates mostly with the distribution of Al and Fe well. The linear relation between these two metals is also good in some profiles (P09 and P16). The distribution of zinc in the carbonate containing profiles (P09 and P15) is very similar to the copper distribution.

Among the studied metals zinc is the least available: only 0-9 % of total zinc is available for plants. In general the highest amounts of soluble zinc (5-9% of total zinc) are found it the topsoil, while the subsoil contains negligible amount of soluble zinc. This suggests the role of the amount of soil organic matter in availability of zinc for plants, which is also shown by their good correlation. In most cases (P14, P15, and P16) the amount of available zinc decreases with increasing clay mineral content, showing the high affinity of zinc for clay minerals.

CONCLUSIONS

Distributions of total and soluble metal concentrations are generally similar in the studied profiles, significant differences were observed only in case of Zn. Their bioavailability differs from metal to metal, and the following sequence was observed: Pb > Cu > Ni > Zn.

Both the distributions of total and available amounts of Cu are uniform in all of studied profiles independent of variation of chemical and mineralogical composition of soils. Distribution of Pb in soils is determined by the distribution and amount of organic matter in soils. It is also supported by the fact that the extractability of Pb increases with the increasing organic matter content of soils. In case of Ni, neither the total nor the soluble amounts of this metal show any variations with depth. There is no general factor that would determinate its distribution. Similarly, there is no general rule for the distribution of total Zn contents of soils either. On the other hand, the amount of bioavailable Zn increases with increasing organic matter content of soils.

Obvious effect on trace metal distribution was observed only in case of organic matter content of soils. It influences not only the bioavailable amount of Pb and Zn, but the total amount of Pb, as well. In the latter case the atmospheric fallout of heavy metals can play role in the decreased amount of lead in topsoil. The Cu and Zn contents show good correlation with total Al and Fe contents of soils, which may be due to the retention by amorphous oxides, but the characterization of this relation needs further studies. Stronger retention of trace metals by clay minerals is suggested in cases of Pb, Ni, and Zn by the good negative correlation of clay mineral and available metal contents of soils. These two components have contrary effects on heavy metal retention in soils.

The quality of bedrock influences the clay mineral composition of soils, thus it has an effect on heavy metal distribution in soils, which is, however, also influenced by other constituents independent of bedrock. The common effects of these factors form the actual distribution of heavy metals in soils.

ACKNOWLEDGEMENTS

This study was financially supported by Hungarian National Research Found (OTKA No. T-043445). The author is grateful to Dr. Magdolna Hetényi for the Rock-Eval measurements.

REFERENCES

ADRIANO, D. C. (1986): Trace elements in the terrestrial environment. Springer Verlag, New York.

BAIZE, D., STRECKEMAN, T. (2001): Of the necessity of knowledge of the natural pedo-geochemical background content in the evaluation of the contamination of soils by trace elements. The Science of the Total Environment, **264**, 127-139.

CAVALLARO, N., MCBRIDE, M. B. (1978): Copper and cadmium adsorption characteristics of selected acid and calcareous soils. Soil Science Society of America Journal, **42**, 550-556.

DAVIES, B. E., BIFANO, C., PHILLIPS, K. M., MOGOLLON, J. L., TORRES, M. (1999): Aqua regia extractable trace elements in surface soils of Venezuela. Environmental Geochemistry and Health, **21**, 227-256.

DE MATOS, A. T., FONTES, M. P. F., DA COSTA, L. M., MARTINEZ, M. A. (2001): Mobility of heavy metals as related to soil chemical and mineralogical characteristics of Brazilian soils. Environmental Pollution, **111**, 429-435.

DRIESSEN, P., DECKERS, J., SPAARGAREN, O., NACHTERGAELE, F. (2001): Lecture notes on the major soils of the world. FAO of United Nations, Rome.

DUDLEY, L. M., MCLEAN, B. L., FURST, T. H., JURINAK, J. J. (1991): Sorption of Cd and Cu from an acid mine waste extract by two calcareous soils: column studies. Soil Science, **151**, 121-135.

ECHEVERRÍA, J. C., MORERA, M. T., MAZKARIÁN, C., GARRIDO, J. J. (1998): Competitive sorption of heavy metal by soils. Isotherms and fractional factorial experiments. Environmental Pollution, **101**, 275-284.

FUJIKAWA, Y., FUKUI, M.; KUDO, A. (2000): Vertical distributions of trace metals in natural soil horizons from Japan. Part 1. Effect of soil types. Water Air and Soil Pollution, **124**, 1-21.

FUJIKAWA, Y., FUKUI, M. (2001): Vertical distribution of trace metals in natural soil horizons from Japan. Part 2: Efects of organic components in soil. Water Air and Soil Pollution, **131**, 305-328.

GOMES, P. C., FONTES, M. P., DA SILVA, A. G.; DE S. MENDOCA, E., NETTO, A. R. (2001): Selectivity sequence and competitive adsorption of heavy metals by Brazilian soils. Soil Science Society of America Journal, **65**, 1115-1121.

Hungarian Standard MSZ 21470-50 (1998): Environmental protection. Testing of soils. Determination of total and soluble toxic element, heavy metal and chromium(VI) content (in Hungarian). Magyar Szabványügyi Testület.

KETTLER, T. A., DORAN, J. W., GILBERT, T. L. (2001): Simplified method for soil particle-size determination to accompany soil-quality analyses. Soil Science Society of America Journal, **65**, 849-852.

MAROSI, S., SOMOGYI, S. (1990): Magyarország kistájainak katasztere II. MTA Földrajztudományi Kutatóintézet, Budapest.

MASKALL, J., THORNTON, I. (1996): The distribution of trace and major elements in Kenyan soil profiles and implications for wildlife nutrition. In Appleton, J. D.; Fuge, R.; McCall, G. J. H. (eds.): Environmental Geochemistry and Health, Geological Society Special Publication No. **113**, 47-62.

MCLEAN, J. E., BLEDSOE, B. E. (1992): Behavior of metals in soils. EPA Ground Water Issue, EPA/540/S-92/018.

PALUMBO, B., ANGELONE, M., BELLANCA, A., DAZZI, C., HAUSER, S., NERI, R., WILSON, J. (2000): Influence of inheritance and pedogenesis on heavy metal distribution in soils of Sicily, Italy. Geoderma, **95**, 247-266.

PASIECZNA, A., LIS, J. (1999): Relationship between the geochemistry of soils and the geological basement in the Lower Silesian Coal Basin, SW Poland. Journal of Geochemical Exploration, **66**, 219-227.

PULS, R. W., POWELL, R. M., CLARK, D., ELDRED, C. J. (1991): Effect of pH, solid/solution ratio, ionic strength, and organic acids on Pb and Cd sorption on kaolinite. Water, Air, and Soil Pollution, **57-58**, 423-430.

STEFANOVITS, P. (1971): Brown forest soils of Hungary. Akadémiai Kiadó, Budapest.

TACK, F. M. G., VERLOO, M. G., VANMECHELEN, L., VAN RANST, E. (1997): Baseline concentration levels of trace elements as a function of clay and organic carbon contents in soils in Flandres (Belgium). The Science of the Total Environment, **201**, 113-123.

Received: June 5, 2003; accepted: September 17, 2003

Acta Mineralogica-Petrographica, Szeged 2003, Vol. 44, pp. 51-56

ACTA
Mineralogica
Petrographica

PETROGRAPHY AND MINERAL CHEMISTRY OF RHÖNITE IN OCELLI OF ALKALI BASALT FROM VILLÁNY MTS, SW HUNGARY

ZSUZSANNA NÉDLI, TIVADAR M. TÓTH

Department of Mineralogy, Geochemistry and Petrology, University of Szeged
H-6701 Szeged, P. O. Box 651, Hungary
e-mail: nedlizs@yahoo.com

ABSTRACT

In ocelli of alkali basalts from the Villány Mts (SW Hungary) rhönite has been found recently. This is among the first reports of rhönite from ocelli in basaltic dykes, as well as from the southern part of the Pannonian Basin. This new occurrence of rhönite has been analysed and described in this paper, in light of the hypotheses of formation of ocelli and crystallisation conditions of rhönite. On the basis of textural observations and mineral chemistry, we suggest that the ocelli was formed in the late stage of the crystallisation of magma, near the Earth's surface, at relatively high temperature but low pressure. Rhönite in ocelli crystallised as a primary phase in these conditions.

Key words: rhönite, ocelli, basalt, Villány Mts, Hungary.

INTRODUCTION

Rhönite is a relatively rare accessory constituent of magmatic rocks, because due to its minor grain size and semi-opaque character, its exact optical determination is difficult. Nevertheless, recently it is thought to be more frequent than it was described before. In the last decades it has been found in very different magmatic environments from being an accessory phase in groundmass of undersaturated volcanic rocks (e.g. Downes et al., 1995; Prestvik et al., 1999; Fodor and Hanan, 2000) to being a constituent in silicate melt inclusions and pockets of ultramafic mantle xenoliths (Kóthay and Szabó, 1999; Kóthay et al., 2001, 2003; Sharygin et al., 2003) and meteorites (Nazarov et al., 2000). To the best of our knowledge, there is only one occurrence known from ocelli (Sabatier, 1999), so, any new description may have a great importance that can contribute to specify the crystallisation conditions of both ocelli and rhönite.

The main aim of this paper is to present the textural and chemical circumstances of rhönite from ocelli. This also is the first report of rhönite from the southern part of Tisza Unit; namely from the Villány Mts alkali basalts. We also attempt to interpret the formation of ocelli and rhönite crystals in light of the previous descriptions and experimental studies of both, giving in this way some contributions to the hypotheses about formation of ocelli, as well as to the crystallisation conditions of rhönite.

GEOLOGICAL BACKGROUND

In the Villány Mts, Mesozoic dykes of basaltic composition are present sporadically as small bodies (Fig. 1). Altered basalt dykes, containing high amount of ocelli crosscut Aptian – Albian limestones near Beremend and Máriagyűd. They are alkali basalts containing several mafic and felsic xenocrysts, as well as ultramafic spinel lherzolite xenoliths of upper mantle origin (Nédli and M.Tóth, 1999a). Based on whole rock K-Ar data (Molnár and Szederkényi, 1996; Harangi and Árváné Sós, 1993) and the geochemical characteristics, these dykes are thought to have formed in the Late Cretaceous by intraplate magmatism (for details see Nédli, 1999; Nédli and M.Tóth, 1999a, b, 2003).

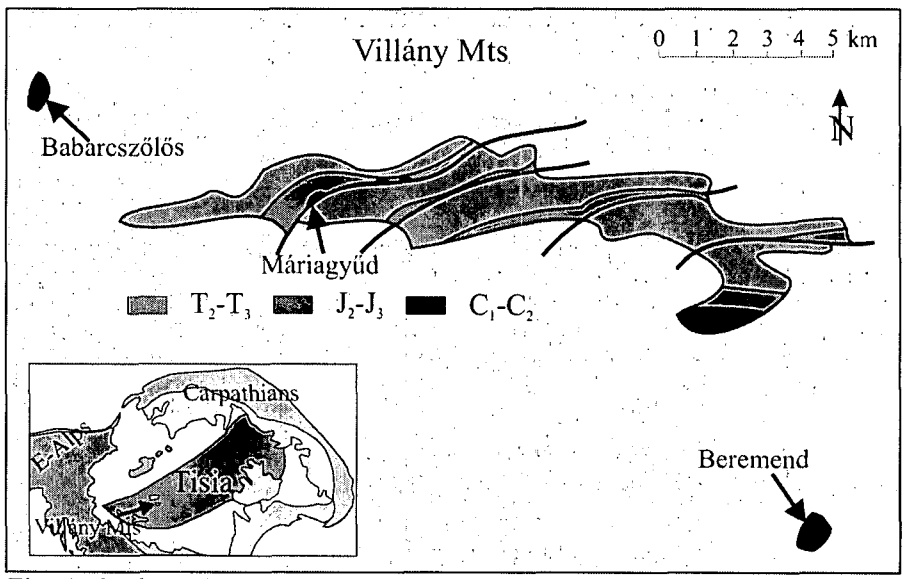

Fig. 1. Geological sketch map of the Villány Mts (after Fülöp, 1966). Surface outcrops of alkali mafic dykes at Máriagyűd and Beremend as well as the sill at Babarcszőlős are highlighted. Inset: Position of the Tisza Block in the Alp-Carpathian-Dinaric system (T_2-T_3: Diverse Triassic carbonate formations; J_2-J_3: Szársomlyó Limestone; C_1-C_2: Nagyharsány Limestone).

Petrography

The Villány Mts dyke group consists of porphyritic basalt with partially or entirely altered olivine and clinopyroxene phenocrysts, at places overgrown by amphibole rims, settled in a fine-grained, pyroxene-rich groundmass. Plagioclase is present only in the groundmass, where it occurs together with euhedral amphibole and biotite crystals, Fe-Ti-oxide grains and apatite needles. Secondary minerals (chlorite, clay minerals and calcite) compose variable amounts of groundmass, up to 20-30 vol%.

Felsic, globular ocelli frequently occur in the dykes. They are mostly ellipsoidal or spherical, rarely irregular in shape (Fig. 2A) of 1-5 mm in diameter. Most ocelli contain anhedral carbonate core surrounded by a complex rim of silicate minerals (Fig. 2B). The rim contains two types of microphenocrysts; the 0.3-0.5 mm long, greenish, euhedral amphibole prisms usually overgrow a clinopyroxene core (Fig. 2B, C). The rhönite grains are small (0.1-0.2 mm), semi-opaque or dark brown in colour (Fig. 2C, D). There is no textural reason for assuming any post-magmatic reaction between the amphibole and rhönite phases; they are regarded co-existing minerals. In addition to microphenocrysts, apatite needles occur in the weakly altered plagioclase-rich or glassy matrix. Plagioclase grains in the ocelli are significantly larger (0.5-1 mm) than those in the groundmass. Ocelli usually have a sharp contact with the groundmass; occasionally the groundmass pyroxene is aligned tangentially to the rim of the ocelli (Fig. 2A, B.). A few ocelli are composed only of carbonate minerals.

High amount of spinel lherzolite xenoliths of upper mantle origin and at some places resorbed quartz xenocrysts are present in the Beremend dyke (Nédli and M.Tóth, 1999a;2003). Significant textural variation can be observed in the hand specimens studied; those with high amounts of ultramafic xenoliths contain a few ocelli and felsic xenocrysts, whereas the highest amount of ocelli occurs mainly in the xenolith-free samples.

ANALYTICAL METHODS

Quantitative mineral chemical analyses were performed on representative rhönite, amphibole and pyroxene grains of ocelli on an upgraded *ARL-SEMQ 30* electron microprobe equipped with 4 wavelength-dispersive spectrometers (WDS) with TAP, LiF and PET diffraction crystals at

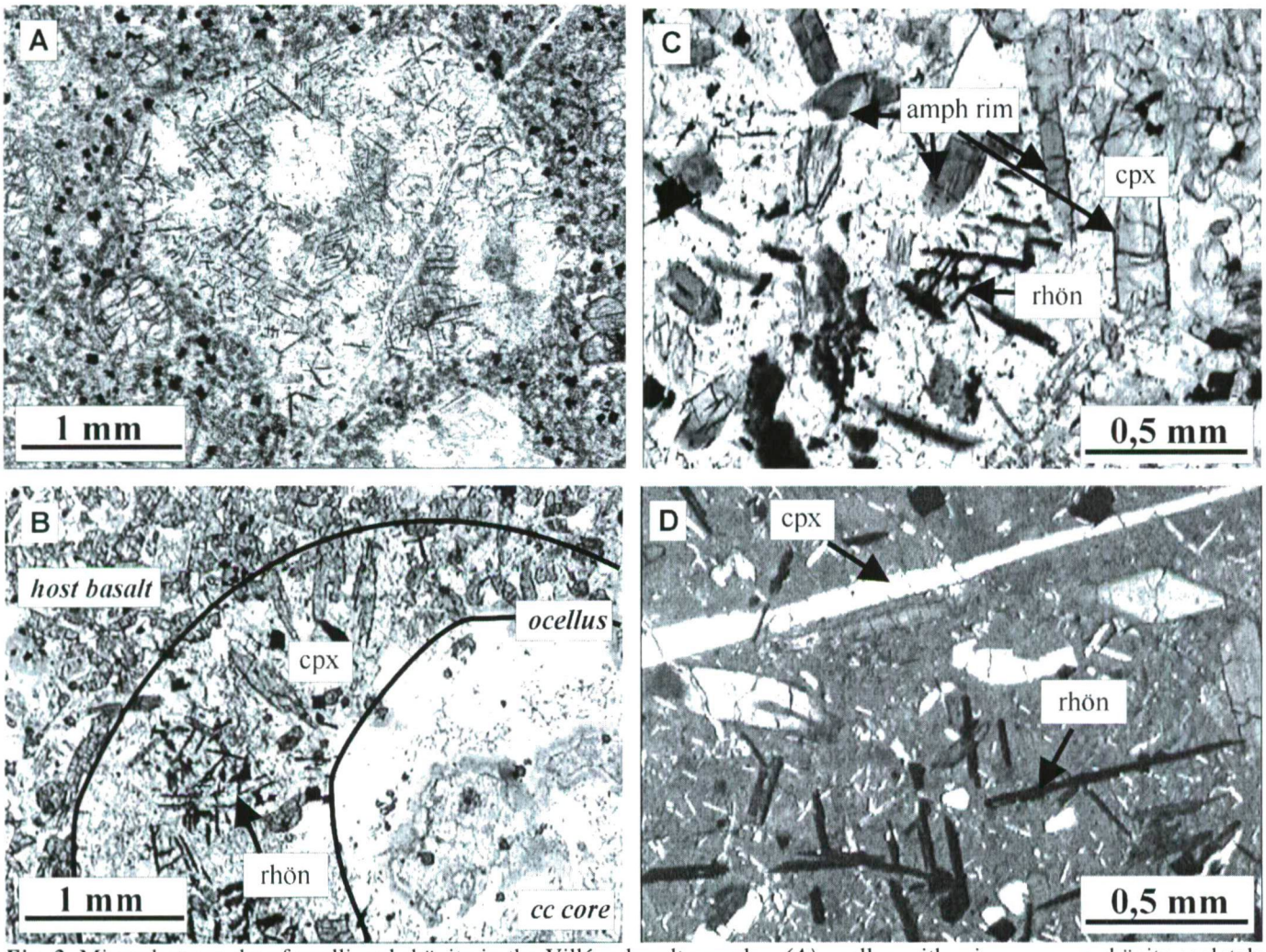

Fig. 2. Microphotographs of ocelli and rhönite in the Villány basalt samples. ***(A)*** ocellus with minor opaque rhönite sceletals (Máriagyűd basalt dyke, 1N). ***(B)*** typical occelus with carbonate core surrounded by a complex rim with clinopyroxene and rhönite microphenocrysts (Beremend basalt dyke, 1N). ***(C)*** opaque and semi-opaque rhönite crystals in ocellus with amphibole rimmed clinopyroxene and amphibole grains (Beremend basalt dyke, 1N). ***(D)*** clinopyroxene and rhönite microphenocrysts in ocellus (Beremend basalt dyke, +N).

Montanuniversität, Leoben (Austria) with 15 kV accelerating voltage, 20 nA beam current. For calibration synthetic and natural standards were used.

MINERAL CHEMISTRY

Compositions of selected pyroxene, amphibole and rhönite grains from the ocelli are listed in Table 1. Single pyroxene grains (cpx I.) have similar compositions to those rimmed by amphibole (cpx II.). Amphibole is maximal in Al^{IV}, and also is rather high in Ti and $(Na+K)^{A}$, while the most important pressure indicators Na^{M4} (Thieblemont et al., 1988) and Al^{VI} (Leake, 1965, 1971; Raase, 1974; Spear, 1981) are remarkably high too. The optically dark brown, small, elongated microphenocrysts are rhönite. Data suggest a high-silica variety with a clear change in compositions from the core to the rim; Si and Mg decrease rimwards, whereas Ti, Na and Fe tend to increase.

Table 1. Selected microprobe analysis of rhönite, pyroxene and amphibole in ocelli in Beremend basalt dyke.

	Beremend basalt, ocellus					
	rhönite		cpx-I/1	cpx-I/2	cpx-II.	tschermakite
	core	rim			core	rim
SiO_2	28,09	27,74	45,54	44,35	41,97	39,59
TiO_2	6,66	7,30	2,55	2,62	4,13	3,40
Al_2O_3	14,33	13,85	9,03	9,30	11,79	15,17
Cr_2O_3	0,03	0,00	0,01	0,00	0,00	0,00
Fe_2O_3	0,00	0,00	0,00	0,00	0,00	0,00
FeO	25,67	26,25	9,97	9,87	9,30	15,43
MnO	0,28	0,21	0,29	0,20	0,13	0,40
MgO	12,07	10,87	9,23	9,26	9,06	9,17
CaO	10,35	10,44	20,73	21,20	21,68	10,26
Na_2O	1,34	1,69	0,91	0,91	0,70	2,41
K_2O	0,00	0,00	0,03	0,01	0,00	0,89
Total	98,82	98,35	98,29	97,72	98,76	96,72
Si	3,91	3,90	1,748	1,718	1,611	6,25
Al-IV	2,35	2,30	0,252	0,282	0,389	1,75
Al-VI			0,157	0,143	0,145	1,08
Ti	0,70	0,77	0,074	0,076	0,119	0,40
Cr	0,00	0,00	0,000	0,000	0,000	0,00
Mg	2,50	2,28	0,528	0,535	0,518	2,16
Fe+2	2,99	3,09	0,320	0,320	0,299	2,04
Mn	0,03	0,03	0,009	0,007	0,004	0,05
Ca	1,54	1,57	0,852	0,880	0,892	1,74
Na	0,36	0,46	0,068	0,068	0,052	0,74
Cation	14,40	14,40	4,01	4,03	4,03	16,20
O	20	20	6	6	6	24

Rhönite structural formulae based on 20 oxygen atoms (after Anthony et al., 1995). In the calculations Fe_2O_3/FeO ratio was set to ~ 0.5 following suggestions of Prestvik et al. (1999).

DISCUSSION

Origin of ocelli

Ocelli are characteristic textural elements of mafic rocks with high volatile contents. They principally occur in lamprophyres (Cooper, 1979; Foley, 1984; Rock, 1991). Their origin is still debated; in fact they have been interpreted either as amygdales, or nucleation cores of leucocratic minerals, or vesicles filled with late phase crystallisation minerals, or as products of immiscibility or pegmatitic immiscibility (Cooper, 1979; Foley, 1984; Philpotts, 1976; Sabatier, 1999).

Ocelli found in dykes in analysis are rounded with sharp boundaries. They contain coarser grains than the surrounding matrix; tangentially arranged grains around the ocellus and a zoned structure with spherical, carbonatic core are common. They are very similar to ocelli in lamprophyre dykes from the Alcsútdoboz-2 borehole (Szabó et al., 1993), whereas the ocelli described from the Mecsek Mts (SW Hungary) miss the silicate rim around the carbonate core and have different mineralogical composition (Demény and Harangi, 1996) being less similar to those in analysis. The ocelli of Villány Mts are also similar to the type II globular structures found in the sannaite dykes from Aillik Bay, Labrador (Foley, 1984) and to those described by Philpotts (1976) in lamprophyres of the Monteregian alkaline province of Quebec, as well as others described from the Massif Central (Sabatier, 1999). The formation of such globular structures has been explained by segregation of a late-stage melt into bubbles after much of the groundmass had crystallised (Smith, 1967; Foley, 1984). The internal, carbonate core can be interpreted as a bubble that originally was occupied by a gas phase. The outer zones may have derived during solidification of a late-stage silicate melt. The origin of the core from a gas bubble is based on its common spherical shape (Smith, 1967; Foley, 1984), which is well shown by the ocelli from the dyke in analysis.

The high amount of ocelli in the studied subvolcanic bodies points to a high volatile content of the injected magma. The systematic appearance of the ocelli in the xenolith-free samples of the dyke provides evidence of gravitational differentiation between the denser, xenolith-rich and the lighter, volatile-rich melt during crystallisation.

Chemical zoning of ocellus forming minerals is well described for some ocellar lamprophyres. In type II ocelli from Labrador (Foley, 1984), the common trends show a rimward increase of acmite component in clinopyroxenes coupled with a drop in Mg and Ca. In micas decrease of Mg, Al, Ti and rise in Ca and Mn is also observed (Foley, 1984). Zoned kaersutites of ocelli are progressively enriched form core to rim in Fe, Ca and Na and depleted in Mg in lamprophyres form New Zealand (Cooper, 1979). Clinopyroxenes from ocelli of lamprophyres in Hungary (AD-2) show normal zoning with rimward increase of Ti, Al and Fe (Szabó et al., 1993). These trends are in agreement with the interpretation of these ocelli as they represent late stage segregation melts (Foley, 1984).

Pyroxene crystals of the ocelli in question are identical to those appear in the host basalt suggesting an identical origin. Single amphibole grains and amphibole overgrowth (tshermakite, according to Leake et al., 1997) around pyroxene grains occur rarely outside the ocelli and so must have formed from the segregated volatile-rich material simultaneously with rhönite laths.

Based on the petrographic similarities between the Villány Mts ocelli and those from lampyrophyre dykes wordwide (Philpotts, 1976; Cooper, 1979; Foley, 1984; Szabó et al., 1993) we think that the common complex ocelli in the studied Villány Mts basalts derived by segregation of the volatile-rich segment of the magma in the late phase of the crystallisation and solidified after separation of carbonate-rich and silicate-rich parts into the carbonate-bearing bubble and the silicate mantle. Pyroxene grains rarely develop in the ocelli, rather they are inherited from the basalt matrix, based on their similar composition and on the fact that they crosscut the ocellus-host basalt boundary.

Crystallisation of rhönite

Rhönite is a rare aluminosilicate belonging to the aenigmatite group minerals. The general crystal-chemical formula of rhönite may be written as $A_2B_6T_6O_{20}$, where A = Ca, B = Mg, Fe^{2+}, Fe^{3+}, Ti, T = Si, Al. Rhönite has been described from different magmatic environments; mostly from groundmass of undersaturated alkali volcanics and intrusives e.g. melilite, nepheline basalt, basanite, alkali syenite (Kylie and Price, 1975; Magonthier and Velde, 1976; Johnston and Stout, 1985; Fodor and Hanan, 2000; etc.) In groundmass it occurs as small, opaque or semi-opaque, dark brown, euhedral grains, together with plagioclase, pyroxene and opaque minerals. Rhönite is known from other conditions as well; from meteorites as rounded grains included in fassaite crystals in melilite-fassaite paragenesis, considered as a metastabile phase in the melts (Nazarov et al., 2000; references therein) and from silicate melt inclusions of olivine phenocrysts as small, dark brown crystals together with augite, minor Al-spinel, pure CO_2 and sulfide blebs (Kóthay and Szabó, 1999; Kóthay et al., 2001, 2003). Secondary formation of rhönite from breakdown of Ti-bearing amphiboles is also reported (Kunzmann, 1999). Presence of rhönite in ocelli is rather infrequent worldwide; rhönite may afford important information about the crystallisation conditions of the ocelli, but its exact formation conditions are still lesser known.

There are only a few measurements available of rhönite worldwide (Kyle and Price, 1975; Magonthier and Velde, 1976; Johnston and Stout, 1985; Kunzmann, 1989, 1999; Downes et al., 1995; Prestvik et al., 1999; Fodor and Hanan, 2000; Grapes et al., 2003) but no one from ocelli. Comparing the rhönite from the Villány Mts basalt ocelli (Table 1, Fig. 3A, B) to those described from the more similar geological environment (groundmass), we can find some compositional differences. The rhönite in analysis is of higher Si, Fe and Na content while lower in Ti, Al and Ca than the samples described in several mafic magmatics (Downes et al., 1995; Prestvik et al., 1999; Fodor and Hanan, 2000). Fig. 3A shows the Ti vs. Na + ^{IV}Si plot of the Villány Mts rhönite and some published rhönite data from alkali mafic magmas, according to the nomenclature of Kunzmann (1999). The Villány Mts samples fall within the rhönite range, but they are slightly higher in Na + ^{IV}Si than the other samples. On the (Na + ^{IV}Si) vs.(Ca + ^{IV}Al) diagram (Fig. 3B) the Villány Mts samples also are well separated from the other data due to their higher Na + ^{IV}Si and lower Ca + ^{IV}Al values; only one sample from Kyle and Price (1975) falls near to them. Comparison of terrestrial rhönite data (Grapes et al., 2003) shows that systematically high Na + ^{IV}Si and low Ca + ^{IV}Al is characteristic of rhönite formed as a breakdown product of kearsutite in mantle xenoliths or in gabbroic rocks, whereas rhönite phenocrysts and microphenocrysts or groundmass consituents normally have lower Na + ^{IV}Si, but higher Ca + ^{IV}Al. Such a chemical classification, however, depends essentially upon the bulk composition (Grapes et al., 2003), and so does not define clear genetic classes.

Several experiments have aimed to reveal the exact formation conditions of rhönite. According to conclusion of Kunzmann (1989), its formation under magmatic conditions requires pressure below 600 bars, temperature between 840 and 1200°C and presence of a hydrous fluid phase, however there is no limit of oxygen fugacity. Huckenholz et al. (1988)

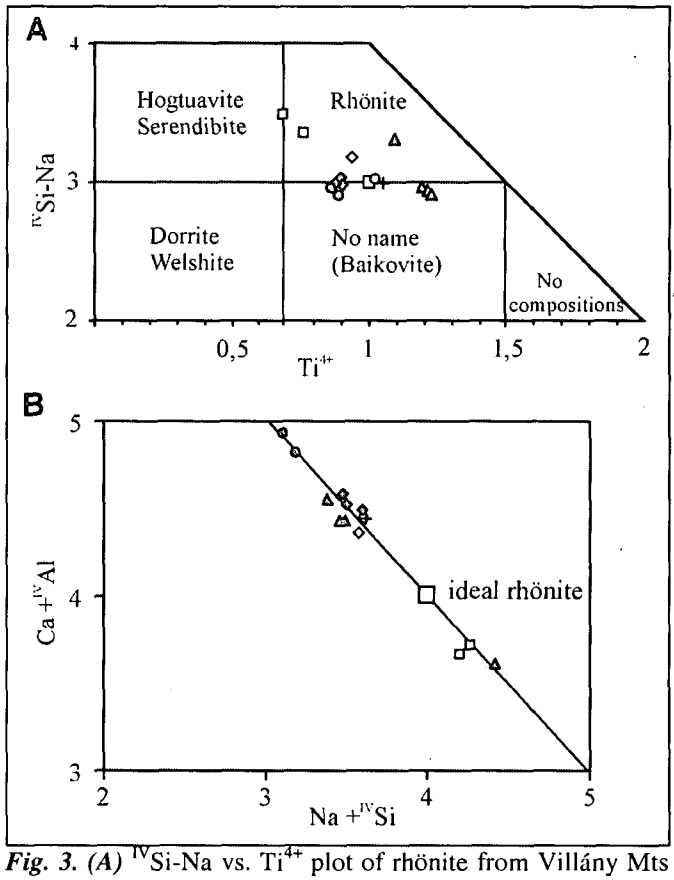

Fig. 3. (A) ^{IV}Si-Na vs. Ti^{4+} plot of rhönite from Villány Mts basalt in comparison with published data of rhönite as groundmass constituent (after Kunzmann, 1999). ***(B)*** Ca+^{IV}Al vs. Na+^{IV}Si plot of Villány Mts rhönite in comparison with some published data for rhönite as groundmass consituent. Black filled squares: Villány Mts; grey filled diamonds: Magonthier & Velde (1976); grey filled triangles: Kyle & Price (1975); grey filled circles: Prestvik et al. (1999); open circle: Downes et al. (1995); open diamond: Camerun et al. (1970); cross: Boivin (1980); open square: "ideal" $Ca_2(Mg_3Fe^{2+}Fe^{3+}Ti)(Si_3Al_3)O_{20}$ rhönite composition (Kunzmann, 1999).

determined the stability field for coexistence of rhönite and amphibole under magmatic conditions in an even narrower range of temperature and pressure: between 0.5 kbar, 1050°C and 0.2 kbar, 1000°C. They suggested that in ascending basalt, the formerly crystallised amphiboles leaving their stability field breakdown into an assemblage of rhönite + plagioclase at low pressure (below 0.5 kbar) and high temperature (1050-1140°C), and rhönite coexists with amphibole in the reaction assemblage only in the above mentioned very narrow PT range.

Experimental study of Boivin (1980) aimed to determine the chemical controls of the formation of rhönite. According to this experiment rhönite formation is independent of fO_2 conditions, but significantly depends on the chemical composition of the magma, especially on Ca and Ti activity of the liquid; TiO_2 content above 2.5 w% is required for the crystallisation of rhönite. If the Ca-content of the melt exceeds 11 mol%, rhönite coexists with plagioclase in groundmass, otherwise rhönite is the only crystallised phase. Rhönite normally occurs below 1 kbar, at about 1170-1100°C, accompanied by plagioclase.

Petrographic studies on rhönite in meteorites (Nazarov et al., 2000) and several recent microthermometric analyses on silicate melt inclusions (Kóthay and Szabó, 1999; Kóthay et al., 2001, 2003; Sharygin et al., 2003) have, however, proved that rhönite can form as a primary phase at rather high PT conditions.

Conclusions

The evolution of Villány Mts basalts, according to Nédli (1999), Nédli and M.Tóth (1999a, b, 2003) and unpublished data, can be outlined as follows. The magma was generated from a metasomatised spinel lherzolite mantle source, by a low degree (approx. 1-5%) partial melting. Ascending from the mantle it included fragments of the heterogeneous, metasomatised mantle, while at shallow depth the magma contaminated the crustal material, as well. Previous estimations (Kovács et al., 2001; Nédli and M. Tóth, 2003) showed that the ascending velocity of the magma was high enough (max.10-30 cm/s) to arrive near surface to form dykes. When intruding Mesozoic carbonates, the temperature could drop rapidly causing the separation of volatile-rich constituents from the crystallised basalt matrix. At the end of the crystallisation history the segregated melt solidified in ocelli.

Comparing the experimentally determined data and petrographical observations about the formation of rhönite to the evolution of the studied samples contradictory results may be got. Data suggest that the ocelli were formed in the late stage of the crystallisation of the basalt, certainly below 1000°C and 8 kbar, which are the crystallisation conditions of the clinopyroxene phenocrysts, according to method of Lindsley (1983). According to the method of Otten (1984), amphibole in ocelli records formation temperature around 980 °C as a minimum estimation through co-existing with another Ti-phase (rhönite). Taking also the fact into account that high ascent velocity of magma is supposed (Kovács et al., 2001; Nédli and M.Tóth, 2003), ocelli probably formed near the Earth's surface, at relatively low pressure but high temperature, like in the experiments of Kunzmann (1989) and Boivin (1980). Composition of co-existing amphiboles of the ocelli confirms formation at high temperature through high Ti (Raase, 1974; Ernst and Liu, 1998), Al^{IV} (Bard, 1970; Blundy and Holland, 1990) and $(Na+K)^{A}$ values, significant Al^{VI} and especially Na^{M4} data, however exclude crystallization under extremely low pressures (Hammarstrom and Zen, 1986; Ernst and Liu, 1998). Several recent studies on rhönite in silicate melt inclusions (Kóthay and Szabó, 1999; Kóthay et al., 2001, 2003; Sharygin et al., 2003) also doubt crystallization of rhönite at very low pressures.

As a conclusion we can state that rhönite in the ocelli of the Villány basalt dykes are of primary igneous origin, which crystallized from the late, segregated volatile-rich part of the magma. Based on petrographic observations and composition of the co-existent amphibole, rhönite certainly developed under rather high temperature, but at significantly higher pressure than most experiments suggest.

Acknowledgments

The DCM Limestones Mine Co. is gratefully acknowledged for making the fieldwork and sampling possible. Pongrácz L., Péró Cs., Rálischné Felgenhauer E., Kassai M., Szabó Cs. are thanked for serving hand specimens and thin sections. The authors wish to give special thank to the members of the Lithosphere Fluid Research Lab (Eötvös L. University, Budapest) for constructive discussions and to Szabó Cs. for his indispensable suggestions and review of the manuscript. L. W. Diamond is thanked for making microprobe measurements at the Montanuniversität, Leoben possible.

References

Anthony, J. W., Bideaux, R. A., Bladh, K., W., Nichols, M. C. (1995): Handbook of mineralogy, Vol. II. Silica, silicates, Part 2. Mineral Data Publishing, Tucson, AZ, p. 683.

Bard, J. P. (1970): Compositions of hornblendes during the Hercynian progressive metamorphism of the Aracene metamorphic belt (SW Spain). Contrib. Mineral. Petrol., **28**, 117-134.

Blundy, J. D., Holland, T. J. B. (1990): Calcic amphibole equilibria and a new amphibole-plagioclase geothermometer. Contrib. Mineral. Petrol., **104**, 208-224.

Boivin, P. (1980): Données expérimentales préliminaries sur la stabilité de la rhönite à 1 atmosphère. Application aux gisements naturels. Bull. Minèral., **103**, 491-502.

Camerun, K. L., Carman, M. F., Butler, J. C. (1970): Rhönite from Big Bend National Park, Texas. Am. Mineral., **55**, 864-874.

Cooper, A. F. (1979): Petrology of ocellar lamprophyres from Western Otago, New Zealand. J. Petrology, **20**, 139-163.

Downes, H., Vaselli, O., Seghedi, I., Ingram, G., Rex, D., Coradossi, N., Pécskay, Z., Pinarelli, L. (1995): Geochemistry of late Cretaceous – early Tertiary magmatism in Poiana Rusca (Romania). Acta Vulcanol., **7(2)**, 209-217.

Ernst, W. G., Liu, J. (1998): Experimental phase equilibrium study of Al- and Ti-contents of Ca-amphibole in MORB – A semiquantitative thermobarometer. Am. Mineral., **83**, 952-969.

Fodor, R. V., Hanan, B. (2000): Geochemical evidence for the Trinidade hotspot trace: Columbia seamount ankaramite. Lithos, **51**, 293-304.

Foley, S. F. (1984): Liquid immiscibility and melt segregation in alkaline lamprophyres from Labrador. Lithos, **17**, 127-137.

Fülöp, J. (1966): A Villányi-hegység krétaidőszaki képződményei (The Cretaceous rocks of the Villány Mts). Geol. Hun. Ser. Geol., **15**, 12-15. (in Hungarian)

Grapes, R. H., Wysoczanski, R. J., Hoskin, W. O. (2003): Rhönite paragenesis in pyroxenite xenoliths, Mount Sidley volcano, Marie Byrd Land, West Antarctica. Min. Mag., **67(4)**, 639-651.

HAMMARSTROM, J. M., ZEN, E. (1986): Aluminium in hornblende: an empirical igneous geobarometer. Am. Mineral., **71**, 1297-1313.

HARANGI, SZ., ÁRVÁNÉ SÓS, E. (1993): A Mecsek hegység alsókréta vulkáni kőzetei I. Ásvány- és közettan. (Early Cretaceous volcanic rocks of the Mecsek Mountains, S Hungary, I. Mineralogy and petrology). Földt. Közl., **123/2**, 129-165. (in Hungarian with English abstract)

HUCKENHOLZ H. G., KUNZMANN T., SPICKER C. (1988): Stability of titanian magnesio-hastingsite and its breakdown to rhönite-bearing assemblages. Terra Cognita, **8**, 66.

JOHNSTON, A. D., STOUT, J. H. (1985): Compositional variation of naturally occurring rhönite. Am. Mineral., **70**, 1211-1216.

KÓTHAY, K., SZABÓ, CS. (1999): Silicate melt inclusion study on olivine phenocrysts from the Hegyestű basalt, Balaton Highland, Hungary. Terra Nostra, **99/6**, 15th ECROFI XV, Potsdam, June 21-24, 1999. Abstracts, 170-173.

KÓTHAY, K., SZABÓ, CS., SHARYGIN, V. V., TÖRÖK, K. (2001): Silicate melt inclusion study on olivine phenocrysts and clinopyroxene microphenocrysts in the Hegyestű basalt, Bakony-Balaton Highland, Hungary. Memórias, **7**, 237-240.

KÓTHAY, K., PETŐ, M., SHARYGIN, V. V., TÖRÖK, K., SZABÓ, CS. (2003): Silicate melt inclusions in olivine phenocrysts from Hegyestű (Bakony-Balaton Highland) and Pécskő alkaline basalts (Nógrád-Gömör), Hungary. Geophysical Research Abstracts, **5**, 00748

KOVÁCS, I., NÉDLI, ZS., KÓTHAY, K., BALI, E., ZAJACZ, I., SZABÓ, CS. (2001): Quartz and feldspar xenocrysts in mafic lavas from Nógrád-Gömör volcanic field, Balaton-Bakony Highland volcanic field and Villány Mountains (Hungary). Mitteilungen der Österreichischen Mineralogischen Gesellschaft, **146**, 155-156.

KUNZMANN, T. (1989): Rhönit: mineralchemie, paragenese und stabilitat in alkalibasaltischen vulkaniten. Ein beitrag zur minerogenese der Rhönit-anigmatit-mischkristallgruppe. Doctoral dissertation, Ludvig-Maximillians University, Munich, 152.

KUNZMANN, T. (1999): The aenigmatite-rhönite mineral group. Eur. J. Mineral., **11**, 743-756.

KYLE, P. R., PRICE, R. C. (1975): Occurrences of rhönite in alkalic lavas of the McMurdo Volcanic Group, Antarctica, and Dunedin Volcano, New Zealand. Am. Mineral., **60**, 722-725.

LEAKE, B. E. (1965): The relationship between tetrahedral aluminium and the maximum possible octahedral in natural calciferous and subcalciferous amphiboles. Am. Mineral., **50**, 843-854.

LEAKE, B. E. (1971): On aluminous and edenitic hornblendes. Mineral. Mag., **38**, 389-407.

LEAKE, B. E., WOOLLEY, A. R., ARPS, C. E. S., BIRCH, W. D., GILBERT, M. C., GRICE, J. D., HAWTHORNE, F. C., KATO, A., KISCH, H. J., KRIVOVICHEV, V. G., LINTHOUT, K., LAIRD, J., MANDARINO, J., MARESCH, W. V., NICKEL, E.H., ROCK, N. M. S., SCHUMACHER, J. C., SMITH, D. C., STEPHENSON, N. C. N., WHITTAKER, E. J., YOUZHI, G. (1997): Nomenclature of amphiboles: report of the Subcommittee on amphiboles of the International Mineralogical Association Commission on new minerals and mineral names. Mineral. Mag., **61**, 295-321.

LINDSLEY, D. H. (1983): Pyroxene thermometry. Am. Mineral., **68**, 477-493.

MAGONTHIER, M. C., VELDE, D. (1976): Mineralogy and petrology of some Tertiary leucite-rhönite basanites from central France. Mineral. Mag., **40**, 817-26.

MOLNÁR, S., SZEDERKÉNYI, T. (1996): Subvolcanic basaltic dyke from Beremend, Southeast Transdanubia, Hungary. Acta Min.-Petr., **37**, 181-187.

NAZAROV, M. A., PATCHEN, A., LAWRENCE, A. T. (2000): Rhonite-bearing Ca, Al-rich inclusions of the Efremovka (CV3) chondrite. In Lunar and Planetary Science XXXI, Abstract 1242, Lunar and Planetary Institute, Houston (CD-ROM).

NÉDLI, ZS. (1999): Mezozoós szubvulkáni kőzettestek vizsgálata a Villányi-hegységben (Study on Mesozoic subvolcanic dykes in the Villány Mts, SW Hungary) Szakdolgozat, JATE, Szeged (Thesis, in Hungarian)

NÉDLI, ZS., M.TÓTH, T. (1999a): Mantle xenolith in the mafic dyke at Beremend, Villány Mts, SW Hungary. Acta Min. Petr., **40**, 97-104.

Nédli, Zs., M.Tóth, T. (1999b): Igneous records of the Meso-Alpine (Upper Cretaceous) subduction in the Villány Mts (Tisia block, SW Hungary). In Székely et al. (eds.): Tübinger Geowissenschaftliche Arbeiten, Series A., **52**, 188-189.

NÉDLI, ZS., M.TÓTH, T. (2003): Felső kréta alkáli bazalt vulkanizmus a Villányi-hegységben. (Upper Cretaceous alkali basalt volcanism in the Villány Mts (SW Hungary)). Földt. Közl., **133/1**, 49-67. (in Hungarian with English abstract)

OTTEN, M. T. (1984): The origin of brown hornblende in the Artfjället gabbro and dolerites. Contrib. Mineral. Petrol., **86**, 189-199.

PHILPOTTS, A. R. (1976): Silicate liquid immiscibility: its probable extent and petrogenetic significance. Am. J. Sci., **276**, 1147-77.

PRESTVIK, T., TORSKE, T., SUNDVOLL, B., KARLSSON, H. (1999): Petrology of early Tertiary nephelinites off mid-Norway. Additional evidence for an enriched endmember of the ancestral Iceland plume. Lithos, **46**, 317–330.

RAASE, P. (1974): Al and Ti contents of hornblende, indications of pressure and temperature of regional metamorphism. Contrib. Mineral. Petrol., **45**, 231-236.

ROCK, N. M. S. (1991): Lamprophyres. Blackie and Son, Glasgow-London-New York, 43-46.

SABATIER, H. (1999): Pegmatitoïdes et basaltes globuleux dans le Massif central français: l'immiscibilité pegmatitique et son double intérêt pour la différenciation magmatique (Evidence of a kind of immiscibility between dry and "wet" fractions of a basic melt. The double bearing of such a process on magmatic differentiation). C.R.Acad.Sci.Paris, Sciences de la terre et des pianétes/Earth&Planetary Sciences, **329**, 645-652.

SHARYGIN, V. V., KÓTHAY, K., PETŐ, M., TÖRÖK, K., TIMINA, T. J., VAPNIK, Y., KUZMIN, D. V., SZABÓ, CS. (2003): Rhönite in alkali basalts: studies of silicate melt inclusions in olivine phenocrysts. ECROFI XVII, 5-7 June, 2003, Budapest, Acta Min.-Petr., Abstract Series 2, Szeged, 2003, 182-183.

SMITH, R. E. (1967): Segregation vesicles in basaltic lava. Am. J. Sci., **265**, 696-713.

SPEAR, F. S. (1981): An experimental study of hornblende stability and compositional variability in amphibolite. Am. J. Sci., **281**, 697-734.

SZABÓ, CS., KUBOVICS, I., MOLNÁR, ZS. (1993): Alkaline lamprophyre and related dyke rocks in NE Transdanubia, Hungary: The Alcsútdoboz-2 (AD-2) borehole. Min. Petrol., **47**, 127-148.

THIEBLEMONT, D., TRIBOULET, C., GODARD, G. (1988): Mineralogy, petrology and P-T-t path of Ca-Na amphibole assamblages, Saint-Martin des Noyers formation, Vendée, France. Journal of Metamorphic Geology, **6**, 697-715.

Received: September25, 2003; accepted: December 8, 2003

Acta Mineralogica-Petrographica, Szeged 2003, Vol. 44, pp. 57-61

ACTA
Mineralogica
Petrographica

PETROGRAPHIC STUDIES ON THE NASA LUNAR SAMPLE THIN SECTION SET: I. THE TEXTURAL SEQUENCE OF THE BASALTIC SAMPLES AND THIER DESCRIPTION BY CELLULAR AUTOMATA MOSAIC MODEL AND TENTATIVE TTT-DIAGRAM

SZANISZLÓ BÉRCZI[1], SÁNDOR JÓZSA[2]

[1] Department of General Physics, Cosmic Materials Space Research Group, Eötvös Loránd University
H-1117 Budapest, Pázmány Péter sétány 1/C, Hungary
[2] Department of Petrology and Geochemistry, Eötvös Loránd University
H-1117 Budapest, Pázmány Péter sétány 1/C, Hungary
e-mail: bercziszani@ludens.elte.hu

ABSTRACT

NASA Lunar Sample Educational Set is a valuable source for planetary petrology education. Using the basaltic thin sections and clast from breccias of the Apollo expedition lunar samples we made cosmopetrographic comparisons between the lunar and a terrestrial sequence. We made a tentative parallel layered sequence of the textures from a lunar mare cross section and a terrestrial pillow lava gradient from outside to inside. On the basis of textural comparisons we compiled a tentative TTT diagram for the lunar mare cooling rates and pillow lava textures.

INTRODUCTION

During the last 10 years (see Appendix) Eötvös University received on loan the NASA Lunar Sample Thin Section Educational Set from Johnson Space Center, Houston. We made various new applications on the basis of this valuable set. One main topics was the comparison of extraterrestrial materials and selected thin sections from terrestrial rocks. We also used industrial materials for textural comparisons, where the operations in the technology manufacturing sequence give a good descritpion of the transformations of the phases (Bérczi et al., 1997, 1999, 2001). Added textures multiplied and extended the possibilities to form complex concepts: how to constitute complex material maps by starting from a sequence of textural types? (inter-connections, basic physical and textural relations of igneous rocks, and other compositions from material science, as ceramics, metallurgy).

Here we report about the study on basalts of NASA Lunar Educational Thin Section Set with comparisons to terrestrial pillow lava textures. On the basis of parameters read from lunar and terrestrial textures the tentative TTT diagram (T-TTT diagram) of basalts can be sketched. In this work we also used the basaltic clasts from breccias and soil samples. First we determined the paragenetic sequences of the samples on the basis of textural characteristics and then estimated cooling rates were determined. In the construction of T-TTT diagram some materials of corresponding technologies (cooling rates, industrial TTT diagrams of hardening steel and forming industrial textures) were also compared.

TEXTURES OF BASALTIC LAYERS REPRESENTED IN THE NASA SET

Many studies on basaltic textural types of the NASA lunar samples, from paragenetic sequence, grain size, crystal morphology, and their systematic relation with the cooling rates in the magma body were studied earlier (Meyer, 1987; Bence and Papike, 1972; Lofgren et al., 1974). In our study we first estimated these parameters from the paragenetic textural sequence from the surface edge toward the deeper layers of gradually coarser fabrics of basaltic samples in an undisturbed magma body. Both textural types, crystal morphology, were used in a cellular automata description to deduce paragenetic sequences for different lunar basalt types of the NASA Lunar Set, in a 8-10 meters thick lunar basaltic flow (Bence and Papike, 1972; Lofgren et al., 1974; Grove, 1977; Grove et al., 1973, 1977), and finally their tentative TTT diagrams (correspondence of cooling rates and textural gradual changes) were constructed.

In the second part of the course we compared basaltic samples of the lunar set, with some similar Carpathian Basin basalts and gabbros of which basalts we selected an ophiolitic textural series of the Darnó Hill, Heves C., Hungary (Józsa, 2000). where a continuous sequence of textures was found parallel with the lunar samples (Grove, 1977).

BASALTIC SAMPLES AND CLASTS IN NASA LUNAR SET IN TEXTURAL SEQUENCE

On the basis of the sequence of terrestrial textures we estimated (interpolated) the place (probable original depth) of the lunar set textures in a lunar basaltic lava flow. We also used literature data for cooling rates. The samples in a sequence starting from the greatest cooling rate are:

74220 The "highest" position (the greatest cooling rate) had the orange soil spherules in the 74220, because their ejection as a lava fountain (Meyer, 1987; Delano and Livi, 1981; McKay and Wentworth, 1992) had glass quenching cca. 1000 C/min. cooling rate (Dungan and Brown, 1977).

68501 Variolitic clast. In an earlier loan of the NASA Lunar set No. 6. the 72275,509 breccia contained a larger

vitrophyric-variolitic clast. 72275 is the thin section with the largest surface in the lunar set. The No. 4. set contains a clast with spherulitic-variolitic texture among the soil grains of 68501 This clast had second highest cooling rate in our sequence (tentatively: some hundred degrees Celsius per day).

12002 This Apollo 12 porphyritic sample 12002 represents slower initial cooling rate for the large olivine grains and higher cooling rate (wide range) for the surrounding (variolitic) laths of clinopyroxenes and plagioclase feldspars (Dungan and Brown, 1977). In a revised model cooling rates may vary from some degrees Celsius to 2000 C/hour (Walker et al., 1975).

14305 The breccia 14305 contains intergranular type clasts, such representing the third texture in the cooling rate sequence (tentatively: hundred degrees Celsius per week)

72275 The subophitic clast of 72275,128 breccia represents an even slower cooling. Over breccias all three basaltic samples represent well crystallized beautiful specimens.

70017 This poikilitic sample of 70017 has paragenetic sequence similar to A-11 High Ti- basalts (Grove, 1977), rich occurrence of sector zoned clinopyroxenes. The rich population of ilmenites make dark the thin section: this ilmenite rich specimen has a counterpart near to Darnó Hill (at Szarvaskő), in a gabbro with high ilmenite cont. bw. 8-10 % wt.)

12005 The Apollo 12 poikilitic 12005 sample had the slowest cooling, so this specimen closes our cooling rate series. It contains large, zoned pyroxene oikocrystals with embedded idiomorphic (euhedral) olivine grains of chadacrysts (Dungan and Brown, 1977).

TERRESTRIAL COUNTERPART TEXTURES: AN OPHIOLITIC SEQUENCE OF DARNO HILL

In the Darnó Hill (basalts and microgabbros) textural sequence of ophiolitic gabbros and basalts can be found. From the outer edge high cooling rate textures to the inner part of the magmatic body (as to the center of a pillow lava "sphere") the following textures represent this series: spherulitic, variolitic, intersertal, intergranular, subophitic, ophitic, poikilitic (Józsa, 2000). Although important details are different in a terrestrial flow and in a lunar flow (chemical compositions, - e.g. 74220 and 12002 are picritic basalts (Nord et al, 1975; Grove et al., 1973; Walker et al., 1974) - water content can change paragenetic sequence of crystallization for plagioclase feldspar and pyroxene), the main textural characteristics determined by cooling rates remains important basis for comparisons and TTT diagrams.

COOLING RATES FOR LUNAR AND TERRESTRIAL BASALTS AND TENTATIVE TTT DIAGRAM FOR THE LUNAR BASALTS

On the basis of experimental determination of the cooling rates and also from TEM measurements of clinopyroxenes both cooling rate sequences and TTT-diagrams were studied and determined (Bence and Papike, 1972; Grove, 1977, 1982; McConell, 1975; Nord et al, 1975). The lunar basalt layer was 8-10 meter thick (Grove, 1982; Nord et al, 1975). This thickness is larger, but comparable to pillow lava units as terrestrial pairs.

Table 1. Texture vs. cooling rate relations in a cooling pillow lava body.

textural type	cooling rate	depth in a pillow lava	length of cooling time
glassy	45000 - 1800 C / min.	1 centimeter	1 min.
spherolitic	22000 - 1000 C / min.	some centimeters	some minutes
variolitic	1000 - 200 C / min.	decimeter	10 minutes - 0,5 hour
intersertal	200 - 30 C / min.	some decimeters	0,5 - 2 hours
inter-granular	0,5C / min.	central region of pill.l.	1 - 2 days

A pillow lava cools during 2 days, but 8-10 meters thick lunar layers cooled for months or years in their inner regions. In a pillow lava textural sequence only the intergranular texture could be reached because of the quick cooling and smaller lava body size. In the lunar basalt case all textural types in our sequence could be reached. The corresponding cooling rates were given by Grove (1977) as 3 C/min. for a vitrophyric, 30 C/hr for a coarser vitrophyric and 3 C/day for a porphyritic Apollo 15 sample. Data of a pillow lava are in Table 1. as follows: (Józsa, 2000; Szakmány, 1995).

SYNOPTIC VIEW BY COMPLEX MATERIAL MAPS

Textural structure contains a versatile characterization possibility for rocks. Microscopic studies give comparative possibilities with other materials. In material science and technology we frequently summarize the behaviour of a metal (or ceramics) by a path of state changes in the field of different physical parameters: we call them material maps. (This synoptic-synthetic view is also used in biology, by the niches. Niches are parameter-cells, where living beings occupy distinct, or partly overlaping regions.) We developed synoptic view in interplanetary comparative petrography by materail maps.

The basaltic samples of the NASA lunar set form a sequence from quick to slow cooling. They represent stages (phases from different depth) from a cross section of a cooling lava flow. (The samples are: 74220 - Orange Soil - volcanic spherules, 12002, porphyric-variolitic texture, 70017, and 12005, ophitic-poikilitic texture (Józsa, 2000). These stages of a sequence represent gradually slower cooling rates. They also represent different SiO_2 ranges: while ranges of picritic (74220 and 70017) and basaltic (12002 and 12005) rocks involve the SiO_2 classification, the cooling rates involves TTT diagrams to be attached (and other C-rurves from metallurgy). While compositional evolution brings the Bowen type ternary and quaternary system diagrams, the TTT diagrams brings the volcanic, subvolcanic and plutonic distinction for igneous rocks. The extended fields bring other lunar samples to "appear" on material maps, as representatives of plutonic type rocks (60025, anorthosite, 78235, norite). Step by step the material maps can be extended by new parameters, and both terrestrial and Martian (meteorite) rocks may be involved into such material maps.

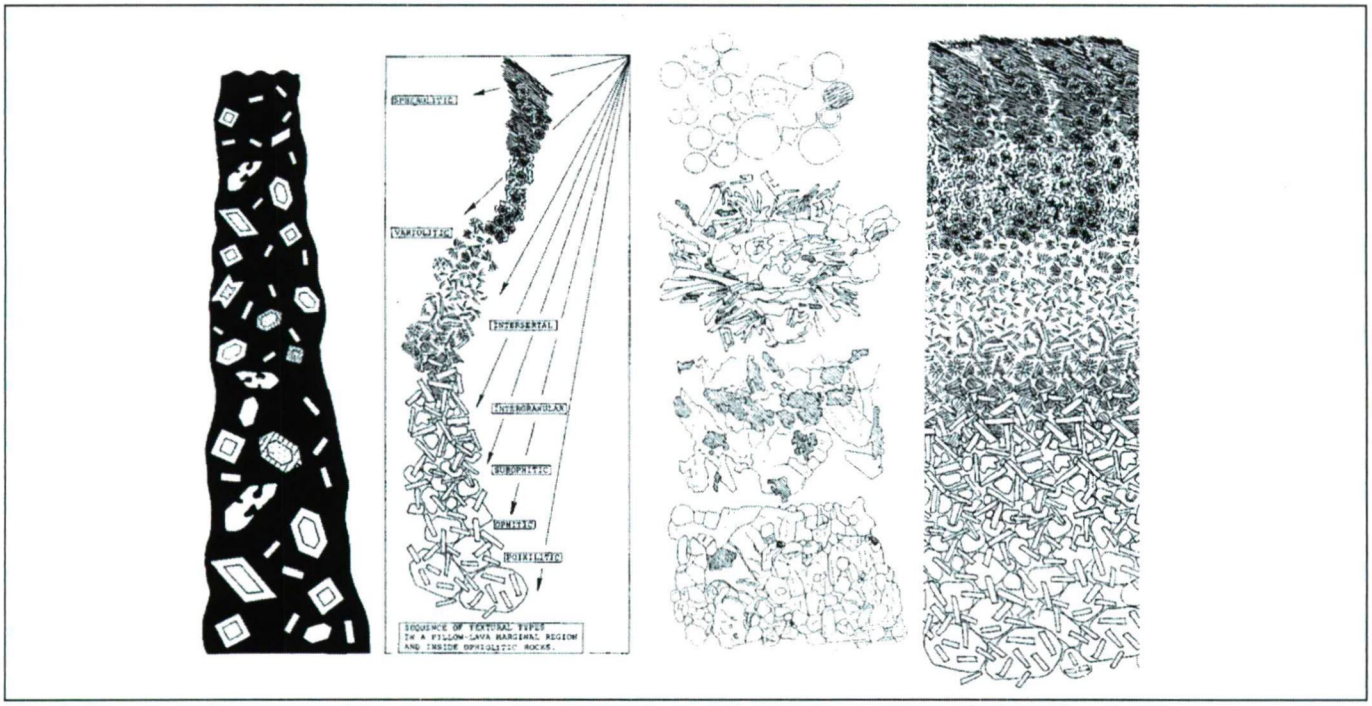

Fig. 1. Sequence of textures and the corresponding T-TTT diagram for the cross section of a lunar lava layer.

CELL-MOSAIC AUTOMATA MODEL DESCRIPTION OF PETROLOGIC TEXTURAL TRANSFORMATIONS

Cell-mosaic automata model helps to formulate all those descriptions we do in practice during textural analyses. The sequence of discrete changes in a cell-mosaic system is formulated on two hierarchy levels: on cellular one (minerals), and on global one (texture itself). (Bérczi, 1990, 1993) The cell-automata mosaic's flow-chart has a framework of description: it is composed from two parts. The first one gives the structure and initial conditions of the cellular background, the second one gives the transitional functions (Bérczi, 1993). Both parts form a pair of approach: a local and a global one, as follows (Fig. 1.)

The advantages of the cell-automata mosaic model come from this separability of local and global picture: both for conditions and operations, and from the expressed connections (feedback possibility) between the local and global characteristics. We made such style of descriptions of sequence of crystallization of 70017 high Ti basalt texture, a metamorphic sequence of terrestrial textures (Vollmar, 1978), Grossman type CAI condensational sequence (this last one was almost in this form (Grossman, 1974), and carbonaceous chondritic aqeous alteration sequence (Krot et al., 1998; Sztrókay et al, 1961).

DESCRIPTION OF PETROLOGIC TEXTURAL TRANSITIONS BY CELLULAR AUTOMATA

We can formulate descriptions of textural analyses by cell-mosaic automata model. It helps to reconstruct the sequence of discrete changes in a cell-mosaic system. The model is formulated on two hierarchy levels: One level is that of minerals (that of cellular one) and that of the texture (global one). The "flow-chart" of the cell-automata mosaic's is composed from two parts: A) that of the structure and initial conditions of the cellular background, and B) that of the transitional functions (Bérczi, 1993). Both parts form a pair of approach on a local and a global one.

The cell-automata mosaic model has advantages coming from the separability of local and global picture. One is the feedback possibility between the of sequence of crystallization of 70017 high Ti basalt texture was made in the paragenetic sequence. From this we reconstructed a

Table 2. Local vs global level of descriptions in a cellular-automata mosaic model.

	a. LOCAL (CELL-LEVEL)	b. GLOBAL (TEXTURAL)
A.. *CELLULAR BACKGROUND*	Aa. Local characteristics of the cell-mosaic system give the cells, as actors in events, the form of the cells, their connections (i.e. faces) and neighbourhood relations.	Ab. Global characteristics of the cell-mosaic system give the texture and the sum up of the local relations. (i.e. the texture is a piokilitic type, because of enclosing relations)
B. *TRANSITIONAL FUNCTIONS*	Ba. Local transitional function for cell mosaic elements which are individual automata (discrete function in space and time, step by step transforming cell-states, i.e. how distinct minerals change)	Bb. Global transitional function for the whole surface populated by the cell-mosaic system (sequence of stages of the texture taken step by step, as a consequence of summed up (for all cells) of the local transitional functions.)

tentative TTT diagram. This texture solidifies between 1250 and 950 C, contains the textural fabrics of a sequence, with the cooling rates from glassy quenching 1000 C/min. rate till 0.5-0.05 C/hr.

CONCLUSIONS

We studied the basaltic samples of the NASA Lunar Set and the comparing pillow lava sequence of the Darno-hill ophiolitic thin section set from the Bükk Mts. Hungay. We constructed from lunar basaltic textural characteristics via cellular automata modeling paragenetic and cooling rate sequences, and a tentative TTT-diagram of lunar basalts (lava flows). In this program we compared lunar textural layers to that of a terrestrial pillow lava textural layers and we also compared basaltic TTT diagrams to steel industrial TTT diagrams. In this work role of textural studies of unusual materials for studies of industrial ones were also emphasized. This way studies of planetary materials has a spin-of direction in space science education, too. Another space science educational outreach of this program was the application of the cellular automata type description to textural transformations.

ACKNOWLEDGEMENTS

Thanks to NASA Lyndon B. Johnson Space Center for loan of the Lunar Educational Thin Section Set between 1993 and 2003. Thanks to the Hungarian Space Office for Fund of No. TP-154/2002 and 2003 supporting the loan and research of the NASA Lunar Samples.

REFERENCES

BENCE, A.E., PAPIKE, J. J. (1972): 3th LSC, 59-61.

BÉRCZI, SZ. (1985): Technology of Materials I. (Lecture Note Series of Eötvös University), J3-1333. Tankönyvkiadó, Budapest. (in Hungarian)

BÉRCZI, SZ. (1990): In Gruber, B, Yopp, J. H. (eds.): Symmetries in Science IV. Plenum Press.

BÉRCZI, SZ. (1993): Double Layered Equation of Motion: Platonic and Archimedean Cellular Automata in the Solution of the Indirect Von Neumann Problem on Sphere for Transformations of Regular Tessellations. Acta Mineralogica et Petrographica, Szeged, **39**, 96-117.

BÉRCZI, SZ., FÖLDI, T., KUBOVICS, I., LUKÁCS, B., VARGA, I. (1997): Comparison of Planetary Evolution Processes Studying Cosmic Thin Section Sets of NASA and NIPR. In Lunar and Planetary Science XXIX, LPI. Houston, p. 101.

BÉRCZI, SZ., JÓZSA, S., KABAI, S., KUBOVICS, I., PUSKÁS, Z., SZAKMÁNY, GY (1999): NASA Lunar Sample Set in Forming Complex Concepts in Petrography and Planetary Petrology, Lunar and Planetary Science, **30**, #1038, LPI, Houston (CD-ROM)

BÉRCZI, SZ., JÓZSA, S., SZAKMÁNY, GY., DIMÉN, A., DEÁK, F., BORBÉI, F., FLOREA, N., PETER, A., FABRICZY, A., FÖLDI, T., GÁL, A., KUBOVICS, I., PUSKÁS, Z., UNGER, Z. (2001): Tentative TTT-diagram from Textures of Basalts and Basaltic Clasts of the NASA Educational Set: Comparisons to Terrestrial Basalts. 26th NIPR Symposium Antarctic Meteorites, Tokyo.

CODD, E. F. (1968): Cellular Automata. Academic Press, New York, [23] von Neumann J. (1966) Theory of Self-Reproducing Automata. Edit./completed: A.W.Burks. Urbana, Illinois.

DELANO, J. W., LIVI, K. (1981): Lunar Volcanic Glasses. GCA 45, 2137.

DUNGAN, M. A., BROWN, R. W. (1977): The Petrology of the Apollo 12 Basalt Suite. Proc. Lunar Sci. Conf. 8th. 1339.

GROSSMAN, L. (1974): Condensation of the Solar System. Reprint from McGraw-Hill Yearbook, 1974, San Francisco.

GROVE, T. L. ET AL. (1973): 4th LSC, 323-325.

GROVE, T. L. (1977): 8th LSC, 380-382.

GROVE, T. L., BENCE, A.E. (1977): 8th LSC, 383-385.

GROVE, T.L. (1982): Am. Min. 67, 251-268.

JÓZSA, S. (2000): Thesis. Eötvös University, Dept. Petrology and Geochemistry, ELTE, Budapest.

KROT, A. N., PETAEV, M. I., SCOTT, E. R. D., KEIL, K. (1998): Progressive metamorphism of the CV3 chondrites, Lunar and Planetary Science, **29**, 1552.pdf.

LOFGREN, G. E., DONALDSON, C. H., WILLIAMS, R. J., MULLINS, O. (1974): 5th LSC, 458-460.

MCCONELL, J. D. C. (1975): An. Rev. Earth. Planet Sci., **3**. 129.

MCKAY, D. S., WENTWORTH, S. J. (1992): Geology of Apollo 17 Landing site, WS., LPI Techn. Rep. No. 92-09, Part 1. p.31.

MEYER, C. (1987): The Lunar Petrographic Thin Section Set. NASA JSC Curatorial Branch Publ. No. 76. Houston, Texas, USA.

NORD, G. L., HEUER, A. H., LALLY, J. S., CHRISTIE, J. M. (1975): 6th LSC, 601-603.;

SZAKMÁNY, Gy. (1995): The main textural types of igneous rocks. Eötvös Univ. Lect. N. Ser. Dept. Petrology. (In Hungarian)

SZTRÓKAY, K., TOLNAY, V., FÖLDVÁRINÉ VOGL, M. (1961): Acta Geol. Hung., **7**, p. 17.

VOLLMAR, R. (1978): Algorithmen in Zellularautomaten. Verlag B. G. Teubner, Stuttgart.

WALKER, D. (1974): 5th LSC, 814-816.

WALKER, D., KIRKPATRICK, R. J., LONGHI, J., HAYS, J. F. (1975): 6th LSC, 841-843.

Received: September 2, 2003; accepted: October29, 2003

THE NASA LUNAR SET

The 384 kg of lunar samples collected and brought to the Earth by Apollo expeditions revealed the main petrologic events of lunar thermal history. Four main rock types (anorthosites, basalts and breccias, solis) are represented in the NASA set. The anorthosites and basalts can be corresponded to the two great geologic provinces on the Moon: anorthosites to terra and basalts to mare. These two main rock types represent two great differentiation periods in the lunar thermal history. Using NASA Lunar thin sections we can show these the two main differentiation periods: Crust formation and later basaltic volcanism. Soils and brecciated impact rocks always were produced during the lunar history.

A. Anorthositic crust formation

Two thin sections represent lunar terra. the 60025 anorthosite exhibits all important and nice characteristics of the shocked and brecciated ancient rocks which once had cumulate texture but impacts transformed it. The three main shock phenomena of (a) undulatory extinction, (b) kink banding and (c) twinning are all well represented in textural regions of 60025 anorthosite sample. The largest shock effect of diaplectic glass formation is shown on 78235 norite sample. It represents the other terra rock type, the intrusive ANT suite, and its plagioclase feldspar was mostly transformed to maskelynite. Summary of these first differentiation: magma ocean, flotation of plagioclase feldspars, accumulating anorthositic crust, into which ANT suite rocks later intruded. The great basin forming impacts continue the lunar history.

B. Basaltic volcanism

Basins were flooded by basalt flows on the near side. 3 very nice thin sections of 12002, 12005 and 70017 represent them (Meyer, 1987). Both exhibit somewhat different texture corresponding to the depth of crystallization in a ca. some 10 m thick lava flow. 12002 shows porphyritic texture with variolitic matrix, 70017 is extremely rich in sector zoned pyroxenes embedded ophitically/poikilitically into large feldspars, while 12005 has the most slowly crystallized texture. 74220 orange glass sample can also be connected with this second part of lunar volcanism, but they represent pyroclastic soil, the orange soil. These spherules are primary liquid compositions from lunar mantle, spread by a lava-fountain activity.

C. Breccias and soils

Impacts always formed brecciated rocks and soils on the Moon. Breccias are represented by 3 samples in the set. The 14305 breccia contains large anorthositic recrystallized fragment and a poikilitic basalt grain. The 72275 sample has breccia-in-breccia hierarchic texture referring to repeated impacts. 65015 sample is representing breccias which were partially melted during the impact event.

There are 3 soil samples, together with the 74220 orange glass sample. They are filtered fractions. 68501 represents soil from the highlands, 70181 represents the mare soils. Sample 15299 is a soil breccia which also contains lunar impact spherules (Meyer, 1987).

INSTRUCTIONS FOR AUTHORS

GENERAL

Acta Mineralogica-Petrographica (AMP) publishes articles (papers longer than 4 printed pages but shorter than 16 pages, including figures and tables), notes (not longer than 4 pages, including figures and tables), and short communications (book reviews, short scientific notices, current research projects, comments on formerly published papers, and necrologies of 1 printed page) dealing with crystallography, mineralogy, ore deposits, petrology, volcanology, geochemistry and other applied topics related to the environment and archaeometry. Articles longer than the given extent can be published only with the prior agreement of the editorial board. Occasionally, in the form of supplement issues AMP publishes materials of conferences, or other events of scientific interest.

The journal accepts papers that represent new and original scientific results, which have not appeared elsewhere before, and are not in press either.
All articles and notes submitted to AMP are reviewed by two referees (short communications will be reviewed only by one referee) and are normally published in the order of acceptance, however, higher priority may be given to Hungarian researches and results coming from the Alpine-Carpathian-Dinaric region. Of course, the editorial board does accept papers dealing with other regions as well, let they be compiled either by Hungarian or foreign authors.
The manuscripts (prepared in harmony of the instructions below) must be submitted to the Editorial office in triplicate. All pages must carry the author's name, and must be numbered. At this stage (revision), original illustrations and photographs are not required, though, quality copies are needed. It is favourable, if printable manuscripts are sent on disk, as well. In these cases the use of Microsoft Word or any other IBM compatible editing programmes is suggested.

LANGUAGE

The language of AMP is English.

PREPARATION OF THE MANUSCRIPT

The different parts of the manuscript need to meet the instructions below:

Title

The title has to be short and informative. No subtitles if possible. If the main title is too long, an additional shortened title is needed for the running head.

Author

The front page has to carry (under the main title) the full name(s) (forename, surname), affiliation(s), current address(es), e-mail address(es) of the author(s).

Abstract and keywords

The abstract is required to be brief (max. 250 words), and has to highlight the aims and the results of the article. The abstracts of notes are alike (but max. 120 words). As far as possible, citations have to be avoided. In the near future the abstracts are going to be distributed in digital form, as well.
The abstract has to be followed by 4 to 10 keywords.

Text and citations

The format of the manuscripts is required to be: double-spacing (same for the abstract), text only on one side of the page, size 12 Times New Roman fonts. Margin width is 2.5 cm, except the left margin, which has to be 3.5 cm wide. Underlines and highlights ought not be used. Please avoid the use of foot and end notes. Accents of Romanian, Slovakian, Czech, Croatian etc. characters must be marked on the manuscript clearly.
When compiling the paper an Introduction – Geological setting – Materials and Methods – Results – Conlclusions structure is suggested.
The form of citations is: the author's surname followed by the date of publication e.g. (Szederkényi, 1996). In case of two authors: (Rosso and Bodnar, 1995) If there are more than two authors, after the first name the co-authors must be denoted as "et al.", e.g. (Roser et al., 1980).

REFERENCES

The reference list can only consist of published papers, M.Sc., Ph.D. and D.Sc. theses, and papers in press.
Only works cited previously in the text can be put in the reference list.
Examples:

BAKKER, R. J. (2002): http://www.unileoben.ac.at/~buero62/minpet/Ronald/Programs/Computer.html. accessed: June 15, 2003.

LE MAITRE, R. W. (ed.) (1989): A Classification of Igneous Rocks and Glossary of Terms. Blackwell, Oxford.

PÁL-MOLNÁR, E. (1998): Geology and petrology of the Ditró Syenite Massif with special respect to formation of hornblendites and diorites. PhD. thesis, University of Szeged, Szeged, Hungary.

ROSSO, K. M., BODNAR, R. J. (1995): Microthermometric and Raman spectroscopic detection limits of CO_2 in fluid inclusions and the Raman spectroscopic characterization of CO_2. Geochimica et Cosmochimica Acta, **59**, 3961-3975.

SZEDERKÉNYI, T. (1996): Metamorphic formations and their correlation in the Hungarian part of Tisia Megaunit (Tisia Megaunit Terrane). Acta Mineralogica-Petrographica, **37**, 143-160.

ZIEGLER, A. M., SCOTESE, C. R., BARETT, S. F. (1983): Mesosoic and Cenozoic paleogeographic maps. In Borsche, P., Sundermann, J. (eds.): Tidal Friction and the Earth's Rotation, II. Springer Verlag, New York, 240-252.

The full titles of journals ought to be given. In case more works of the same author are published in the same year, then these has to be differentiated by using a, b, etc. after the date.

ILLUSTRATIONS

Finally, each figure, map, photograph, drawing, table has to be attached in three copies, they must be numbered and carry the name of the author on their reverse. All the illustrations ought to be printed on separate sheets, captions as well if possible. Foldout tables and maps are not accepted. In case an illustration is not presented in digital form then one of the copies has to be submitted as glossy photographic print suitable for direct reproduction. Photographs must be clear and sharp. The other two copies of the illustrations can be quality reproductions. Coloured figure, map or photograph can only be published at the expense of the author(s).
The width of the illustrations can be 56, 87, 118, or 180 mm. The maximum height is 240 mm (with caption).
All figures, maps, photographs and tables are placed in the text, hence, it is favourable if in case of whole page illustrations enough space is left on the bottom for inserting captions. In the final form the size of the fonts on the illustrations must be at least 1,5 mm, their outline must be 0,1 mm wide. Digital documents should be submitted in JPG-format. The resolution of line-drawings must be 400 dpi, while that of photographs must be 600 dpi. The use of Corel Draw for preparing figures is highly appreciated, and in this case please submit the .CDR file, as well.

PROOFS AND OFFPRINTS

After revision the author(s) receive only the page-proof. The accepted and revised manuscripts need to be returned to the Editors either on disc, CD or as an e-mail attachment. Proofreading must be limited to the correction of typographical errors. If an illustration cannot be presented in digital form, it must be submitted as a high quality camera-ready print.
The author(s) will receive 25 free offprints. On payment of the full price, further offprints can be ordered when the corrected proofs are sent back.

Manuscripts for publication in the AMP should be submitted to:

Dr. Pál-Molnár Elemér
e-mail: palm@geo.u-szeged.hu
Phone: 00-36-62-544-683; Fax: 00-36-62-426-479
Department of Mineralogy, Geochemistry and Petrology
University of Szeged
P. O. Box 651
H-6701 Szeged, Hungary

Published in 450 copies/issue (300 in Hungary, 150 abroad).
Distributed by the Department of Mineralogy, Geochemistry and Petrology, University of Szeged, Szeged, Hungary.
Price of volume 44, 2003 (including Postage): HUF 4000 in Hungary, USD 40 in all other countries.

established in 1922

ACTA MINERALOGICA-PETROGRAPHICA

VOLUME 44 2003

HU ISSN 0365-8066

CONTENTS:

ARTICLES

NOTES

MISCELLANEOUS

Printed in Hungary by Páskum Nyomda, H-7103 Szekszárd, P.O. Box 627